ACCELERATED CORROSION TESTING OF GROUTS FOR PT STEEL STRAND

FINAL REPORT

Project BDV29-977-44
(800002803)

Submitted To
FDOT Research Center
605 Suwannee Street
Tallahassee, FL 32399

Project Manager
Matthew Duncan
Florida Department of Transportation, State Materials Office
5007 NE 39th Avenue
Gainesville, FL 32609

Principal Investigator: Kingsley Lau

Submitted By

Kingsley Lau
Florida International University
10555 W. Flagler Street
Miami, FL 33174

April 2021

Report Prepared by:
Samanbar Permeh
and Kingsley Lau

DISCLAIMER

This investigation was supported by the Florida Department of Transportation. The opinions, findings, and conclusions expressed here are those of the authors and not necessarily those of the Florida Department of Transportation or the U.S. Department of Transportation.

The contributions by Rutambara Sonawane to the work is acknowledged here. The assistance provided by Jonathan Hadad is greatly appreciated.

APPROXIMATE CONVERSIONS TO SI UNITS

SYMBOL	WHEN YOU KNOW	MULTIPLY BY	TO FIND	SYMBOL
LENGTH				
in	inches	25.4	millimeters	Mm
mils	mils	25.4	micrometers	Mm
ft	feet	0.305	meters	M
yd	yards	0.914	meters	M
mi	miles	1.61	kilometers	km

SYMBOL	WHEN YOU KNOW	MULTIPLY BY	TO FIND	SYMBOL
AREA				
in^2	square inches	645.2	square millimeters	mm^2
ft^2	square feet	0.093	square meters	m^2
yd^2	square yard	0.836	square meters	m^2
ac	acres	0.405	hectares	ha
mi^2	square miles	2.59	square kilometers	km^2

SYMBOL	WHEN YOU KNOW	MULTIPLY BY	TO FIND	SYMBOL
VOLUME				
fl oz	fluid ounces	29.57	milliliters	mL
gal	gallons	3.785	liters	L
ft^3	cubic feet	0.028	cubic meters	m^3
yd^3	cubic yards	0.765	cubic meters	m^3
NOTE: volumes greater than 1000 L shall be shown in m^3				

SYMBOL	WHEN YOU KNOW	MULTIPLY BY	TO FIND	SYMBOL
MASS				
oz	ounces	28.35	grams	g
lb	pounds	0.454	kilograms	kg
T	short tons (2000 lb)	0.907	megagrams (or "metric ton")	Mg (or "t")

SYMBOL	WHEN YOU KNOW	MULTIPLY BY	TO FIND	SYMBOL
TEMPERATURE (exact degrees)				
^{o}F	Fahrenheit	5 (F-32)/9 or (F-32)/1.8	Celsius	^{o}C
SYMBOL	WHEN YOU KNOW	MULTIPLY BY	TO FIND	SYMBOL
ILLUMINATION				
fc	foot-candles	10.76	lux	lx
fl	foot-Lamberts	3.426	candela/m^2	cd/m^2

SYMBOL	WHEN YOU KNOW	MULTIPLY BY	TO FIND	SYMBOL
FORCE and PRESSURE or STRESS				
lbf	pound force	4.45	newtons	N
lbf/in^2	pound force per square inch	6.89	kilopascals	kPa

APPROXIMATE CONVERSIONS TO US. CUSTOMARY UNITS

SYMBOL	WHEN YOU KNOW	MULTIPLY BY	TO FIND	SYMBOL
LENGTH				
mm	millimeters	0.039	inches	in
µm	micrometers	0.039	mils	mils
m	meters	3.28	feet	ft
m	meters	1.09	yards	yd
km	kilometers	0.621	miles	mi

SYMBOL	WHEN YOU KNOW	MULTIPLY BY	TO FIND	SYMBOL
AREA				
mm^2	square millimeters	0.0016	square inches	in^2
m^2	square meters	10.764	square feet	ft^2
m^2	square meters	1.195	square yards	yd^2
ha	hectares	2.47	acres	ac
km^2	square kilometers	0.386	square miles	mi^2

SYMBOL	WHEN YOU KNOW	MULTIPLY BY	TO FIND	SYMBOL
VOLUME				
mL	milliliters	0.034	fluid ounces	fl oz
L	liters	0.264	gallons	gal
m^3	cubic meters	35.314	cubic feet	ft^3
m^3	cubic meters	1.307	cubic yards	yd^3

SYMBOL	WHEN YOU KNOW	MULTIPLY BY	TO FIND	SYMBOL
MASS				
g	grams	0.035	ounces	oz
kg	kilograms	2.202	pounds	lb
Mg (or "t")	megagrams (or "metric ton")	1.103	short tons (2000 lb)	T

SYMBOL	WHEN YOU KNOW	MULTIPLY BY	TO FIND	SYMBOL
TEMPERATURE (exact degrees)				
^oC	Celsius	1.8C+32	Fahrenheit	^oF

SYMBOL	WHEN YOU KNOW	MULTIPLY BY	TO FIND	SYMBOL
ILLUMINATION				
lx	lux	0.0929	foot-candles	fc
cd/m^2	$candela/m^2$	0.2919	foot-Lamberts	fl

SYMBOL	WHEN YOU KNOW	MULTIPLY BY	TO FIND	SYMBOL
FORCE and PRESSURE or STRESS				
N	newtons	0.225	poundforce	lbf
kPa	kilopascals	0.145	poundforce per square inch	lbf/in^2

Technical Report Documentation Page

1. Report No.	2. Government Accession No.	3. Recipient's Catalog No.
4. Title and Subtitle Accelerated corrosion testing of grouts for PT steel strand		5. Report Date April 2021
		6. Performing Organization Code
7. Author(s) Samanbar Permeh and Kingsley Lau		8. Performing Organization Report No.
9. Performing Organization Name and Address Florida International University 10555 W. Flagler St. Miami, FL 33174		10. Work Unit No. (TRAIS)
		11. Contract or Grant No. BDV29-977-44
12. Sponsoring Agency Name and Address Florida Department of Transportation 605 Suwannee St. MS 30 Tallahassee, FL 32399		13. Type of Report and Period Covered: Draft Final Report March 2018 – July 30, 2021
		14. Sponsoring Agency Code
15. Supplementary Notes		

16. Abstract

Protection afforded by the post-tension system components often are effective to prevent corrosion of the steel strand; however, there have been cases of corrosion related to grout voids and bleed water. There were cases where the non-bleed thixotropic grouts, used to prevent bleed, had corrosion associated with grout segregation. Prescribed testing generally focused on preventing bleed water formation and chloride contamination but did not address the effects of developed grout deficiencies such as segregation. Other test methods, such as the rapid macrocell, test has also been used in research for steel strand in grouts. It was of interest to assess corrosion testing methods to identify grout robustness and corrosion mitigation to adverse construction. Testing here included methods that promote the development of grout deficiencies, including overwatering, grout prehydration, and flow restrictions for the grouts in vertically deviated setups such as the incline tube test and the inverted-tee test (INT). The work explored modifications to the Post-Tensioning Institute (PTI) accelerated corrosion test and the rapid macrocell test, implementing components of the inverted-tee test. Corrosion testing using the modified incline tube test and electrochemical noise technique were considered as well. Different levels of physical grout deficiencies were visually evident for the thixotropic grout when mixed with excess 10% water. The results showed that the INT setup with the vertical deviation can produce enhanced transport of moisture and sulfate ions towards the top of the tee header and that application of these test specimens can be implemented in existing test guidelines to assess grout robustness and corrosion propensity in deficient grout. Electrochemical noise was shown to be an effective measurement technique to assess the development of localized corrosion of steel in alkaline sulfate solution.

17. Key Word Grout, Post-Tension, Corrosion, Testing, Segregation	18. Distribution Statement		
19. Security Classif. (of this report) unclassified	20. Security Classif. (of this page) unclassified	21. No. of Pages 107	22. Price

EXECUTIVE SUMMARY

Prestressed concrete bridge construction including post-tensioned methods has been widely used. Protection afforded by the tendon duct and the grout often are effective to prevent corrosion of the steel strand; however, there have been several cases of premature corrosion in Florida bridges and elsewhere related to grout voids and bleed water. Non-bleed thixotropic grouts were used to prevent the corrosion development observed previously; however, by 20l1, there were cases of corrosion associated with physically and chemically deficient segregated grout characterized as moisture-rich, low cement content material with high concentrations of sulfate ions. Tests prescribed for corrosion mitigation and quality control of the grout generally focused on preventing bleed water formation and chloride contamination. The Post-Tensioning Institute (PTI) made provisions for an accelerated corrosion test (ACT) that was intended for quality control and developmental purposes but does not address the effects of developed grout deficiencies such as segregation. Other test methods such as the rapid macrocell test has also been used in research for steel strand in grouts. Due to the corrosion tendon failures in a Florida bridge in 2011 associated with a prepackaged thixotropic grout that had developed material segregation, it was of interest to identify corrosion testing methods that would account for grout physical and chemical deficiencies. It would be suggested that testing attuned to grout segregation such as to identify grout robustness and corrosion mitigation could be used to prescribe grouts resistant to the recent corrosion issues. The development of an accelerated corrosion test that considers grout robustness in terms of corrosion ideally could disseminate the beneficial effects of corrosion mitigation technologies such as inhibitor impregnation.

To address these research goals, testing included methods that would promote the development of grout deficiencies. This included adverse mix conditions such as overwatering, grout prehydration, and flow restrictions for the grouts in vertically deviated setups to promote water displacement such as the modified incline tube (MIT) test and the inverted-tee test (INT). The results presented here for the commercially available grouts do not represent material performance as intended following accepted mixing protocols and specifications but were used rather for illustrative purposes to develop corrosion testing protocols that can address grout physical and chemical deficiencies. The work explored test methods, including modifications to the PTI accelerated corrosion test and the rapid macrocell test, to consider grout segregation (such as implementing components of the inverted-tee test). Corrosion testing using the modified incline tube test and electrochemical noise technique were considered as well.

The visual observations of the grout from the various test setups provided important findings for the assessment of grout robustness. Different levels of physical grout deficiencies were visually evident for the thixotropic grout when mixed with excess 10% water. The results showed that the INT setup with the vertical deviation can produce enhanced transport of moisture towards the top of the tee header. The grouts had different yields of leached sulfate ions in the INT header, but higher sulfate levels were generally observed in the tee header than in the tee body, likely relating to the displacement of water. It was apparent that the presence of a high-level flow constriction amplified the water displacement; however, the experiments did not show appreciable effect to enhance sulfate accumulation due to the grout flow constriction.

The results showed that the methodologies prescribed in existing test guidelines can be applicable to assess grout robustness and corrosion propensity in deficient grout. Grout C and expired Grouts C and D, cast with 10% extra water with the most adverse grout segregation showed results that would be considered not meeting acceptance criteria. The results showed that generally Grouts A and B showed a

longer time to corrosion. Accelerated corrosion testing can be used to identify the corrosion performance of passive corrosion mitigation technologies (such as inhibitors and films). Application of protective hydrocarbon films to post-tensioned tendons, such as those already commercially developed can mitigate corrosion. The presence of severe grout deficiencies with continued exposure to adverse corrosion environments can reduce the efficacy of the protective film. The macrocell tests were envisioned to provide an economic alternative to the polarization resistance and potentiostatic tests. However, the outcomes of the research showed that there were complications relating to the electrochemical activity of the individual test cells that would obscure easy interpretation of the galvanic coupling of the cells. Any adverse chemical effects relating to the development of deficient grout by the INT setup was not captured by the macrocell testing. The addition of salt to the anode cell did not provide better outcomes.

The MIT and INT setups can be useful to identify the robustness of grout materials to adverse mixing conditions (such as overwatering and prehydration). The resolved solution resistance of the grout however was strongly differentiated between locations from the top and bottom of the tendon, indicating differentiation in the grout and moisture content. Lower solution resistance was resolved for grout at the top of the tendon than at the lower elevations, further supporting the use of the MIT as means to test grout performance. The corrosion potentials and corrosion current densities for the steel embedded in the MIT specimens and the INT specimens were correlated to the grout sulfate content. The corrosion potential decreases to more electronegative values at the higher sulfate concentrations. Likewise, the corrosion current density showed a general increasing trend with the higher sulfate levels. The values produced from the test program here were consistent with historical data from earlier research, further verifying the adverse effects of elevated sulfate ion concentrations in the segregated grout. The expired grouts developed the highest sulfate ion concentrations and showed the greatest susceptibility for corrosion development.

Lab testing to identify grout robustness requires aggressive test methods; however, overly aggressive test conditions to promote grout segregation is not representative of the required and necessary appropriate quality expected for field construction. Any development of corrosion test methods to address grout robustness must state the expected use and handling of the materials and provide justification for the level of adverse grout conditioning implemented for construction materials beyond that specified by the manufacturer.

Electrochemical noise was shown to be an effective measurement technique to assess the development of localized corrosion of steel in alkaline solution when utilizing appropriate anti-aliasing filters and instrument settings. General statistics such as the mean, rms, standard deviation, skew, and kurtosis of the potential and current time signatures have some experimental scatter but generally revealed the negative the effect of elevated sulfate concentrations on electrochemical noise associated with pitting events. Spectral analysis indicated that the characteristic charge increases and the characteristic frequency decreases with sulfate ion concentration, yet the overall corrosion rate increases, indicating that pitting corrosion develops.

TABLE OF CONTENTS

LIST OF FIGURES

LIST OF TABLES

CHAPTER 1. INTRODUCTION

Prestressed concrete bridge construction including post-tensioned methods has been widely used. It allows the construction of bridges with a long span and opens up a range of design possibilities [1-2]. Corrosion of steel strand in bonded post-tensioned (PT) tendons relating to defects in the grout material has been documented since the 1990s. The grout in PT systems provides barrier protection from the external environment in addition to that afforded by the concrete element and the tendon pipe material [3-4]. As the grout is typically made from portland cement, the steel strand is further protected from corrosion by the development of a passive layer in the alkaline grout pore water solution. These corrosion protection levels often are effective to prevent corrosion of the steel strand; however, there have been several cases of premature corrosion in Florida bridges and elsewhere [5-16]. Many of those cases were related to the inadequate or degraded protection of the strand at joints where moisture and chloride ions can penetrate [8]. Other cases were related to the development of void spaces within the tendon due to the formation of bleed water in neat grouts [5-7]. In those instances, the steel strand were partially exposed in the grout voids in contact with the grout bleed lens. In part due to aggregation of chloride ions by the transport of the bleed water, as well as possible carbonation and moisture recharge due to imperfect duct sealing, macrocell coupling of the developed corrosion anodes at the grout-air interface and the remaining steel (strand embedded in the grout and auxiliary steel components) resulted in accelerated corrosion. Bridge specifications at that time called for redundancy in sealing the duct with the concrete girder (for internal tendons), containment within the PT duct with appropriate coupling and capping, and strand embedment with the PT grout. After early corrosion failures, new material specifications called for grout with non-bleed characteristics. Since the early 2000s, the non-bleed thixotropic grouts were used to prevent the corrosion development observed prior. However, by 20l1, there were cases where corrosion developed in grouts meeting the non-bleed thixotropic grout specifications. The corrosion was not associated with bleed water or void formation and chloride ion concentrations were not significantly elevated in those cases. Some of these cases were associated with physically and chemically deficient segregated grout characterized as moisture-rich, low cement content material with high concentrations of sulfate and alkali ions [17-25].

All of these issues have proven the importance of having good grout quality to extend the service life of bonded post-tensioned tendons. The extent of grout deficiency, moisture presence, aggressive ion accumulation, and grout pore water carbonation contribute to the severity of the defect. Tests prescribed for corrosion mitigation and quality control of the grout generally focused on preventing bleed water formation. These tests included the wick-induced bleed tests, Schupak pressure test, and incline tube test. Field tests often include sounding techniques to identify grout voids. However, case studies and quality control checks of grouted tendons reveal that some level of grout deficiencies such as grout voids and bleed channels often form; and in many cases, corrosion cells do not develop there. Material specifications also maintained chloride limits, often prescribed as a percent of chloride per cement content.

Several testing approaches relating to the corrosion performance of steel strand in the grouts have been considered, including accelerated corrosion testing such as that made for conventional steel reinforcement in concrete [25-31]. Trejo et al., 2009[29] evaluated accelerated corrosion test procedures including the mini-macrocell test, the concrete chloride ion assessment test (also referred to as the concrete corrosion inhibitor association test), and the accelerated chloride threshold test [29]. The application of an anodic potentiostatic test was originally developed in consideration of chloride penetration through damaged tendon ducts as part of a Federal Highway Administration (FHWA)

research project in 1992 on the durability of bonded tendons in post-tensioned bridge structures [32]. The FHWA post-tensioning tendon installation and grouting manual [4] continues to refer to this test method. The test method was further developed by Schokker, 1999 [33], and Hamilton et al, 2000 [34] and addressed complications with the electrochemical polarization test parameters. Pacheco et al, 2006 [35] included the linear polarization resistance method to provide more practical testing than the anodic potentiostatic tests.

Based on the research by Schokker and Hamilton, the Post-Tensioning Institute (PTI) made provisions in the PTI M55 Specification for Grouting of Post-Tensioned Structures for an accelerated corrosion test (ACT) for the assessment of grout materials [36]. The test method was intended for quality control and developmental purposes. It provides criteria for the acceptance of a grout material following a two-step process. The ACT gives provision for acceptance of grout materials that exhibit a polarization resistance greater than 700 $k\Omega \cdot cm^2$ measured by the linear polarization resistance method. The polarization resistance of steel embedded in the test grout material would give a quick indication if there are any components in the grout mixture that would allow depassivation of the steel to occur. A grout material that does not meet this criteria can then be tested by an anodic potentiostatic polarization test of the grouted specimen immersed in chloride solution and polarized to +200 mV_{SCE} where the time to corrosion must exceed that of a neat grout. The polarization would allow fast migration of the chloride ion through the grout and holds the steel at a large anodic polarization that would allow fast detection of corrosion once chloride-induced corrosion initiates. As mentioned earlier, this test component derived from the viewpoint of the ability of the grout to resist chloride penetration through the grout as can occur in scenarios where there is incomplete protection provided by the tendon duct and reinforced concrete structural element but does not address developed grout deficiencies such as segregation. Current specifications in Florida and Virginia require prepackaged grout materials to be tested according to the PTI ACT method. Grouts that exhibit a time to corrosion in the anodic potentiostatic test exceeding 1,000 hours is considered satisfactory. The test method required expensive and sophisticated test equipment including a potentiostat and a multiplexer.

The rapid-macrocell test was developed under the Strategic Highway Research Program (SHRP) [37] for testing of corrosion of steel rebar and has been adopted for testing of corrosion resistant reinforcing steel rebar [38-39] including in standard specifications for testing of stainless steel rebar in ASTM A955 Annex 2.28 The rapid macrocell test has also been used in research for steel strand in grouts[11-13,40-41]. The test method separates two unique test cells, each comprised of a steel electrode embedded in cementitious material or immersed in a representative test solution. The two test cells are electrically coupled with wire and a shunt resistor and ionically coupled via a salt bridge (such as agar admixed with salt). Each test cell is assumed to develop net anodic behavior or net cathodic behavior after its galvanic coupling where a net macrocell current can develop. In order to develop the macrocell, the test grout and electrolyte in each cell should maintain its net anodic or net cathodic condition. With these test conditions controlled, the rapid-macrocell test can be used to differentiate corrosion conditions with small test elements and basic electronic instrumentations. For the case of assessing chemically deficient grouts, the anode component should maintain those characteristics that allow for corrosion initiation (such as pH, chloride concentration, sulfate concentration, etc.) [18-21].

Due to the corrosion tendon failures in a Florida bridge in 2011[9] associated with a prepackaged thixotropic grout that had developed material segregation, it was of interest to identify corrosion testing methods that would account for grout physical and chemical deficiencies. It would be suggested that testing attuned to grout segregation such as to identify grout robustness and corrosion mitigation could be

used to prescribe grouts resistant to the recent corrosion issues. Casting grout in large mockups were made to identify grout segregation. Full scale mockups were used prior to bridge construction in Virginia for grout material selection. Tests such as a modified incline tube test were used in research to identify grout segregation. However, full scale testing is not practical for material selection, material specification or for quality control for the builders or owners, and the modified incline tube test also can be costly. Furthermore, the chemistry of complex grout mix designs can be affected by the many environmental and construction factors including temperature, grout storage, pre-hydration, excess moisture mixing, and etc... As construction can sometimes be difficult, specified grouts that are robust after adverse mixing and grouting conditions can minimize the severity of developed grout defects.

On a related technical note, inhibitor impregnation utilizing a silicon hydrocarbon polymer that forms a protective film was applied on tendons in a FDOT bridge (Jacksonville, FL). Field results showed that inhibitors as part of a commercially-available system could be distributed along the length of the tendon via the strand interstitial spaces. Result of laboratory trials showed that the inhibitor-impregnated specimens had reduced corrosion by more than 90% comparing to untreated samples [42]. The procedure has since been used on PT tendons at risk of corrosion on other bridges, buildings and industrial structures in Florida, Virginia, New York, Ontario, Newfoundland and the UK. The development of an accelerated corrosion test that considers the robustness of grout materials in terms of corrosion durability ideally could disseminate the beneficial effects of corrosion mitigation technologies such as the inhibitor impregnation.

Development of an accelerated corrosion test is proposed to screen materials susceptible to segregation where differentiation of localized grout chemistry could allow corrosion initiation. There are several important questions to be addressed to determine appropriate test methods to identify corrosion development in grouts susceptible to segregation. The major research objectives to be explored include:

1) To characterize the development of physical and chemical grout deficiencies due to excess mix water and water volume displacement.
2) To develop small scale test methodologies that identify deficient grout.
3) To identify corrosion electrochemical characteristics of steel strand in deficient grout.
4) To develop small scale test methodologies to identify steel corrosion in deficient grout.
5) To determine application of small scale test methodologies to assess corrosion mitigation techniques for deficient grout.

To address these research goals, testing included methods that would promote the development of grout deficiencies. This included adverse mix conditions such as overwatering, grout pre-hydration, and flow restrictions for the grouts in vertically deviated setups to promote water displacement such as the incline tube test and the inverted-tee test. The results presented here for the commercially-available grouts do not represent material performance as intended following accepted mixing protocols and specifications but were used rather for illustrative purposes to develop corrosion testing protocols that can address grout physical and chemical deficiencies. The report is divided into sections pertaining to test methods including modifications to the PTI accelerated corrosion test and the rapid macrocell test to consider grout segregation (such as implementing components of the inverted-tee test). Corrosion testing using the modified incline tube test and electrochemical noise technique were considered as well.

CHAPTER 2. METHODOLOGY

Previous research and observations indicated that moisture content was a critical factor for the development of physical and chemical deficiencies in post-tensioned grouts. Another complication was to relate the grout deficiencies with its propensity for the development of corrosion of embedded steel elements. Several exploratory test setups were made to gage the contributing effects of moisture content, casting modality, vertical deviation, and space confinement. Different test setups to measure corrosion activity was assessed as well.

2.1. PTI Accelerated Corrosion Test

2.1.1 Overview

Experiments following the general framework of the Post-Tensioning Institute (PTI) Accelerated Corrosion Test (ACT) for grouts specified in the guide PTI M-55 Appendix B [36] were made but included an approach to assess the robustness of grout materials in terms of segregation by adding 10% additional mix water beyond the grout manufacturer's recommended limit. The PTI ACT is currently specified by the FDOT material specification 938-4.3. The test method includes casting 14-inch, 1-inch diameter grout specimen with an embedded 7-wire prestressing steel strand using a PVC pipe as a mold. Only a 3.5-inch section of the PVC pipe is opened to directly expose the grout specimen to the test solution; however, the electrochemical testing likely would include attenuation of current to polarize an extended length of embedded steel. The grout products were mixed with an electric mixer and hand poured into the PVC mold. The corrosion testing following the ACT protocols included linear polarization resistance and an anodic potentiostatic polarization test at +200 mV_{SCE} in 5% NaCl solution. In the work here, the top portion of the strand at the junction between the grout and the air was covered with an acrylic paint to avoid the effects of carbonation. Specimens were cast as listed in Table 2.1.

Table 2.1. PTI ACT Specimen

Grout	Water	Casting Date	Number of Samples Cast	Grout Curing Time	Specimen Tested[1]
A	10%[2]	07/16/2019	8	28-days	M51*, M52*, M54*, M55*, M56*, M57*
			4	56-days	M53*, M58*, M59*, M510*
	Control[3]	08/16/2019	4	28-days	M5A1, M5A2, M5A3, M5A4
			2	56-days	M5A5, M5A6
B	10%[2]	07/15/2019	8	28-days	M61*, M62*, M63*, M64*, M65*, M66*
			4	56-days	M67*, M68*, M69*, M610*
	Control[3]	08/16/2019	4	28-days	M6A1, M6A2, M6A3, M6A4
			2	56-days	M6A5, M6A6
C	10%[2]	07/10/2019	8	28-days	E1*, E2*, E4*, E5*, E6*, E7*
			4	56-days	E8*, E9*, E10*, E11*
	10%[2]	08/15/2019	4	28-days	E1', E2', E3', E4'
			2	56-days	E5', E6'
	Control[3]	08/15/2019	4	28-days	EA1, EA2, EA3, EA4
				56-days	EA5, EA6
Neat Grout	0.45 w/c[4]	08/05/2019	10	28-days	C1*, C2*, C3*, C4*, C5*, C6*, C7*, C8*, C9*
			2	56-days	C11*, C12*

1. Only defect-free specimens were tested. 2. Pre-Exposed grout. 3.As-received grout. 4. Water to cement ratio

2.1.2. Specimen Preparation Procedures

Preparation of Steel Strand.

PTI ACT specifies a full 14" length of strand of testing where a portion of the strand exits the grouted specimen. The exposed steel at the interface of the grout and air can be subjected to carbonation, especially in the crevice regions between the wire interstitial spaces. To minimize this effect, the center king wire of a 13" length strand was extended one inch and was coated with an acrylic paint (as shown in Figure 2.1a). The paint would ideally provide a barrier coating at the steel grout-to-air interface for the short-term experiments. A gasket was used as a spacer to center the strand within the PVC mold. The work here used a perforated rubber gaskets. The holes were placed in the gaskets to allow greater flowability of the grout within the mold.

PVC Mold Components, Assembly, and Grout Casting

One-inch diameter PVC pipe and caps were cut to size and prepared according the specification guide (Figure 2.1b). A Dremel circular saw with preset cut depth stops was found suitable to make the longitudinal slits for the center PVC section to be opened for exposure to the test solution. The PVC components were assembled connected by silicone and duct tape as shown in Figure 2.1c. Final assembly and grouting hand troweled in place within the mold was made as shown in Figure 1d. Specimens were demolded in two subsets: 28-day and 56-day curing within the mold and stored in 100% RH.

Figure 2.1. PTI Accelerated Corrosion Testing
a. Preparation of steel strand. b. PVC components. c. Assembly of PVC components.
d. Grout casting. e. Electrochemical testing

Electrochemical Testing

The open-circuit potential (OCP) and linear polarization resistance (LPR) measurements were made using a saturated calomel electrode (SCE). The LPR testing was made from the OCP and cathodically polarized 25 mV. The anodic regime of the polarization prescribed by the guide was not followed to avoid the effects of the anodic polarization as well as capacitive charging associated with the interfacial double layer. A scan rate of 0.05 mV/s was used. The analysis region was the linear portion of the scan that typically developed at the last 10 mV. Electrochemical impedance spectroscopy (EIS) was conducted at the OCP condition using a 10 mV AC perturbation in the frequency range of 100,000 > f > 1000 Hz, sampling 10 data points per decade. The solution resistance, Rs, was fit to the high frequency limit of the Randles circuit and was used to correct for the measured polarization resistance by LPR (Rp') following the equation Rp=Rp'-Rs. A saturated calcium hydroxide solution in deionized water (pH=12.6) was used. OCP, LPR, and EIS tests were conducted for all cast specimens. Select specimens were further tested by the anodic potentiostatic polarization tests.

The anodic potentiostatic test was conducted using a Gamry Ref 6 potentiostat and multiplexer as shown in Figure 1e. A stainless steel rod was used as the counter electrode. A 5% NaCl solution was used. Silver/silver-chloride reference electrodes were used for the multiplexed test. It was observed that there was some drift in the reference electrodes during extending testing. For prolonged testing, the polarization was suspended, and the reference electrodes were calibrated before resuming testing. Figure 2.2 shows a schematic of the test setup.

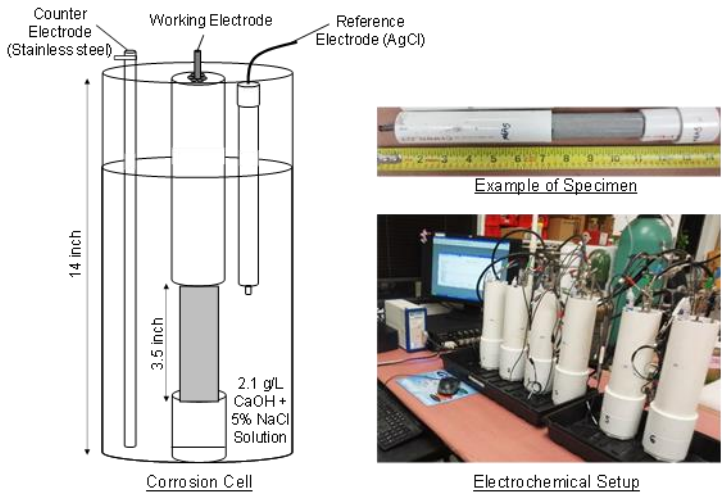

Figure 2.2. Schematic and test setup of the anodic potentiostatic polarization test

2.1.3. Inhibitor Injection

The test specimens used for evaluation of the modified ACT to assess passive corrosion mitigation technologies such as inhibitor impregnation were cast following the general framework of the PTI ACT specified in the guide PTI M-55 Appendix B [36] included an approach to assess the robustness of grout materials in terms of segregation by adding 10% additional mix water beyond the grout manufacturer's recommended limit. Cut sections of select specimens from Table 2.1 (after anodic polarization test) were used. As shown in Figure 2.3, the top section (~6 inch) of the selected specimens for Grout A, B, C, and a neat grout were sectioned (Table 2.2). After cutting the specimens to expose the steel strand cross-section and wire interstitial spaces, an injection port was attached to introduce compressed air and the impregnation media (Figure 2.2). WD-40 was used as a generic medium used for

demonstration purposes. Similar materials were used by Silnutzer et al., 2020 [43]. The medium was injected with compressed air at 20 psi pressure until the medium flowed out of the outlet at the bottom of the specimen.

Figure 2.3. Test specimen

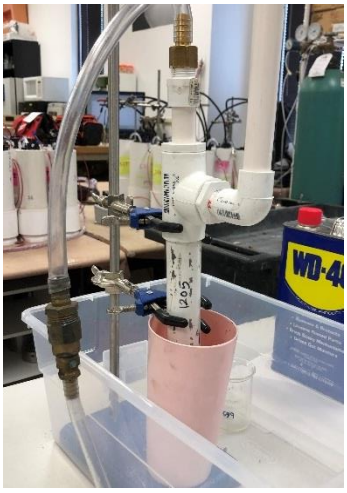

Figure 2.4. Photo of injection port.

After injection, the bottom section was sealed with epoxy. A 2-inch length opening was made in the PVC mold to expose the grouted specimen. The corrosion testing included linear polarization resistance (LPR) and open circuit potential (OCP) in a saturated calcium hydroxide solution and an anodic potentiostatic polarization test at +200 mV_{SCE} in a saturated calcium hydroxide with 5% NaCl solution (following PTI M-55 Appendix B). Supplemental electrochemical impedance spectroscopy (EIS) measurements were made as well. A stainless-steel rod was used as the counter electrode. Silver/silver-chloride electrodes were used as the reference electrodes for the multiplexed test. A saturated calomel electrode was used as a reference electrode for the LPR measurements and supplemental open-circuit potential (OCP) measurements. Figure 2.5 shows the corrosion cell and setup.

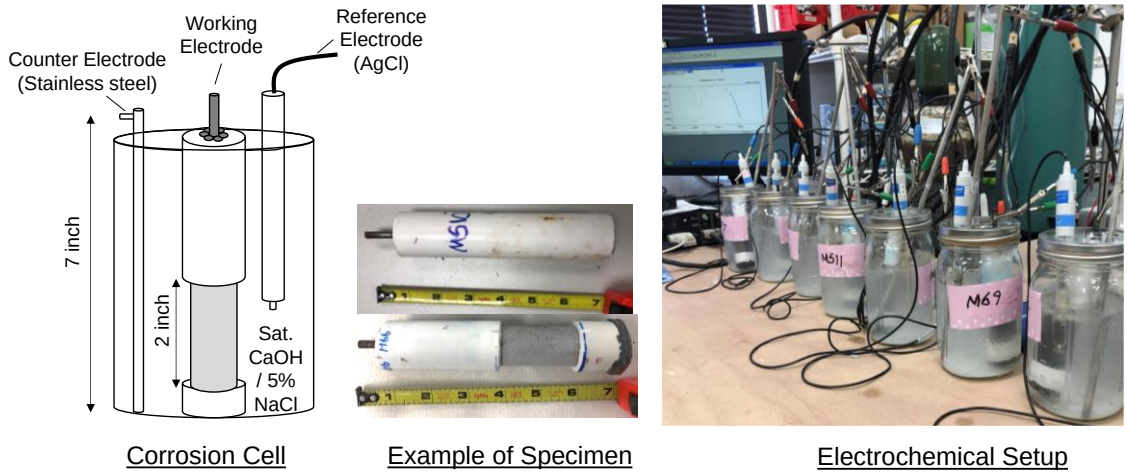

Figure 2.5. Corrosion cell and experimental setup

Table 2.2. Test matrix for ACT assessment of inhibitors

Grout	Mix water	Control	Impregnated with WD-40
A	10% excess	M58, M59	M510, M511
B	10% excess	M63, M66	M67, M69
C	10% excess	E1', E2'	E3', E4'
Neat Grout	0.45 W/C	C1, C2	C7, C11

2.2. Rapid Macrocell Test

2.2.1. Overview

The rapid-macrocell tests was developed under the Strategic Highway Research Program for testing of corrosion of steel rebar subjected to de-icing salts but has been adopted for testing of corrosion resistant reinforcing steel rebar and in research for strand in grouts. In its various incarnations, the test method couples two unique electrochemical cells (made up of steel bar embedded in cementitious material) placed in separate electrolyte. The electrodes were electrically coupled with wire and a 10-ohm shunt resistor. Ionic coupling between the separate electrolyte is made with a salt bridge (constituted of agar admixed with salt to improve conductivity).

A 9-inch 0.75-inch diameter steel bar was used as the metal electrode for both test cells in both the test grout and the control 0.45 w/c neat-grout. The top portion of the steel bar at the junction of the grout and the air was coated with epoxy to avoid the effects of carbonation. Grouted test specimens had an 8" length (top 1" of steel bar extended out) and 1" in diameter. Table 2.3 lists the conditions for the cast test specimens used for these experiments. Table 2.4 shows the conditions for the galvanic coupling of the electrodes with dissimilar grout materials to form the macrocell. The expected net anodic cell labeled as anode was made with the test grouts cast as prescribed by the grout manufacturer or mixed with an excess of 10% mix water. The cell labeled as cathode was made with either the same grout material (with normal or excess 10% mix water) or a control condition with a neat grout with a 0.45 w/c. These sets of experiments were made to identify the suitability of using the grout product or a control neat grout for the cathode.

Table 2.3. Rapid Macrocell Specimen

Grout	Water	Casting Date	Number of Samples Cast	Specimen Tested
A	10% [1]	08/05/2019	4	M5W1, M5W2, M5W3, M5W4
		10/07/2019	4	M5W5, M5W6, M5W7, M5W8
	Control[2]	08/06/2019	2	M51, M52
		10/07/2019	4	M53, M54, M55, M56
		12/18/2019	2	M57, M58
C	10%[1]	08/02/2019	4	EW1, EW2, EW3, EW4
		08/15/2019	4	EW5, EW6, EW7, EW8
	Control[2]	08/02/2019	2	E1, E2
		10/07/2019	4	E3, E4, E5, E6
		12/18/2019	2	E7, E8
Neat Grout	0.45 w/c	08/05/2019	4	C1, C3, C4, C5
		10/07/2019	4	C7, C8, C9, C10
		12/18/2019	4	C11, C12, C13, C14

1. Exposed grout. 2. As-received grout.

The test method has advantages that only small test elements and basic electronic instrumentation is required. However, the testing for various applications require consideration on the supporting test electrolyte to maintain net anodic or net cathodic behavior of the test specimens. For assessment of grout materials, any intrinsic corrosion behavior of the grout (including that due to its chemical makeup and its environment) needs to be maintained. The magnitude of the macrocell is not representative of the actual iron oxidation rate and furthermore, the level of reduction reactions at the cathode may not necessarily be representative to that in actual production. For the case of assessing chemically deficient grouts, the anode component should maintain those characteristics that allow for corrosion initiation (such as pH, chloride concentration, sulfate concentration, etc.).

Table 2.4. Rapid Macrocell Anode-Cathode Coupling

Anode		Cathode	Coupled Pair (Anode-Cathode)
Grout	Mix Water	Mix Water	
A	Control	Control	M53-M54, M55-M56
		Excess 10%	-
		Neat Grout	M57-C11, M58-C12
	Excess 10%	Control	M5W1-M51, M5W2-M52
		Excess 10%	M5W5-M5W6, M5W7-M5W8
		Neat Grout	M5W3-C3, M5W4-C5
C	Control	Control	E3-E4, E5-E6
		Excess 10%	-
		Neat Grout	E7-C13, E8-C14
	Excess 10%	Control	EW1-E1, EW2-E2
		Excess 10%	EW5-EW6, EW7-EW8
		Neat Grout	EW3-C1, EW4-C4
Neat Grout	0.45 w/c	Neat Grout	C7-C8, C9-C10

2.2.2. Sample Preparation Procedures

Preparation of Steel:

Each cell had a steel bar (9-inch length, 0.75-inch diameter) cleaned with acetone and dried. The top of the bar was drilled and tapped to insert a steel screw for electrical connection to copper wires. As shown in Figure 2.6a, the top inch of the bar as well as the base of the steel screw was coated with epoxy to minimize exposure as well as possible carbonation induced corrosion at the bar region at the grout/air interface after casting. Rubber gaskets with additional holes drilled into its flange were used as centering spacers.

PVC Mould Components, and Grout Casting:

The cell molds were comprised of a 7-inch long, 1-inch diameter PVC pipe capped at one end as shown in Figure 2.6b. The steel bar was placed within the mold and the mixed grout was hand-troweled in three lifts. The sides of the mold was tapped to facilitate grout consolidation. Examples of the specimens during fabrication are shown in Figure 2.6c.

Test Cell Assembly:

The anode and cathode specimens were demolded and copper wires were attached to the steel screw. The specimens were subsequently placed and sealed into PVC containers filled with saturated calcium hydroxide solution. The anode and cathode in its respective containers were ionically coupled using a salt bridge following methodology described by Darwin and Strurgeon, 2011 [39]. The salt bridge was a 20" long 5/16"OD, 3/16"ID vinyl tubing filled with an agar mixed with potassium nitrate. As shown in Figure 3d, the tubing was placed through rubber seat washers through the plastic lids for both containers prior to filling to provide an adequate seal and to maintain a continuous medium along the length of the u-shape salt bridge. Both ends of the tubing were immersed in the test solution in its respective container. For 6 salt bridges, a mixture of 41 g of potassium nitrate, 4.5 g agar, and 100 g of tap water, heated to activate the agar and cooled in room temperature, was used. The ionic electrical resistance of each salt bridge was less than 10,000 ohm.

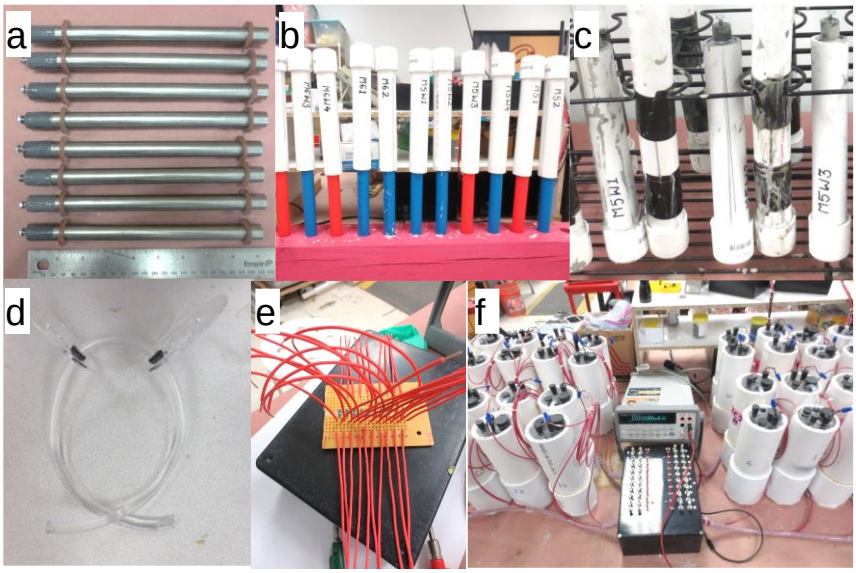

Figure 2.6. Rapid Macrocell Test.
a. Preparation of steel bar. b. PVC mold assembly. c. Grouting. d. Salt bridge assembly. e. Instrumentation assembly. f. Macrocell testing.

Electrochemical Testing

An electrical breakout box was prepared for the rapid macrocell test. The anode and cathode were electrically connected across a 10-ohm shunt resistor. The macrocell current could be calculated from the voltage difference of the anode and cathode across the shunt resistor. Additionally, an electrical switch between the anode and cathode was installed to allow instantaneous electrical current measurements by opening the circuit for a short period (less than 5 seconds) using an ammeter as shown in Figure 2.6f. The mixed potential of the coupled galvanic cell for the anode and cathode was made by placing a saturated calomel electrode in it respective container. Figure 2.7 shows the schematic of the experiment.

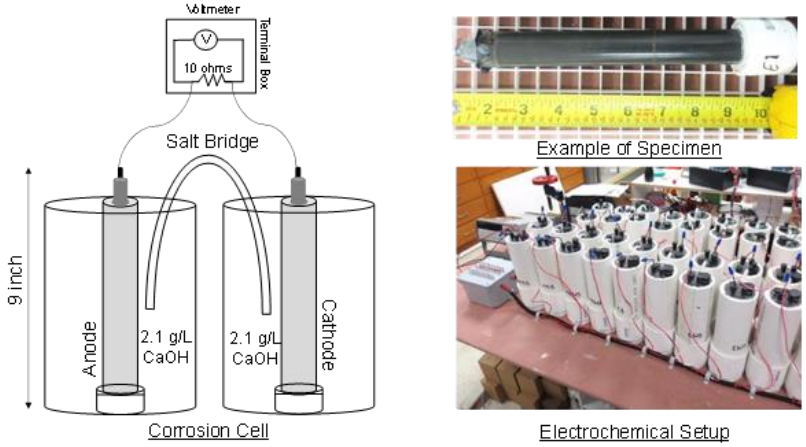

Figure 2.7. Schematic of rapid macrocell test

2.3. Inverted Tee-Test

2.3.1. Overview

From previous research, it was identified that deficient grout can form due to the displacement of water during the pumping stage of the grout installation. An inverted tee-test (INT) was proposed where a dramatic change in the vertical axial cross-section of test specimens was introduced. A schematic of the INT is shown in Figure 2.8. INT specimens were cast with a steel bar for corrosion testing and without steel for grout material testing. The corrosion testing of specimens included methodologies adopting the PTI ACT and the rapid macrocell test. For the latter, cathodes (of similar geometry to the anodes) were made from 0.45 w/c neat grouts where the grout was hand-injected into a horizontal PVC mold and filled by a gravimetric pressure head developed by extending the vertical height of the injection point with a series of two 45-degree PVC angles. The grout material testing included bulk resistance measurements, water absorption and wet resistivity, and chemical analysis for grout segments partitioned as shown in Figure 2.9.

Like the previous sample preparation procedures for the test grouts, an excess of mix water, 10% above the manufacturers' recommended limit, was added. For the INT test, the test grouts were installed by a manual pump rather than hand-troweled as for the ACT and rapid macrocell test described in the preliminary trials described earlier. Test conditions included the grout product, tee-stem height (1 ft to 5 ft), space constriction (with filters), grout prehydration (using expired grouts), and influence of external ion contamination (sulfate and chloride ions). Figure 2.10 shows how filters were placed to create a flow constriction between the tee body and tee stem. In some cases, flow constriction through the filter

prevented complete filling of the tee stem and an alternative partition plan following the top 13” as shown in Figure 2.10 was used.

Tables 2.5 and 2.6 detail the conditions for the corrosion and grout material specimens,

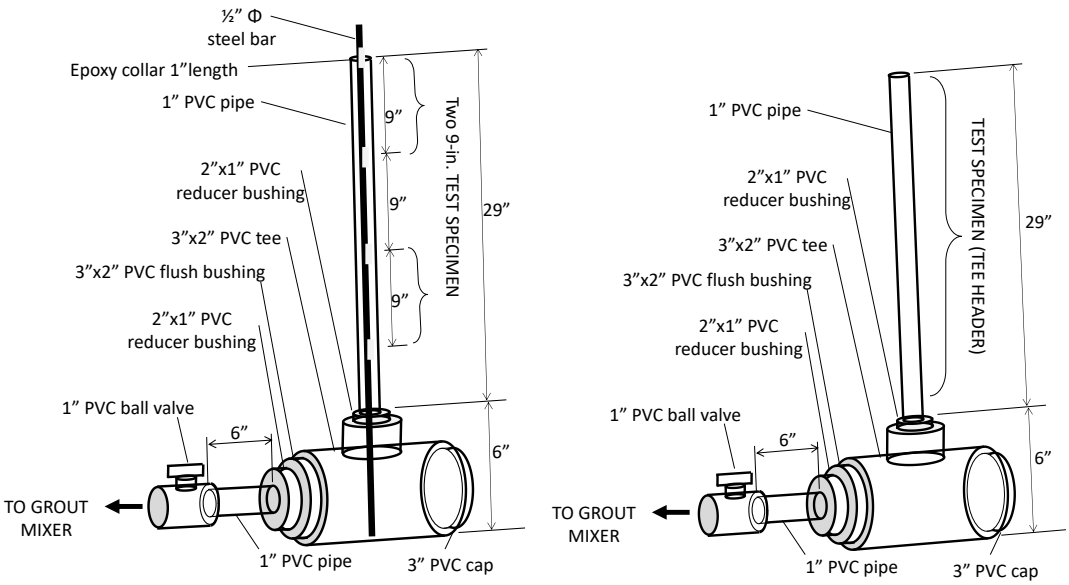

Figure 2.8. Schematic of typical inverted-tee specimen.
In some test cases, different tee header lengths and filters were used.
Left: Corrosion Testing. Right: Grout Testing.

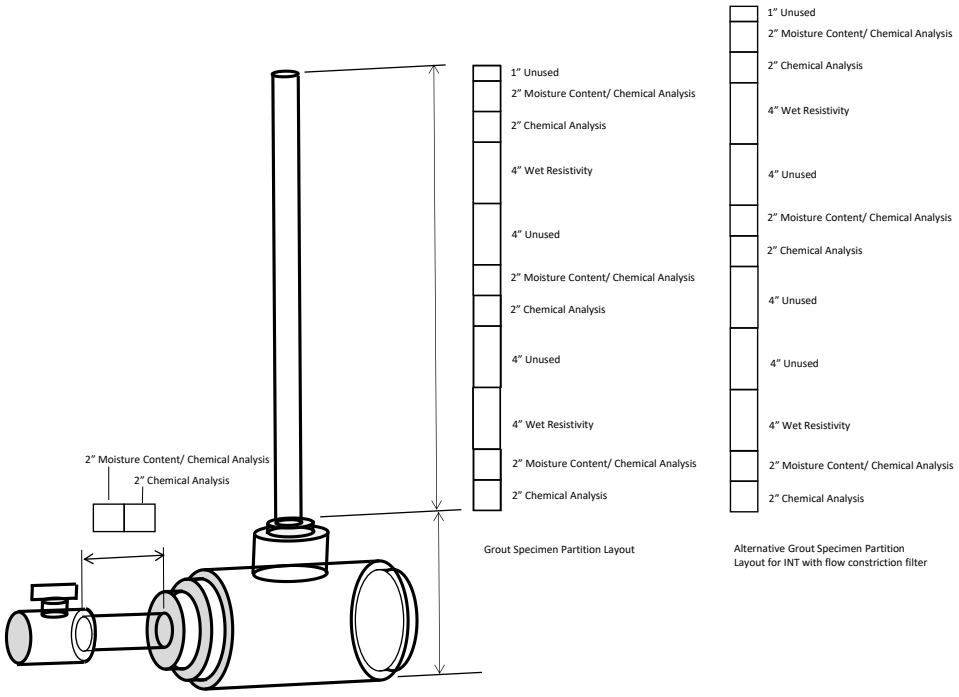

Figure 2.9. INT Grout specimen partition plan.

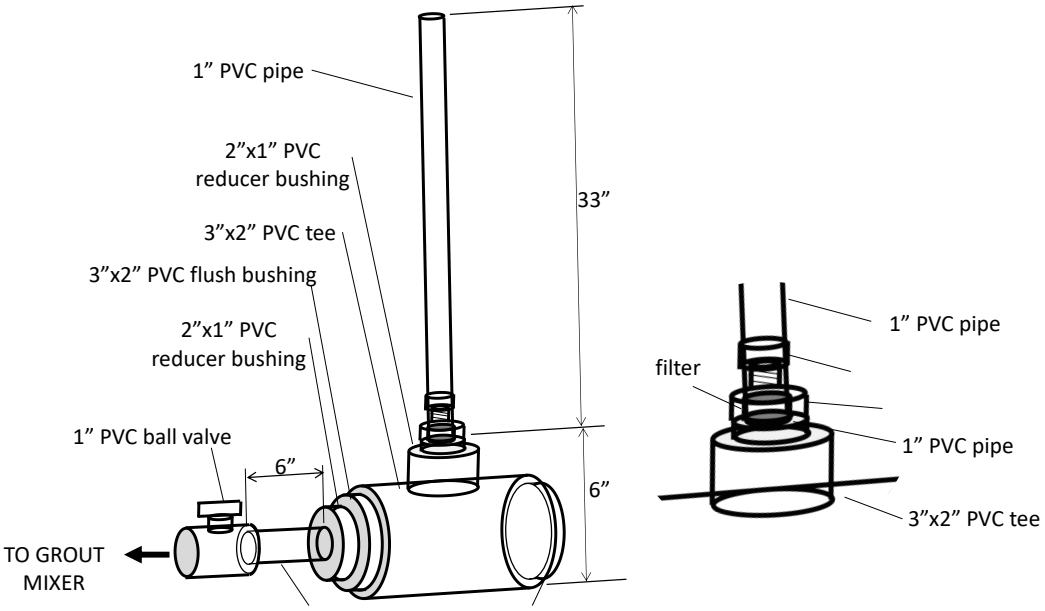

Figure 2.10. Schematic of INT with filter for flow constriction.

Table 2.5. INT Corrosion Test Specimen

Grout	Grout Condition	Name	Date Cast	No. of Specimen[3]
A	AR[1], 10%[2]	IM51*	06/09/2020	2
		IM52*	06/09/2020	2
		IM53*	06/09/2020	2
		IM54*	06/09/2020	2
	AR	IM53	06/08/2020	2
		IM54	06/08/2020	2
B	AR, 10%	IM61*	06/09/2020	2
		IM62*	06/09/2020	2
		IM63*	06/09/2020	2
		IM64*	06/09/2020	2
	AR	IM61	06/08/2020	2
		IM62	06/08/2020	2
C	AR, 10%	IE1	06/08/2020	2
		IE2	06/08/2020	2
		IE3	06/08/2020	2
		IE4	06/08/2020	2
	Expired, 10%	IOE1	08/03/2020	2
		IOE2	08/03/2020	2
		IOE3	08/03/2020	2
		IOE4	08/03/2020	2
D	Expired, 10%[2]	IS1	08/03/2020	2
		IS2	08/03/2020	2
		IS3	08/03/2020	2
		IS4	08/03/2020	2
Neat Grout	0.45 w/c	IC1	06/09/2020	2
		IC2	06/09/2020	2
		IC3	08/03/2020	2
		IC4	08/03/2020	2
	0.45 w/c, H[4]	HC1	06/09/2020	6
		HC2	06/09/2020	6
		HC3	06/09/2020	6
		HC4	06/09/2020	6
		HC5	08/03/2020	6
		HC6	08/03/2020	6

1. As-Received. 2. 10% extra mix water. 3. No. of cut specimens. 4. Cast horizontally.

Table 2.6. INT Grout Material Specimen

Grout	Test Condition		Grout Condition	Name	Date Cast	No. of Specimen[3]	
						header	body
A	Control		AR[1], 10%[2]	IM55	06/10/2020	10	2
				IM56	06/10/2020	10	2
			AR, 10%, S[4]	IM57s	06/12/2020	10	2
			AR, 10%, C[5]	IM58c	06/12/2020	10	2
			AR, 10%, S+C[6]	IM59s+c	06/12/2020	10	2
B	Control		AR	IM63[7]	06/08/2020	10	2
				IM64[7]	06/08/2020	10	2
			AR, 10%	IM65	06/10/2020	10	2
				IM66	06/10/2020	10	2
			AR, 10%, S	IM67s	06/12/2020	10	2
			AR, 10%, C	IM68c	06/12/2020	10	2
			AR, 10%, S+C	IM69s+c	06/12/2020	10	2
	High Constriction		AR	IM610S	06/22/2020	4	2
				IM611S	06/22/2020	5	2
			AR, 10%	IM614S	06/22/2020	6	2
				IM615S	06/22/2020	5	2
	Low Constriction		AR	IM612L	06/22/2020	12	2
				IM613L	06/22/2020	12	2
			AR, 10%	IM616L	06/22/2020	12	2
				IM617L	06/22/2020	12	2
C	Control		AR, 10%	IE5	06/10/2020	10	2
				IE6	06/10/2020	10	2
			Expired, 10%	IOE5	06/10/2020	10	2
				IOE6	06/10/2020	10	2
D	Control		Expired, 10%	IS5	06/10/2020	10	2
				IS6	06/10/2020	10	2
Neat Grout	Control		0.45 w/c	IC5	06/10/2020	10	2
				IC6	06/10/2020	10	2
			AR, 10%, S	IC7s	06/12/2020	10	2
			AR, 10%, C	IC8c	06/12/2020	10	2
			AR, 10%, S+C	IC9s+c	06/12/2020	10	2
	High Constriction		0.45 w/c	IC10S	06/22/2020	12	2
				IC11S	06/22/2020	12	2
	Low Constriction		0.45 w/c	IC12L	06/22/2020	12	2
				IC13L	06/22/2020	12	2
	Vertical Deviation	1’	0.45 w/c	ICV1	05/26/2020	3	2
		2’	0.45 w/c	ICV2	05/18/2020	5	3
		5’	0.45 w/c	ICV3	05/26/2020	14	2
	Vert. Dev. + Constriction		0.45 w/c	ICV4	05/18/2020	6	5

1.As-Received. 2. 10% extra mix water. 3. No. of cut specimens. 4. 2,000 ppm sulfate. 5. 832 ppm chloride. 6. Combined 2,000 ppm sulfate and 832 ppm chloride. 7. Cast with steel bar.

2.3.2. Specimen Preparation Procedures

Preparation of Steel:

Steel bars, 36-inch length and 0.5-inch diameter, were cut and deburred for the corrosion test specimens. The steel bars used for the anode component of the test cell were left in the as-received condition and were only cleaned with acetone and dried with warm air. The steel bars used for the cathode component of the test cell was ground with 80 grit sand paper until a uniform bright finish was made. The bars were then rinsed with tap water to remove residual particles, cleaned with acetone, and dried with war air. As shown in Figure 2.8, the stem portion of the INT sample was partitioned to make two anode test specimens (9-inch length). The steel for the cathode test specimens were also partitioned in 9-inch segments, but were retrieved from grouted samples cast horizontally as introduced earlier. At the location of each partition, a 1-inch length epoxy mask was applied (Figure 2.10a and 2.10b). The epoxy mask served to prevent carbonation-induced corrosion of the steel extended out of the grout at the grout/air interface during testing.

PVC Mold Components, and Grout Casting:

The PVC components of the INT as drawn in Figures 2.8 and 2.9 were collected and assembled as shown in Figure 2.11c, 2.11d, and 2.11e. The PVC mold for the horizontally cast cathode component of the rapid-macrocell test is shown in Figure 2.10f. The steel bar was placed within the INT mold and centered within the tee stem. An example of the centering spacer for the steel bar is shown in Figure 2.11g.

The filters to provide grout flow constrictions were made by casting plastic straws of different diameters in epoxy within a 1.25-inch diameter mold such that a ratio of open space to close space on the transverse area was approximately 2.5 following PTI specifications. The bottom end of the straws were initially plugged with silicone prior to being cast in the epoxy to prevent the epoxy from seeping into the cylindrical spaces within the straws. The silicone could easily be removed after hardening of the epoxy. Two filter sizes were made including using twelve 0.25-inch diameter straws or forty-six 0.12-inch diameter straws. The filters and PVC filter assembly for the flow constriction experiments are shown in Figure 2.11h, 2.11i, and 2.11j.

The completed INT specimen assemblies were placed on wooden racks to ensure vertical stability during the grout pumping process. The grout was mixed using an electric mixer as shown in Figure 2.12a. After mixing, the grout was poured into a manual grout pump (Figure 2.12b) and the grout was pumped into each INT assembly allowing for grout to fill the mold and flow out of the stem prior to closing the inlet PVC ball valve at the tee body.

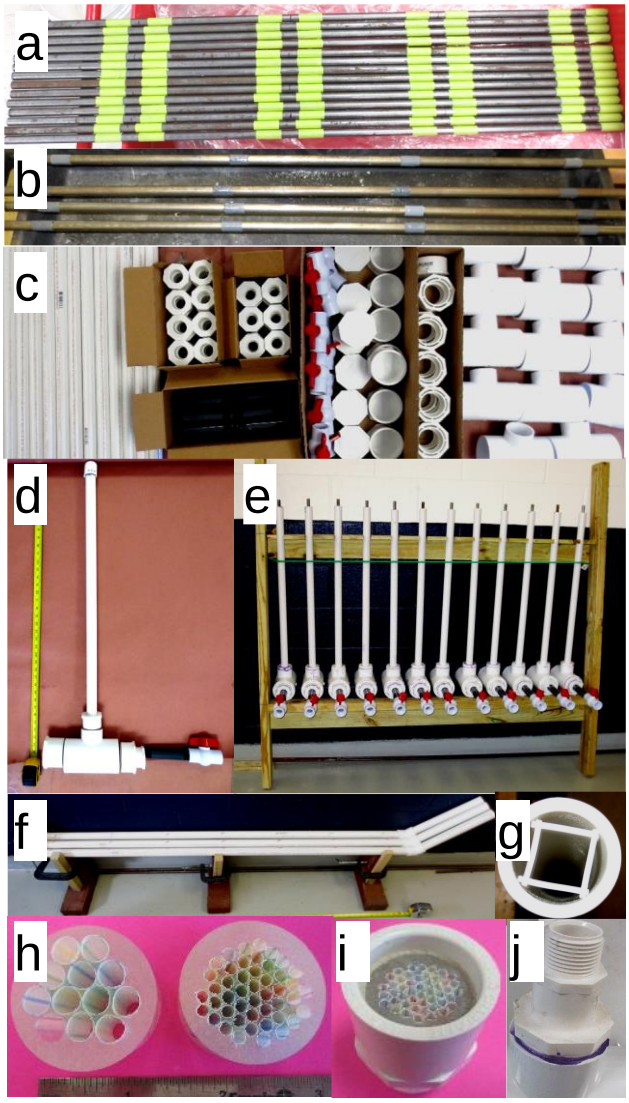

Figure 2.11. INT Assembly.
a. INT anode steel partitioning. b. Macrocell cathode steel partitioning. c. INT PVC components. d. Completed INT assembly. e. INT assembly setup for grouting. f. Macrocell cathode setup for grouting. g. Spacer to center steel bar. h. Filters to introduce flow constriction. h. Internal view of filter assembly. i. External view of filter assembly

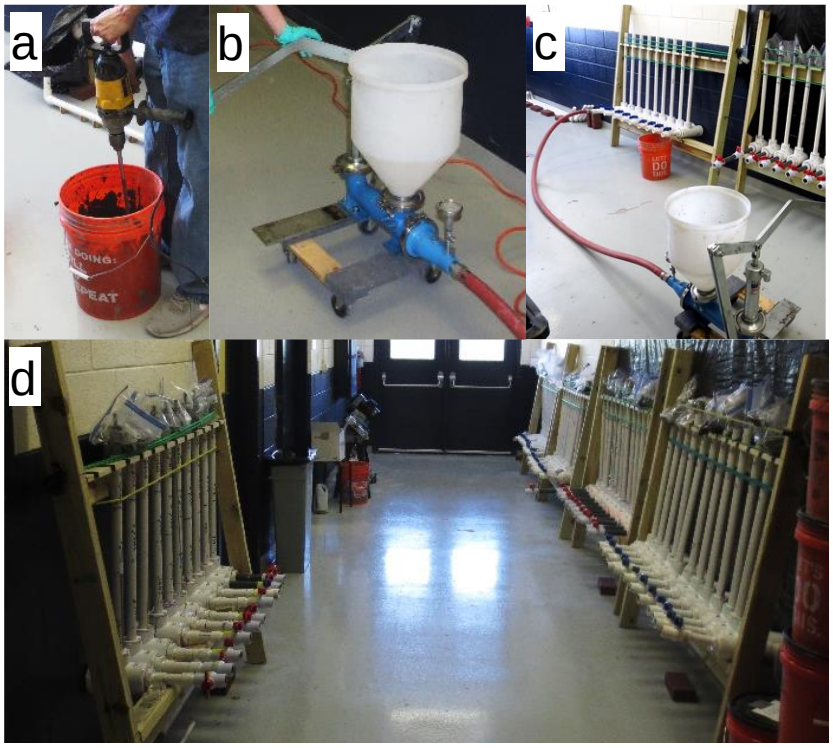

Figure 2.12. Grout Mixing and Pumping for INT.
a. Grout mixing. b. Manual grout pump. c. Setup for INT grout injection. d. Grouted INT specimens.

After 28 days curing within the INT mold or the horizontal mold for the macrocell test cathodes, the PVC was cut at each partition mark for each 9-inch specimen with an electric chop saw such as shown in Figure 2.13a. A 1/8-inch hole was drilled at the top of the exposed steel cross-section of each specimen and a steel screw was inserted so that a hard electrical contact was made. Insulted copper wire was soldered to the steel stud (Figure 2.13b). Both the top and bottom of each specimen were coated with an epoxy (as shown in Figure 2.13c) to mask the exposed steel bar cross-section and the electrical connection. The PVC pipe mold was removed by making two circumferential cuts at the top and bottom of the specimen (~1 cm distance from each end) and two longitudinal slits. An example of an INT test specimen is shown in Figure 2.13d. For the INT grout sampling specimens, cuts were made at each partition mark with a shop saw creating a set of test specimens as shown in Figure 2.13e.

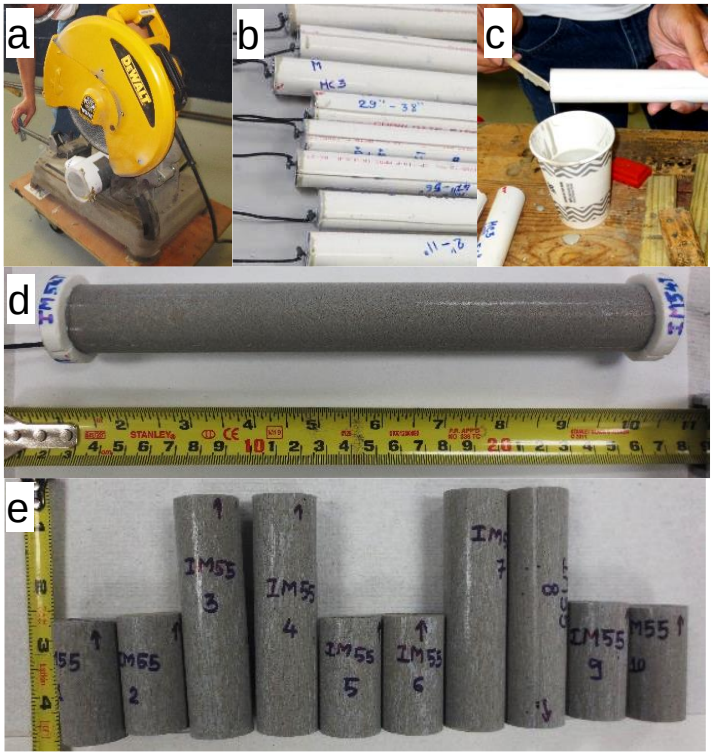

Figure 2.13. INT Test specimen fabrication.
a. Sectioning of INT specimens. b. Electrical connection to steel bar for INT corrosion specimens. c. Sealing exposed steel on INT corrosion specimens. d. INT corrosion specimens. e. INT grout test specimens.

Material Testing:

The INT grout test specimens were cut into segments as shown in Figure 2.9 and Figure 2.13e. Immediately after demolding at 28 days, the grout resistance (R) for each segment (as well as grout from the tee body inlet pipe) was measured by a 2-point method using a soil resistance meter, and the initial grout resistivity (ρ) was calculated by the expression $\rho=RA/L$ where A in the cross sectional area of the 1-inch diameter specimen and L is the length of each grout segment. Also, the moisture content was measured for select specimens from the tee stem and the tee body inlet pipe. The moisture content of the grout samples was determined by ASTM C642. The moisture content was calculated from the mass loss after drying the grout in 110^{o}C until consecutive measurements in 24-hour intervals were within 5% following the expression $MC\%=(m_o-m_f)/m_o$ where m_o is the initial mass and m_f is the mass after drying.

Following Figure 2.9, specimens from the tee header were sorted for chemical analysis or conditioned in 100%RH for mass gain and wet resistivity testing. An ex-situ leaching procedure following a FM 5-618 method was adopted for determination of sulfate and chloride. For the specimens exposed in 100%RH (Figure 2.14a), the mass gain due to moisture uptake was monitored by gravimetric mass measurements using a high precision lab balance. The electrical resistance was also monitored by the 2-point electrical resistance method (Figure 2.14b). For the specimens selected for chemical analysis (including grout specimens from the tee stem and from the tee-body inlet pipe), the grout segments were ground to a powder and collected after sieving through a no. 100 sieve (Figure 2.14c-14f). The grinding process included pre-drying the grout fragments at 60^{o}C. Pre-drying the grout fragments are important practical consideration as the moisture in the grout will create residue on the grinding device.

Furthermore, the pre-drying can normalize grout specimens with different moisture content. The effects of the pre-drying is further considered in the sister project to assess methodologies for sulfate ion analysis.

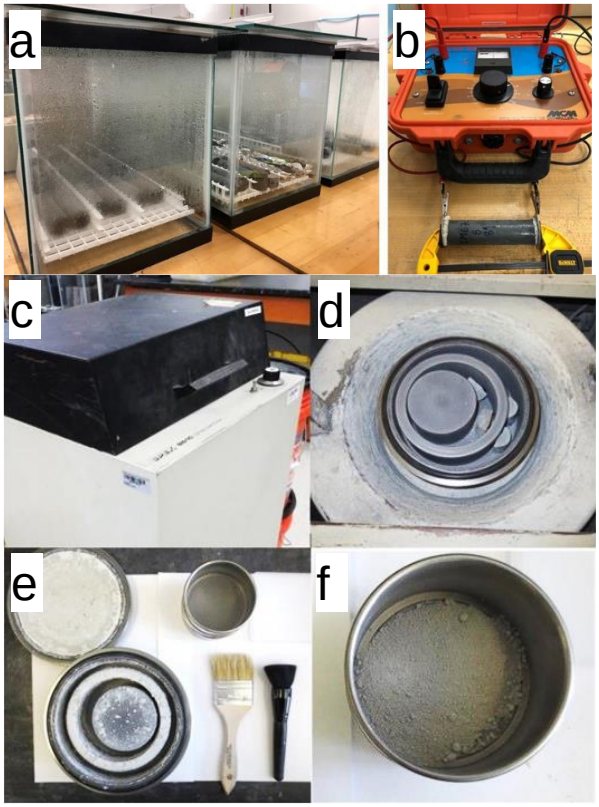

Figure 2.14. INT grout material testing.
a. 100%RH exposure. b. Electrical resistance measurement. c. External view of Shatterbox. d. Grinding grout fragments. e. Collection of ground grout powder. f. Sieving grout powder.

Electrochemical Testing

The open-circuit potential (OCP), linear polarization resistance (LPR), and electrochemical impedance spectroscopy (EIS) was made for all anode INT specimens and cathode specimens. Afterwards, the INT anode specimens were selected for testing following the general procedures prescribed by the PTI ACT and the rapid-macrocell test with the modifications described earlier (Figure 2.15-2.16).

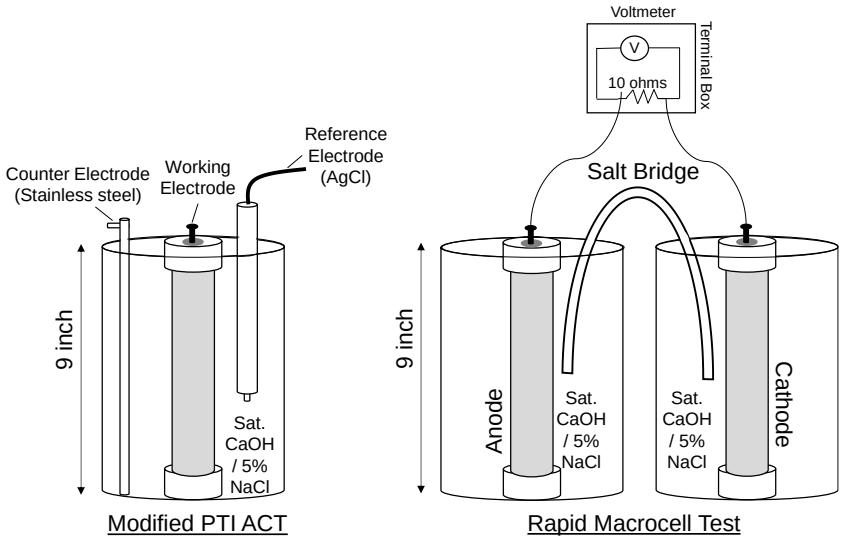

Figure 2.15. Setup for electrochemical testing and corrosion cell

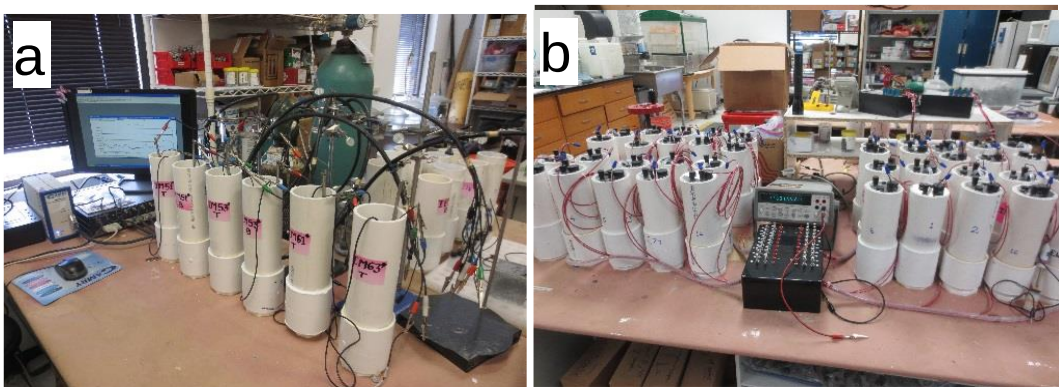

Figure 2.16. INT Corrosion Test Setup.
a. Modified PTI ACT. b. Rapid-Macrocell Test.

The corrosion testing generally followed the PTI ACT protocols including linear polarization resistance (LPR) in a saturated calcium hydroxide solution and an anodic potentiostatic polarization test in 5% NaCl solution. A stainless-steel rod was used as the counter electrode. Silver/silver-chloride electrodes were used as the reference electrodes for the multiplexed test. A saturated calomel electrode was used as a reference electrode for the LPR measurements and supplemental open-circuit potential (OCP) measurements. Figure 2.15 shows the corrosion cell.

The rapid macrocell tests generally followed ASTM A955 Annex 2.25 [27]. Specimens labeled as anodes were the two-cut sections from the INT header made with the test grouts as detailed in Table 2.5. Specimens labeled as cathode were cut sections of a 0.45-w/c neat grout that was cut horizontally in 5-ft segments. Specimen preparation and the test setup were described before. Figures 2.15 and 2.16 show the corrosion cell and experimental testing. The specimens were subsequently immersed in saturated calcium hydroxide solution and sealed in PVC containers. For the comparative testing after 30 days, the test solution was renewed with saturated calcium hydroxide and 5% NaCl solution for another 30-day cycle. The anode and cathode in its respective containers were ionically coupled using a salt bridge as described earlier.

An electrical breakout box was prepared for the rapid macrocell test and the anode and cathode were electrically connected across a 10-ohm shunt resistor. The macrocell current could be calculated from the voltage difference of the anode and cathode across the shunt resistor. Additionally, an electrical switch between the anode and cathode was installed to allow instantaneous electrical current measurements using an ammeter by opening the circuit for a short period (less than 5 seconds).

2.4 Modified Incline Tube Test

The MIT had been shown to promote some level of grout segregation. As such, the setup was used to produce grout samples for further chemical analysis and assessment of sampling procedures. The MIT test generally consists of pumping grout in a 3-inch diameter pipe, along a 15-foot length at a 30 degree incline. A schematic of the specimen assembly used in this research is shown in Figure 2.17. The relatively high grout volume and the vertical deviation could promote transport of moisture if the grout material is susceptible to bleed or segregate. The MIT test also included excess mix water to promote the moisture transport.

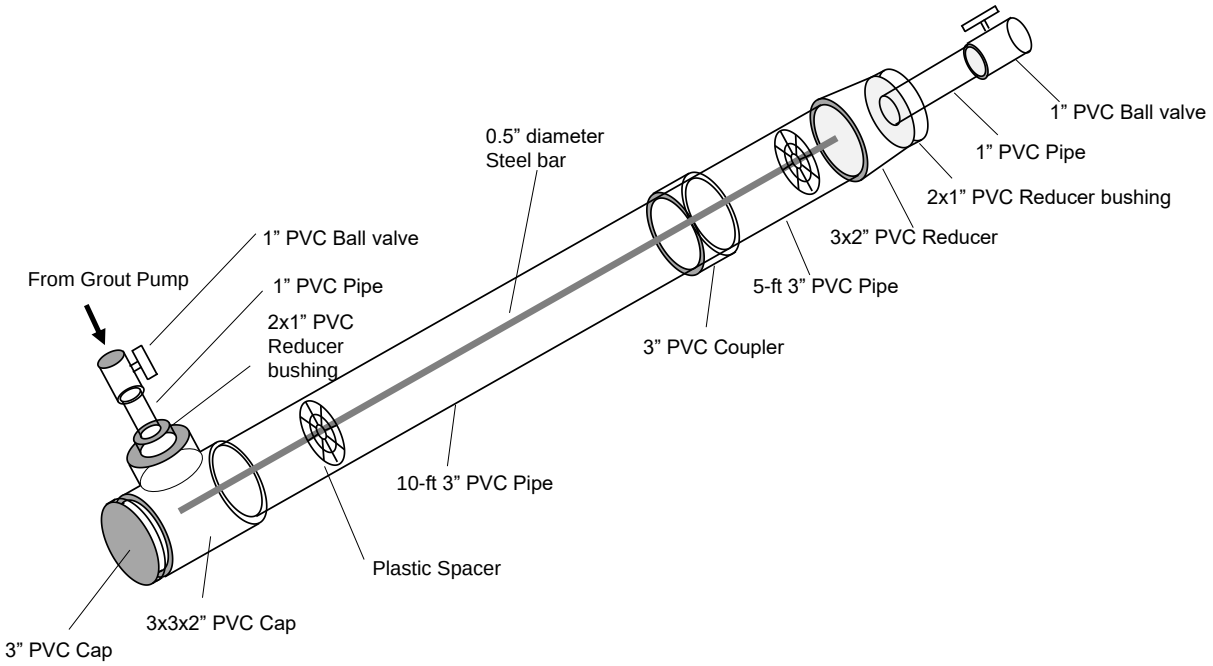

Figure 2.17. MIT test assembly

A 15-foot 0.5-inch diameter steel bar was placed in the MIT for additional corrosion testing. The steel bar was cut to length and cleaned with acetone (Figure 2.18A). The PVC components were assembled according to Figure 2.17 and the steel bar was placed within the pipe, centered with rebar spacers. The specimens were placed on a steel frame with a 30 degree incline, as shown in Figure 2.18B-D.

Figure 2.18. MIT assembly.
A. Steel bar. B. Front view of assembly. C. Side view of assembly. D. View of steel bar near MIT outlet.

Figure 2.19. MIT Grout Mixing and Injection

The Grout A material had been specified for horizontal PT applications and Grout B had been specified for vertical applications. The grout mixes for both products incorporated 10% excess mix water from the manufacturer's recommendation. It was thought that the two products designed for different applications (horizontal and vertical) can be used as a foil, and the two products with non-ideal excess mix water and subject to the vertical deviation in the MIT testing would ideally create differentiation in the grout within the assembly to provide test material for subsequent laboratory testing of deficient grout. For each specimen, four 25-pound batches were weighed and mixed on site and pumped into the PVC assembly. A manual grout pump was used to inject the grout into the MIT assemble (Figure 2.19). Grout was allowed to freely flow out of the PVC outlet. The outlet valve was first closed followed by the inlet valve. Details of the MIT specimens are shown in Table 2.7.

Table 2.7. MIT specimens

Name	Condition	Casting Date	Number of Samples Cast	Specimen Name	Name of cast cylinder mold
Grout A	As-received grout with 10% ext water	11/20/2019	1	MIT-1	1-1[1], 1-2[1], 1-3
		11/21/2019	3	MIT-2	2-1[1], 2-2[1], 2-3
				MIT-3	3-1[1], 3-2[1], 3-3
				MIT-4	4-1[1], 4-2[1], 4-3
		12/03/2019	2	MIT-6	6-1[1], 6-2[1], 6-3
				MIT-8	8-1[1], 8-2[1]
Grout B	As-received grout with 10% ext water	12/04/2019	3	MIT-9	9-1[1], 9-2[1], 9-3
				MIT-10	10-1[1], 10-2[1], 10-3
				MIT11	11-1[1], 11-2[1], 11-3,
		12/17/2019	3	MIT-13	13-1[1], 13-2[1], 13-3,
				MIT-14	14-1[1], 14-2[1]
				MIT16	15-1[1], 15-2[1], 15-3

1. Grout cylinders stored in saturated calcium hydroxide solution.

CHAPTER 3. MATERIAL CHARACTERIZATION

The development of deficient grout by the various test conditions detailed in the previous chapter was assessed in terms of the propensity for active corrosion of the embedded steel and differentiation of grout properties. The manifestation of grout segregation was assessed by moisture content, grout resistivity, and general visual corrosion development. Chemical analysis for sulfate concentration was also carried out for INT test specimen.

3.1. Visual Grout Condition

The grouted specimens from the PTI Accelerated Corrosion Test (ACT), rapid macrocell test, and inverted-tee tests (INT) are shown in detail in Appendix A. It was evident that the fabrication of grouted test specimens in hand-poured batches within rather tight spaces in the 1-inch diameter PVC pipe for the ACT and rapid-macrocell test was difficult and grout defects such as small air voids were observed in many specimens after demolding. Casting in lifts and attempts to rod the material within the tight geometry did not always prevent consolidation issues. Some level of grout segregation was often observed at the location of the spacers for the rapid macrocell-test. The 0.45 w/c neat grout poured in-place by hand typically showed grout consolidation problems. The surface appearance of the thixotropic grouts when mixed following recommended procedures was more uniform and had better overall visual consistency than the neat grout. The injection of thixotropic grout in the normal condition with a grout pump generally provided a more uniform material along the vertical height of the INT specimens. The 0.45 w/c neat grout injected by a pressure head also formed better consolidated material than its hand-poured counterparts, although movement of air along the length of the neat grout was apparent. Comparisons of the grout materials after demolding showed that the mixing with excess 10% water could provide visual grout heterogeneities for all materials although the magnitude of physical grout deficiency differed by grout product. The INT setup showed that deficient grout material created by the excess mix water could accumulate in the tee header.

The visual observations of the grout from the various test setups provided important findings for the assessment of grout robustness. Better grout consolidation within the small geometry test specimens was made when the grout was injected with a grout pump rather than hand-poured. The thixotropic grouts, when mixed following recommended practices, generally formed visually consistent hardened grout and was more robust to consolidation problems than the neat grout. Different levels of physical grout deficiencies were visually evident for the thixotropic grout when mixed with excess 10% water.

3.2. Effect of Grout Mix and Cast Conditions

The INT specimens from the tee header (were cut into 10 sections) as well as from the tee body inlet valve stem were further tested to evaluate the material segregation. The effects of the excess 10% mix water, vertical deviation in the tee header, grout flow confinement, and grout contamination were assessed.

3.2.1. Effect of Vertical Deviation

Figure 3.1 shows the moisture content of the grout from various tee stem heights when cast with up to 5 feet of vertical deviation. The results showed that the INT setup with the vertical deviation can produce enhanced transport of moisture towards the top of the tee header. The grout at greater vertical heights had correspondingly greater moisture content and the moisture content of the grout in the tee header was consistently greater than the grout in the tee body. This effect was observed for test trials with

the tee header made at 1 ft, 2 ft, and 5 ft. Subsequent INT tests were made with a vertical deviation of 3 ft.

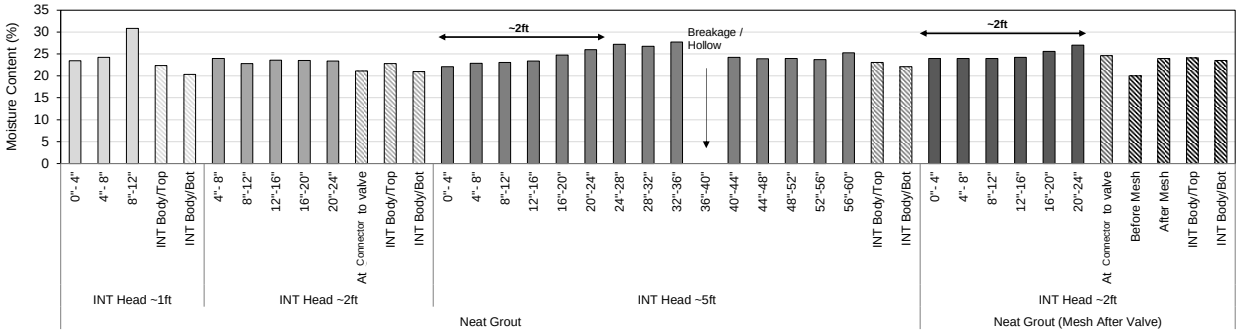

Figure 3.1. Moisture content of neat grout in INT setup with different vertical lengths.

3.2.2. Effect of Excess Mix Water

The effect of excess 10% mix water was initially assessed for grout cast in 3x6" cylinders. As shown in Figure 3.2, the thixotropic grouts in the normal mix condition and with excess mix water were consistently higher than that for the 0.45 w/c neat grout, indicative of the good electrical characteristics of the thixotropic grouts. In the static pour for the cylinder specimens, the effect of the excess mix water on the bulk resistivity was not readily apparent. Indeed, any amount of grout segregation within the cylinder could not be easily differentiated.

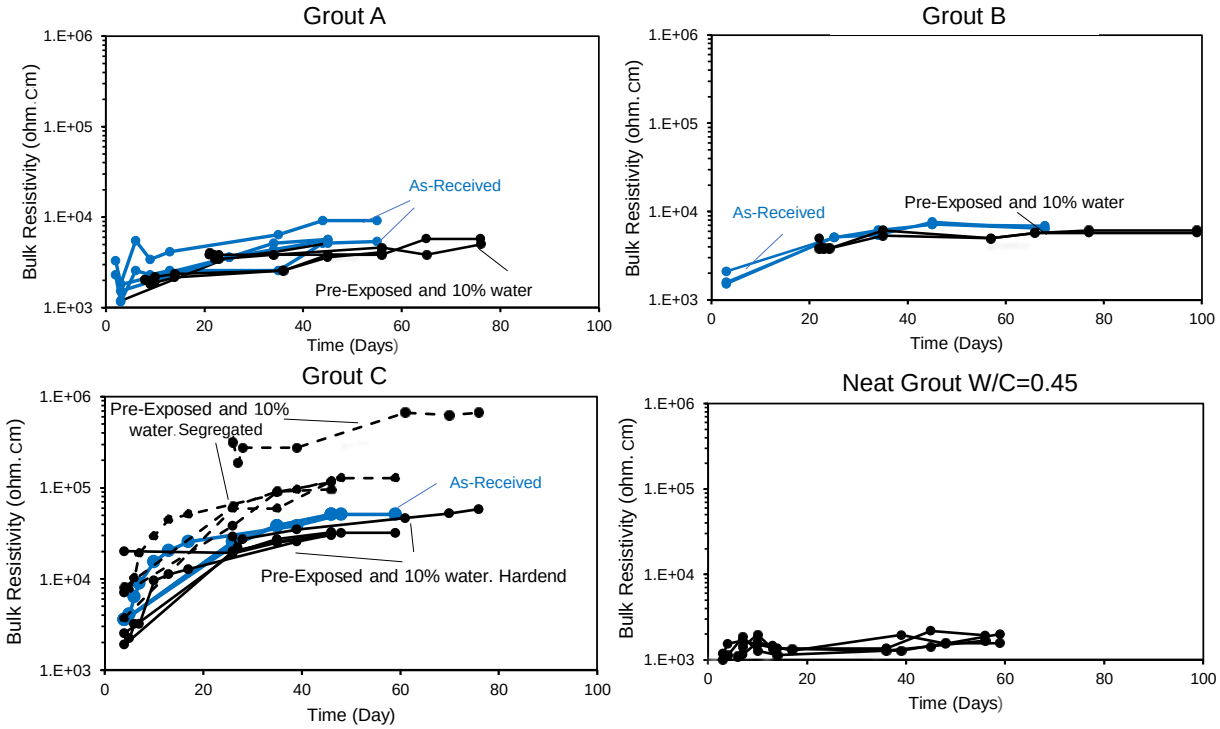

Figure 3.2. Bulk resistivity of grout cast in 3x6"cylinders.

The INT specimens, on the other hand, allowed for a physical separation of grout from the tee header and tee body. The results of the moisture content and bulk resistivity are shown in Figures 3.3 and 3.4. There was distinct differentiation in moisture content for the Grout C, expired Grout C and D. Differences in moisture content of the grout from the tee header and body were less apparent for the

Grout A and B grout. On the other hand, lower grout resistivity was apparent for the grout in the tee header in comparison to the tee body. The grout resistivity of the Grout C grout in the tee header typically resulted in high values due to observed high porosity that resulted from the excess mix water and water displacement in the INT. Grout in the tee body had grout resistivity within the same magnitude of order as the other thixotropic grouts, if not somewhat elevated.

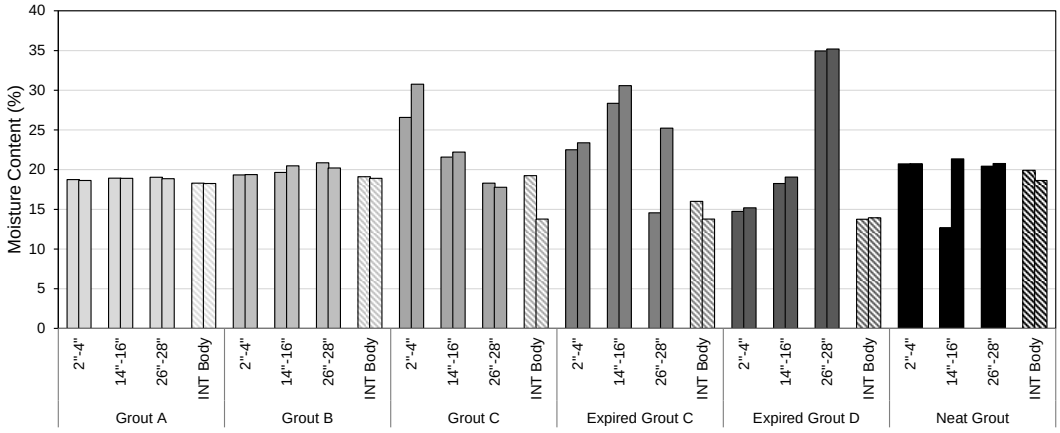

Figure 3.3. Moisture content of grout cast in INT with 10% extra mix water

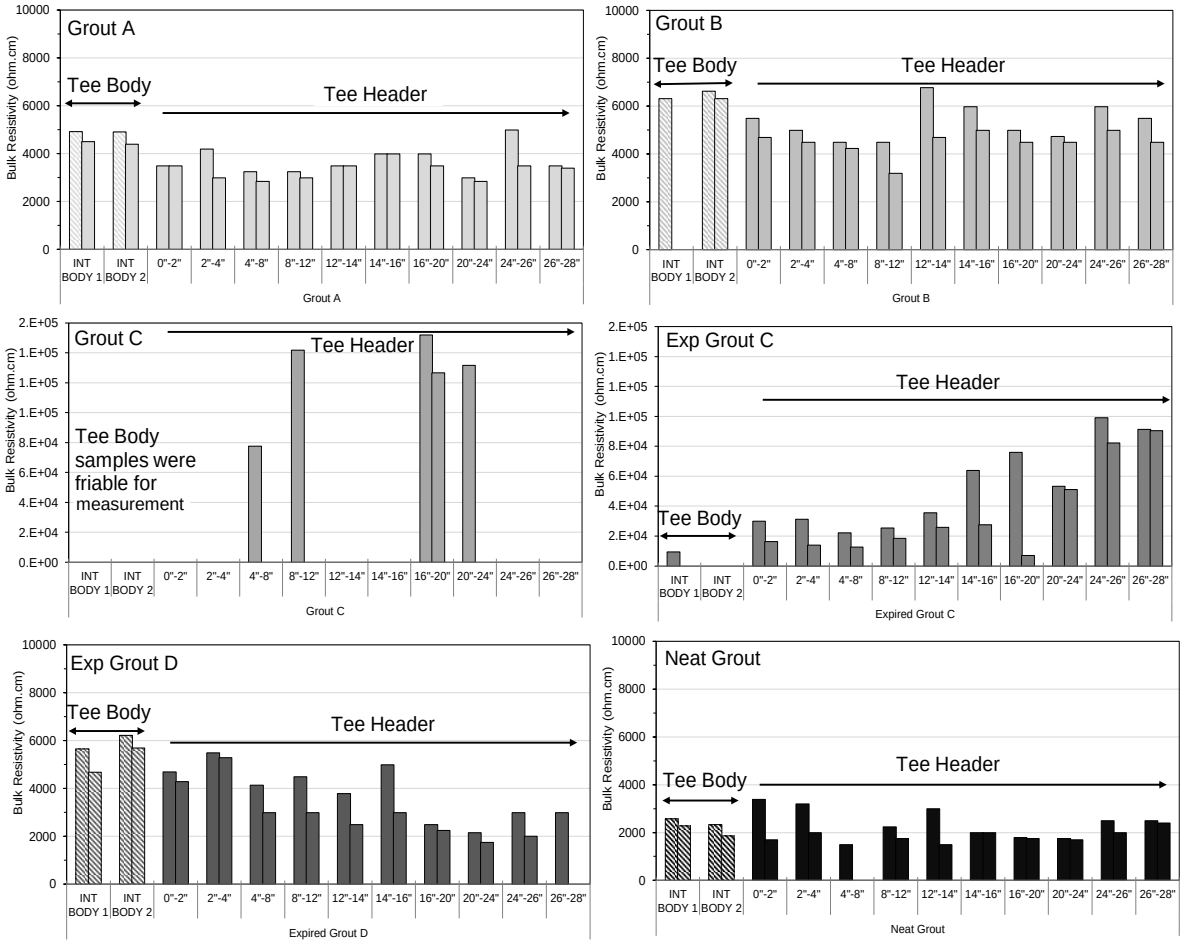

Figure 3.4. Bulk resistivity of grout cast in INT with 10% extra mix water

Figure 3.5 shows the moisture uptake and wet resistivity of the grout specimens during its exposure in 100%RH. As of up to 60 days, the specimens have not reached a saturated moisture condition and have not yet reached a terminal wet resistivity. The resistivity results would have the conflated effect of cement hydration and moisture uptake. In any case, all of the thixotropic grouts show improved permeability and resistivity characteristics over the 0.45 w/c neat grout.

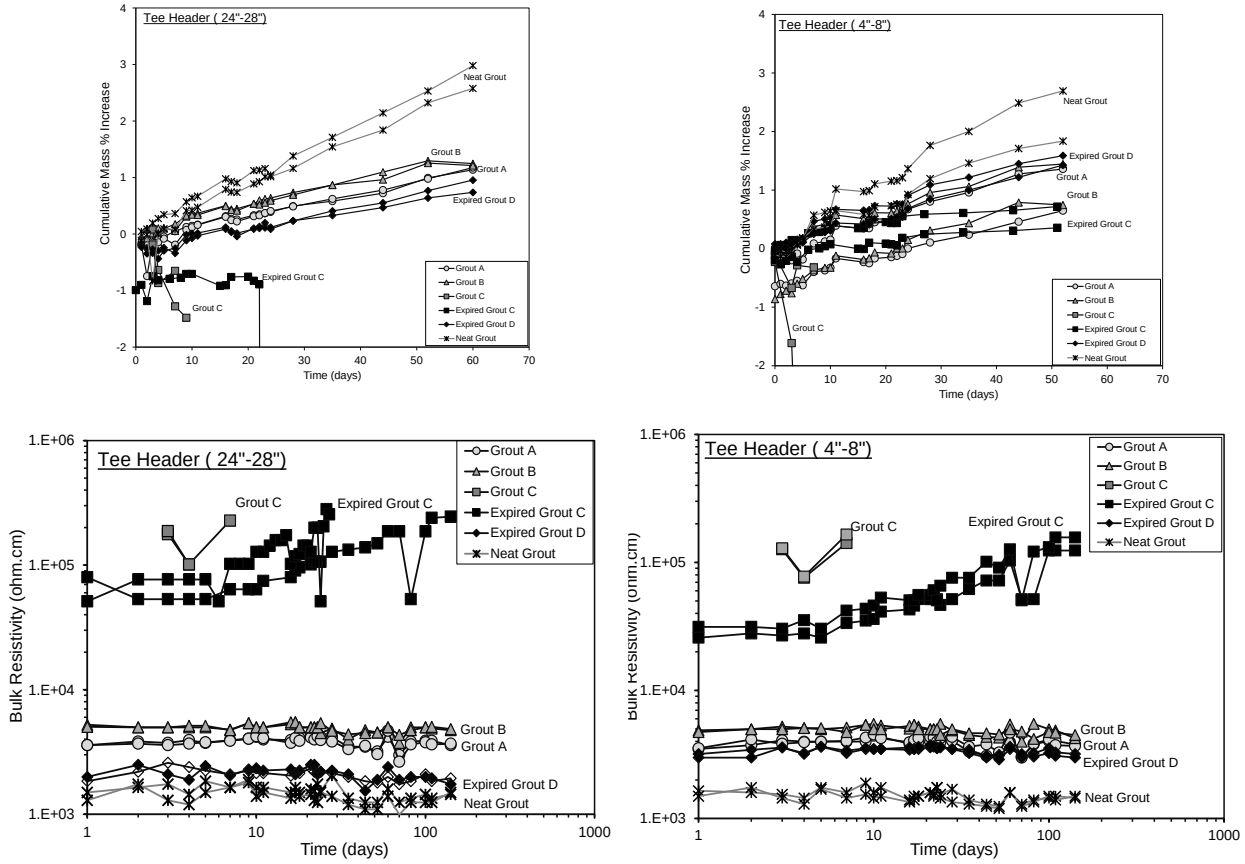

Figure 3.5. Moisture uptake and grout wet resistivity of INT setup cast with 10% extra mix water

3.2.3. Effect of Flow Constriction

Figures 3.6 and 3.7 show the moisture content and bulk resistivity of grout cast in INT setup with the presence of high and low grout flow constriction. Similar to the INT results without the flow constriction, the grout in the tee header had higher moisture content than the grout in the tee body. In all test cases, the excess mix water allowed for enhanced water displacement into the tee header. However, it was apparent that the presence of a high flow constriction amplified this effect. Much higher water contents (>30%) was measured in the grout from tee header.

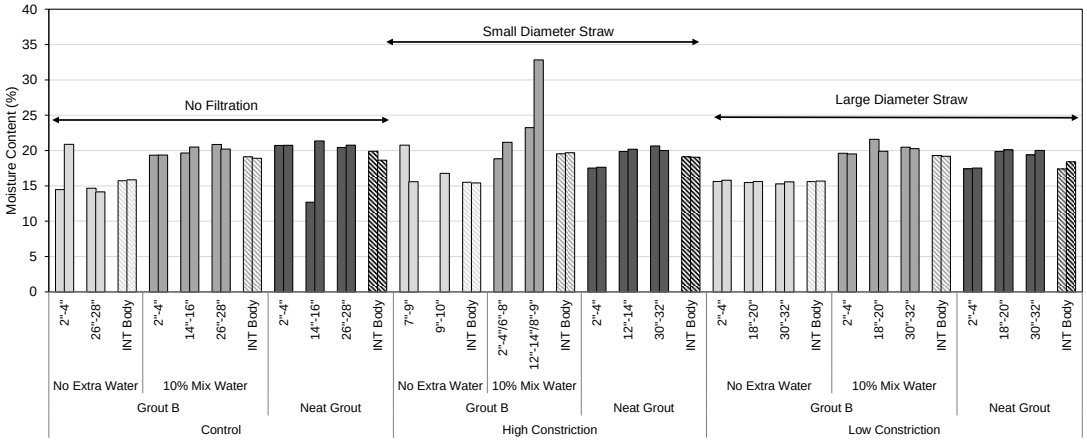

Figure 3.6. Moisture content of grout cast from INT with grout flow confinement.

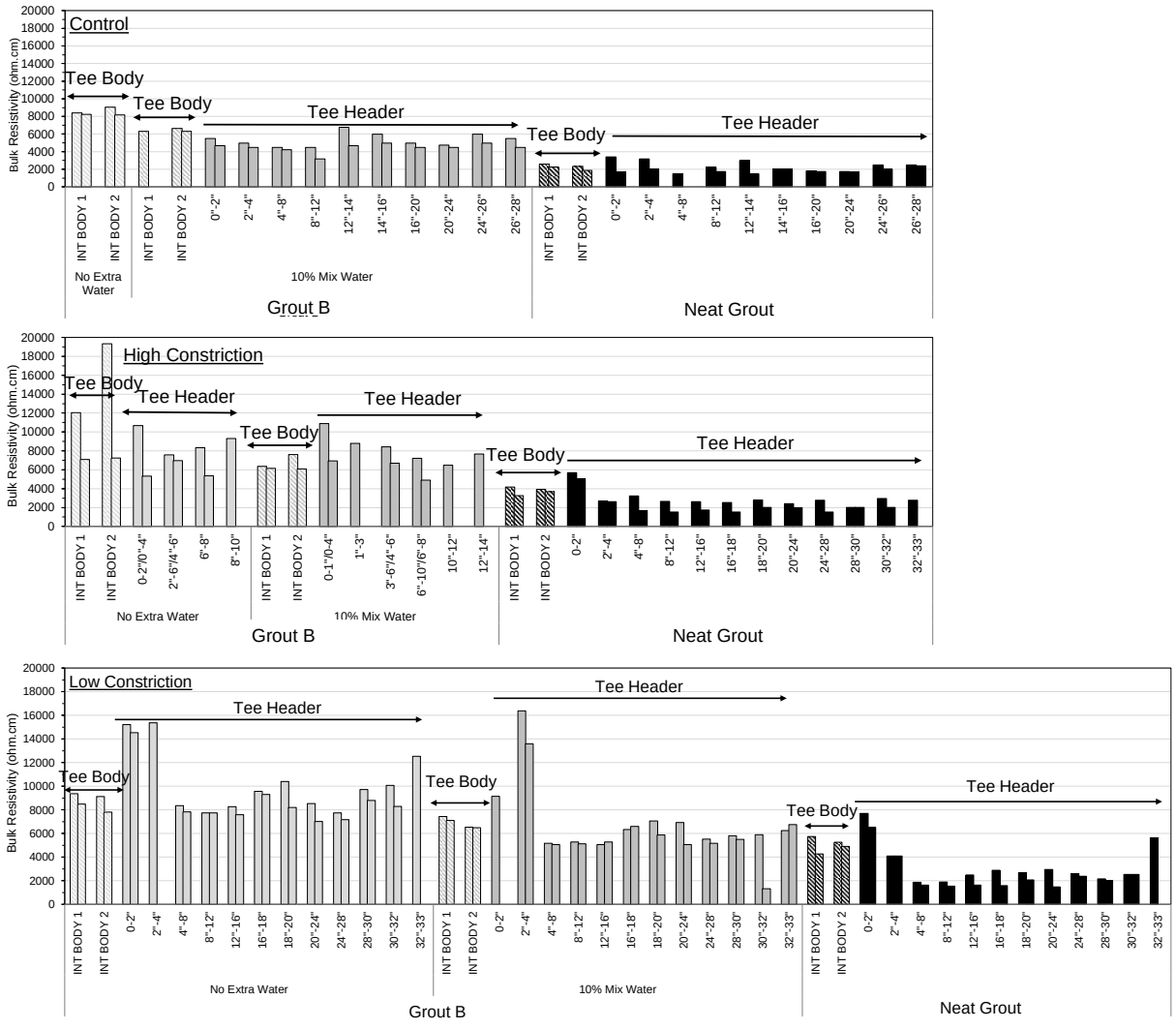

Figure 3.7. Bulk resistivity of grout cast from INT with grout flow confinement.

Although the bulk resistivity showed supporting and consistent results that grout in the tee header had worse electrical characteristics than the grout in the tee body and that the excess 10% mix water allows for greater moisture displacement, the resistivity results did not show clear effect of the grout flow constriction. Even though the moisture content was the greatest in the tee header after grout pumping with high-level flow constriction, the bulk resistivity of the grout before and after the flow constriction (i.e., tee body and tee header) did not reveal a correlating effect. This was due to the fact that the thixotropic grout could not be completely pumped through the high-level constriction filter up to the 3' vertical deviation. It was observed that the filter became clogged with a dense grout material allowing for the higher water content in the grout above. The effect of grout hydration and differential drying upon demolding may also be important. Monitoring of moisture uptake and wet resistivity of the grout conditioned in 100%RH are described next (Figures 3.8 and 3.9).

After up to 40 days of conditioning in 100%RH, the grouts subjected to flow constriction continued to increase in mass due to water uptake, and the wet resistivity dropped accordingly. There is no clear differentiation in the results due to the flow confinement. Consistent with the observations from the other test cases, the thixotropic grouts showed improved characteristics over the neat grout.

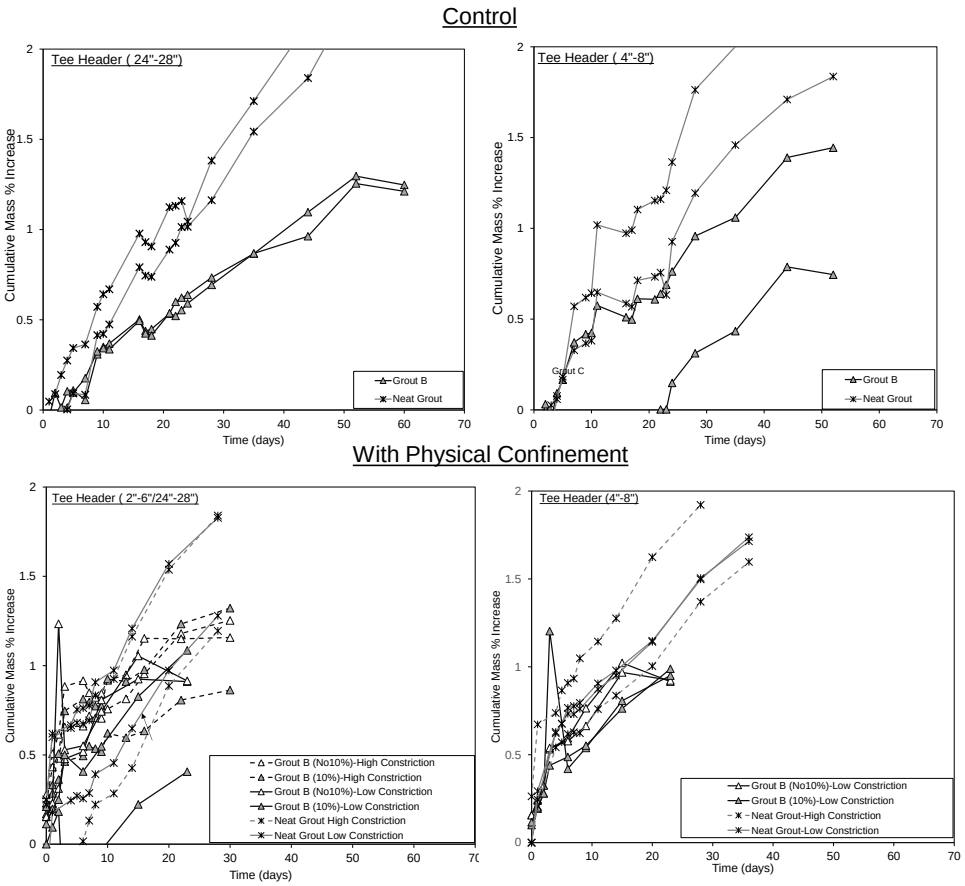

Figure 3.8. Moisture uptake of grout from INT setup cast with grout flow confinement.

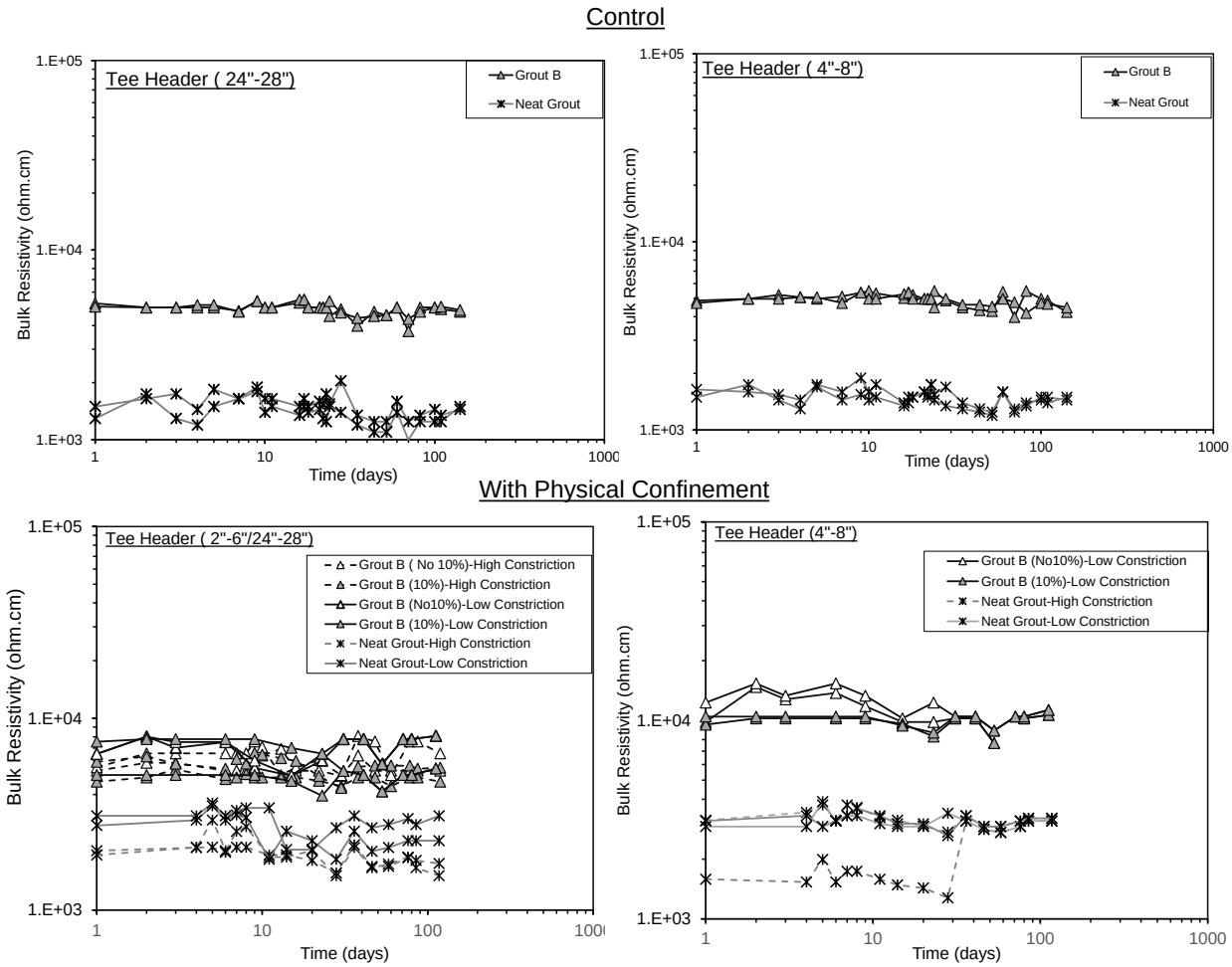

Figure 3.9. Wet resistivity of grout from INT setup cast with grout flow confinement.

3.2.4. Effect of External Ion Contamination

Figures 3.10 and 3.11 show the moisture content and bulk resistivity of the grout specimens cast with chloride and sulfate ion contamination. As expected, the moisture content was higher in the INT header than the INT body. The presence of the chloride and sulfate ions would enrich the ionic concentration of the grout pore water but it was evident that its presence would not be a dominant factor in the grout bulk resistivity. The differentiation in the moisture content of the grout in the tee header and tee body would imply that there was accumulation of moisture in the tee header. The transport of the water would likely allow for differentiation of the chloride and sulfate concentrations along the vertical height of the INT specimen.

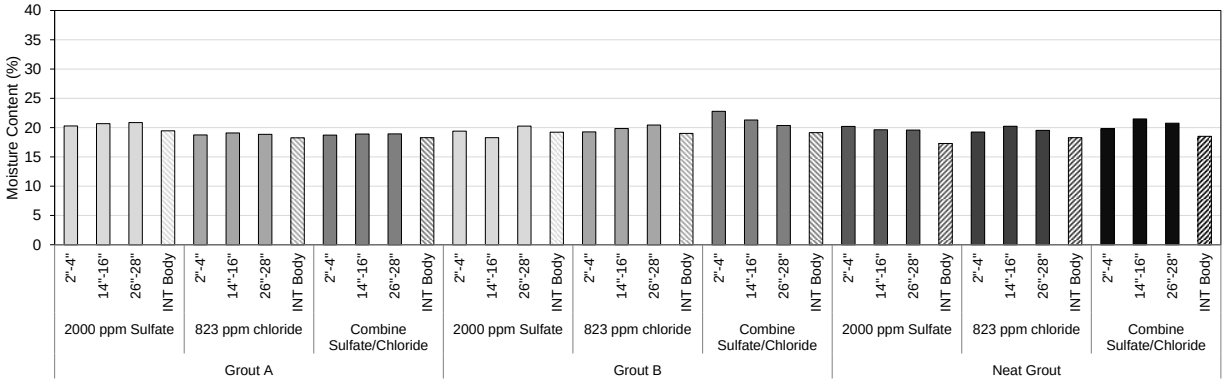

Figure 3.10. Moisture content of grout cast from INT with external ion contamination.

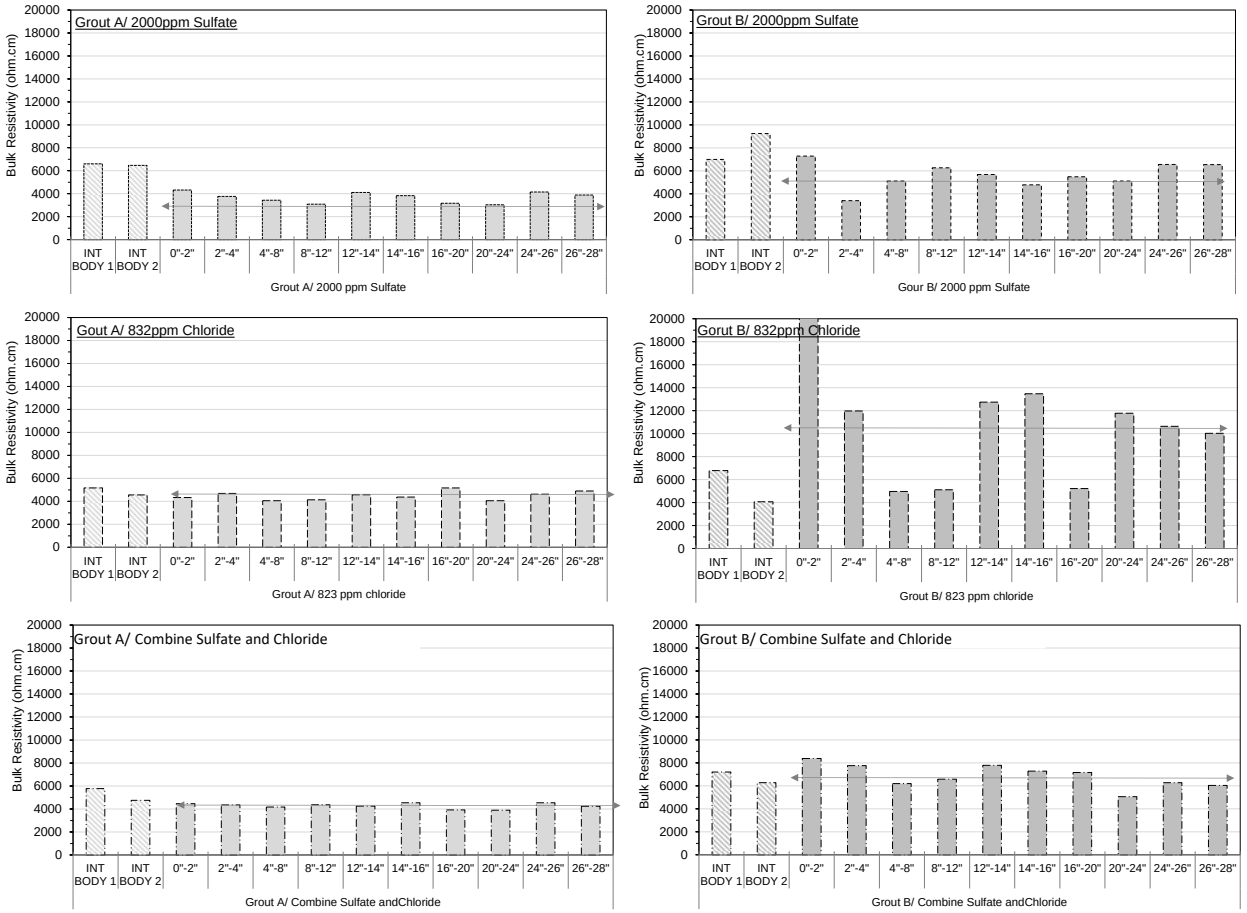

Figure 3.11. Bulk resistivity of grout cast from INT with external ion contamination.

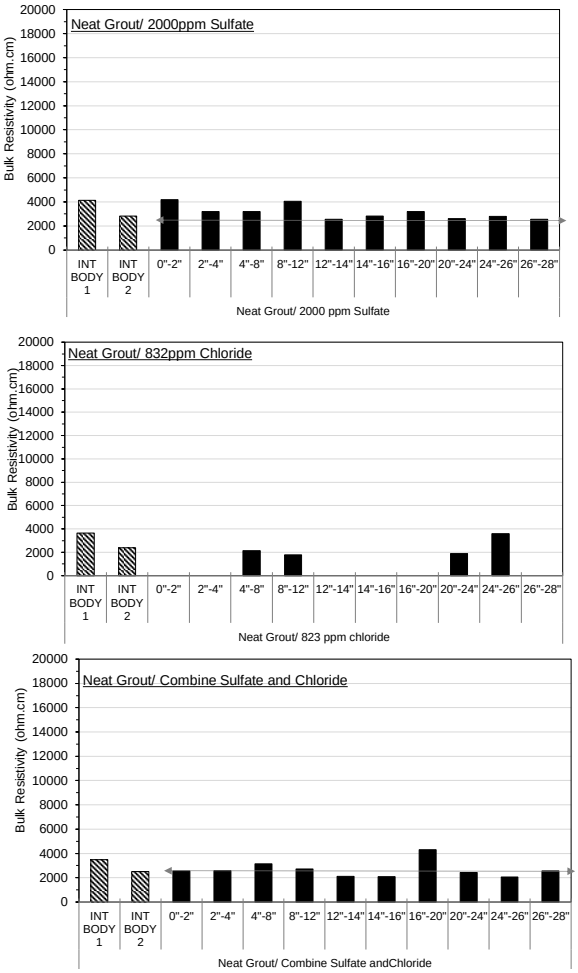

Figure 3.11-continued. Bulk resistivity of grout cast from INT with external ion contamination.

Figures 3.12 and 3.13 show the results water uptake and wet resistivity of specimens conditioned in 100%RH. The transport of ions relating to the chemical deficiencies of segregated grout was posited to be related to movement of water during the grout injection stage. As such, the recorded data below were made for posterity for comparisons of various levels of grout segregation.

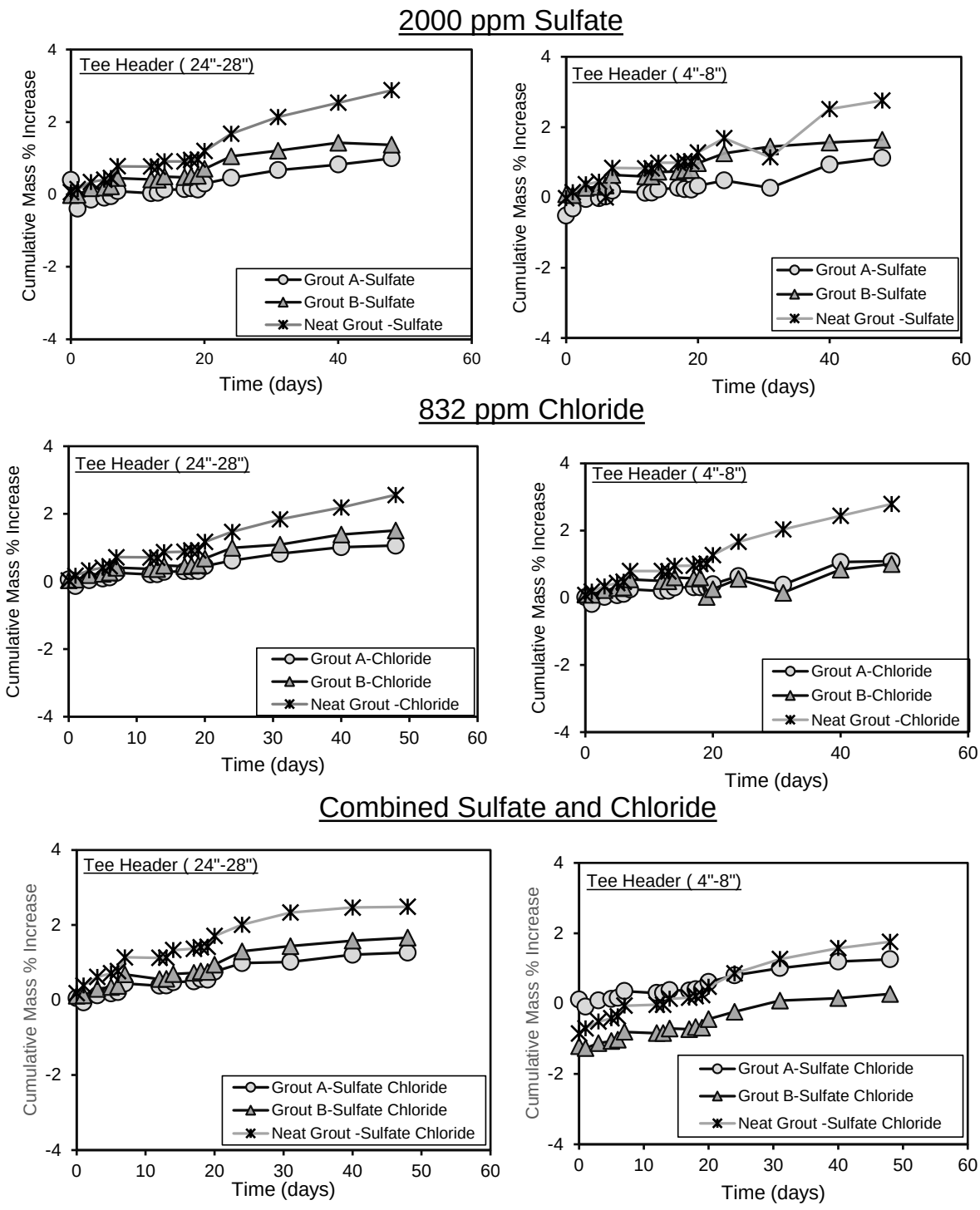

Figure 3.12. Moisture uptake of grout from INT setup cast with external ion contamination.

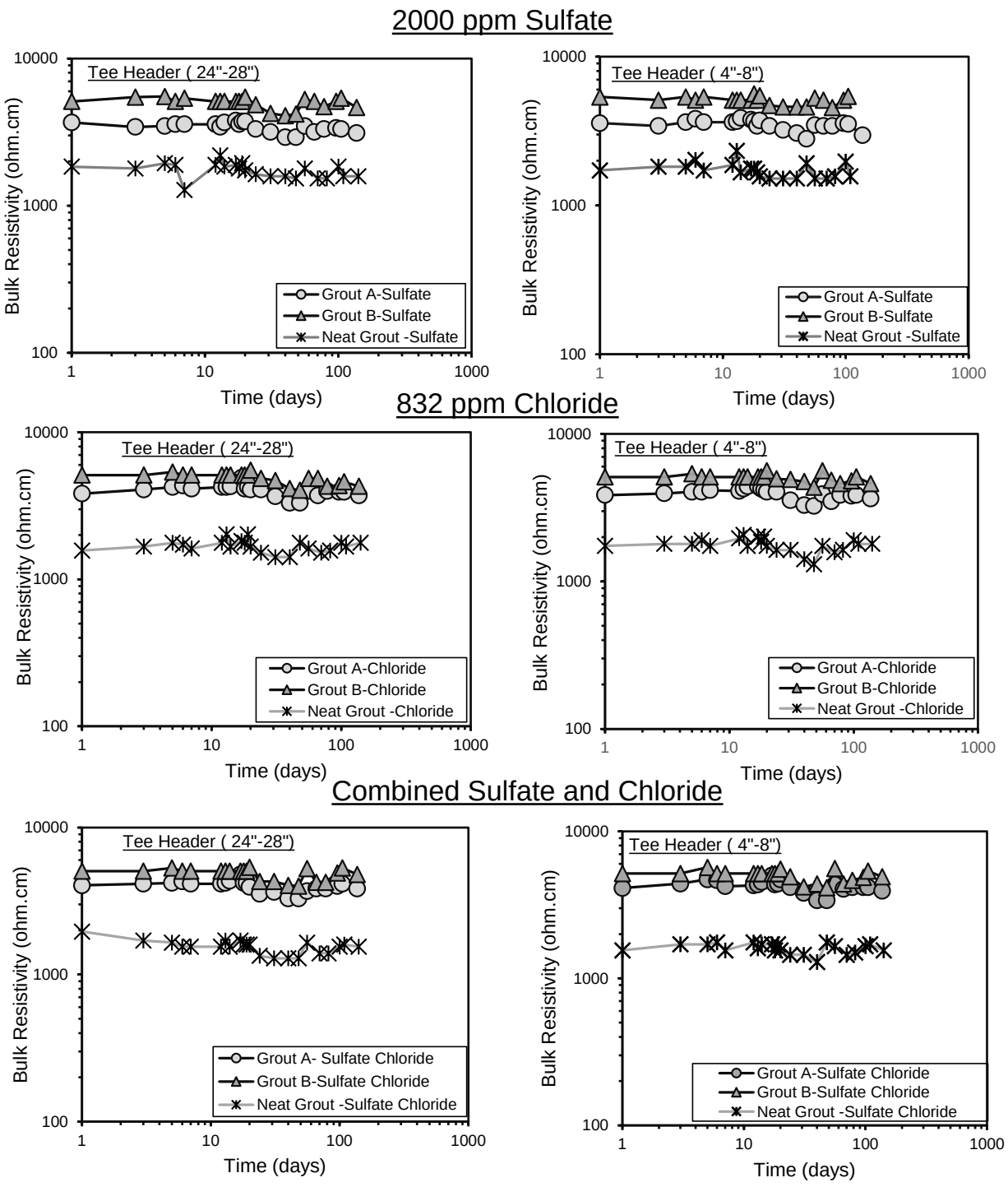

Figure 3.13. Wet resistivity of grout from INT setup cast with external ion contamination.

3.4. Chemical Analysis

The grout from the INT specimens were further tested following FM 5-618 to assess the effects of poor construction on the extent to which sulfate ions can accumulate including overwatering, prehydration, external contamination, and flow constriction. Results are shown in Table 3.1-3.3 and Figures 3.14-3.17.

Table 3.1. Results of Leaching Experiments (Grout A)

Grout	Test Condition	Grout Condition	Name	INT Segment	pH	Sulfate Concentration		Chloride Concentration	
						Leachate (ppm)	Grout (mg/g)	Leachate (ppm)	Grout (mg/g)
A	Control	AR[1], 10%[2]	IM55	1	12.64	5	0.1	5	0.1
				5	11.81	5.6	0.112	5	0.1
				B	12.69	5	0.1	5	0.1
				10	12.67	35	0.7	5	0.1
			IM56	1	12.7	5	0.1	5	0.1
				5	12.66	12	0.24	5	0.1
				A	12.7	5	0.1	5	0.1
				10	12.7	34	0.68	5	0.1
		AR, 10%, S[4]	IM57s	1	12.72	5	0.1	5	0.1
				6	12.7	5.4	0.108	5	0.1
				9	12.66	5	0.1	5	0.1
				A	12.7	5	0.1	5	0.1
		AR, 10%, C[5]	IM58c	1	12.6	5	0.1	5	0.1
				5	12.63	5	0.1	5	0.1
				9	12.6	5	0.1	5	0.1
				A	12.65	5	0.1	5	0.1
		AR, 10%, S+C[6]	IM59s+c	1	12.63	5	0.1	5	0.1
				5	12.62	5	0.1	5	0.1
				9	12.64	5	0.1	5	0.1
				A	12.61	5	0.1	5	0.1

1. As-Received. 2. 10% extra mix water. 3. No. of cut specimens. 4. 2,000 ppm sulfate. 5. 832 ppm chloride. 6. Combined 2,000 ppm sulfate and 832 ppm chloride. 7. Cast with steel bar.

Table 3.2. Results of Leaching Experiments (Grout B)

Grout	Test Condition	Grout Condition	Name	INT Segment	pH	Sulfate Concentration		Chloride Concentration	
						Leachate (ppm)	Grout (mg/g)	Leachate (ppm)	Grout (mg/g)
B	Control	AR	IM63[7]	1	12.53	5	0.1	5	0.1
				9	12.55	5.3	0.106	5	0.1
				B	12.59	5	0.1	5	0.1
			IM64[7]	1	12.57	5	0.1	5	0.1
				9	12.6	5	0.1	5	0.1
				B	12.62	5	0.1	5	0.1
		AR, 10%	IM65	1	12.52	120	2.4	2.5	0.1
				5	12.52	5	0.1	5	0.1
				A	12.54	10	0.2	5	0.1
				10	12.73	66	1.32	5	0.1
			IM66	1	12.56	5	0.1	5	0.1
				5	12.54	6.7	0.134	5	0.1
				A	12.45	5	0.1	5	0.1
				10	12.64	56	1.12	5	0.1
		AR, 10%, S	IM67s	1	12.58	5	0.1	5	0.1
				5	12.61	9.8	0.196	5	0.1
				9	12.64	6.3	0.126	5	0.1
				A	12.65	9.6	0.192	5	0.1
		AR, 10%, C	IM68c	1	12.63	12	0.24	5	0.1
				5	12.66	7.9	0.158	5	0.1
				9	12.67	5	0.1	5	0.1
				A	12.67	6.7	0.134	5	0.1
		AR, 10%, S+C	IM69s+c	1	12.65	5	0.1	5	0.1
				5	12.63	7.1	0.142	5	0.1
				9	12.65	5	0.1	5	0.1
				A	12.58	9	0.18	5	0.1
	High Constrict.	AR	IM610S	3	12.57	5	0.1	5	0.1
				A	12.57	5	0.1	5	0.1
			IM611S	3	12.58	5	0.1	5	0.1
				A	12.57	5.8	0.116	5	0.1
		AR, 10%	IM614S	1	12.51	5	0.1	5	0.1
				5	12.44	8.2	0.164	5	0.1
				A	12.5	5	0.1	5	0.1
			IM615S	2	12.48	6.5	0.13	5	0.1
				A	12.47	14	0.28	5	0.1
	Low Constrict.	AR	IM612L	1	12.61	6.9	0.138	5	0.1
				10	12.55	5	0.1	5	0.1
				A	12.6	5	0.1	5	0.1
			IM613L	1	12.63	5	0.1	5	0.1
				10	12.65	5	0.1	5	0.1
				A	12.64	5.2	0.104	5	0.1
		AR, 10%	IM616L	1	12.5	8.5	0.17	5	0.1
				10	12.47	9.7	0.194	5	0.1
				A	12.49	8.8	0.176	5	0.1
			IM617L	1	12.54	5	0.1	5	0.1
				10	12.53	5	0.1	5	0.1
				A	12.57	5	0.1	5	0.1

Table 3.3. Results of Leaching Experiments (Grout C, D, and neat grout)

Grout	Test Condition	Grout Condition	Name	INT Segment	pH	Sulfate Concentration		Chloride Concentration	
						Leachate (ppm)	Grout (mg/g)	Leachate (ppm)	Grout (mg/g)
C	Control	AR, 10%	IE5	9	12.39	38	0.76	2.5	0.05
				B	12.17	180	3.6	2.5	0.05
			IE6	9	12.4	37	0.74	5	0.1
				B	12.21	120	2.4	5	0.1
		Expired, 10%	IOE5	9	11.92	470	9.4	3	0.06
				A	12.35	8	0.16	5	0.1
			IOE6	9	11.73	3.9	0.078	2.5	0.05
				A	12.15	650	13	3.6	0.072
D	Control	Expired, 10%	IS5	A	12.68	5	0.1	5	0.1
				10	12.69	250	5	5	0.1
			IS6	A	12.66	5	0.1	5	0.1
				10	12.16	410	8.2	3.5	0.07
Neat Grout	Control	0.45 w/c	IC5	1	12.6	19	0.38	5	0.1
				5	12.65	18	0.36	5	0.1
				10	12.74	21	0.42	5	0.1
				A	12.64	19	0.38	5	0.1
			IC6	1	12.65	14	14	5	0.1
				5	12.6	17	17	5	0.1
				10	12.73	36	36	5	0.1
				A	12.52	19	19	5	0.1
		AR, 10%, S	IC7s	1	12.67	8.9	0.178	5	0.1
				5	12.68	5.2	0.104	5	0.1
				9	12.55	12	0.24	5	0.1
				A	12.57	7	0.14	5	0.1
		AR, 10%, C	IC8c	1	12.53	5	0.1	5	0.1
				5	12.68	5	0.1	5	0.1
				9	12.65	5	0.1	5	0.1
				A	12.68	5	0.1	5	0.1
		AR, 10%, S+C	IC9s+c	1	12.64	8.7	0.174	8.2	0.164
				5	12.62	6.5	0.13	5	0.1
				9	12.68	5	0.1	5	0.1
				A	12.67	5	0.1	5	0.1
	High Constriction	0.45 w/c	IC10S	1	12.55	21	0.42	5	0.1
				11	12.61	18	0.36	5	0.1
				A	12.62	19	0.38	5	0.1
			IC11S	1	12.26	20	0.4	5	0.1
				10	12.58	19	0.38	5	0.1
				A	12.6	20	0.4	5	0.1
	Low Constriction	0.45 w/c	IC12L	1	12.58	30	0.6	5	0.1
				10	12.6	27	0.54	5	0.1
				A	12.53	28	0.56	5	0.1
			IC13L	1	12.64	5	0.1	5	0.1
				10	12.67	10	0.2	5	0.1
				A	12.48	7.2	0.144	5	0.1

1. As-Received. 2. 10% extra mix water. 3. No. of cut specimens. 4. 2,000 ppm sulfate. 5. 832 ppm chloride. 6. Combined 2,000 ppm sulfate and 832 ppm chloride. 7. Cast with steel bar.

As discussed earlier, the different grout products had different yields of leached sulfate ions in the INT header. As shown in Figure 3.14, higher sulfate levels were generally observed in the tee header than the tee body likely relating to the displacement of water to the top of the specimen.

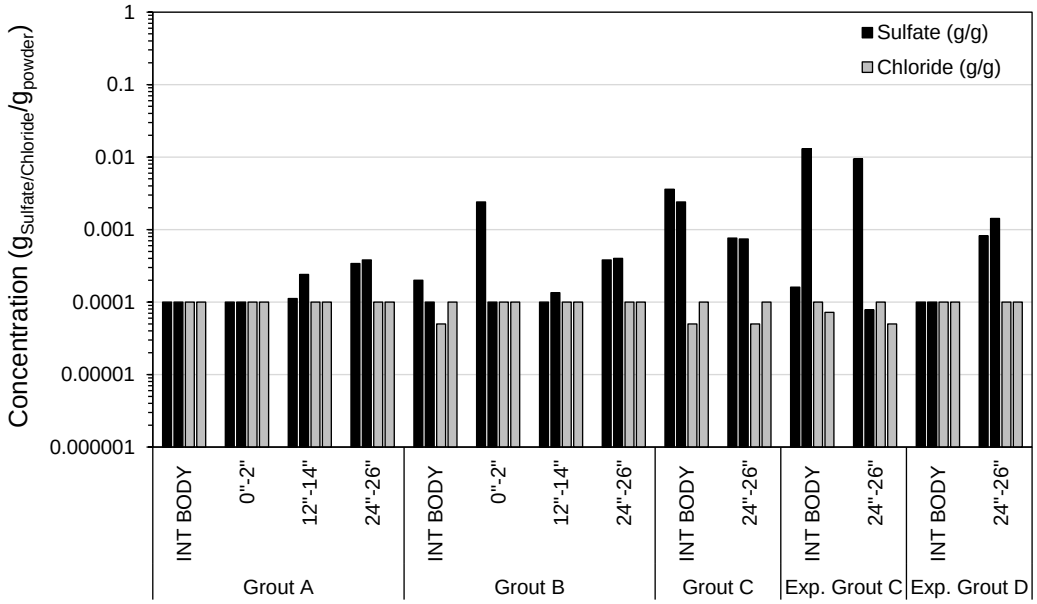

Figure 3.14. Comparison of sulfate ion concentrations in grout from INT tee header and tee body.

Figures 3.15 shows the resolved sulfate concentrations in grouts subjected to sulfate contamination. Consistent with previous research, it was shown that the sulfate ion accumulation in the deficient grout (here in the tee header) can develop without external contamination. In the test conditions with an additional 2,000 ppm sulfate, the resolved sulfate concentrations were lower than the control mix. It was observed that when the additional sodium sulfate was added to the mix water, the grout mix was thicker where less water per solids was present. This would create a lower water-to-cement ratio and overall less water availability to be involved in the material segregation.

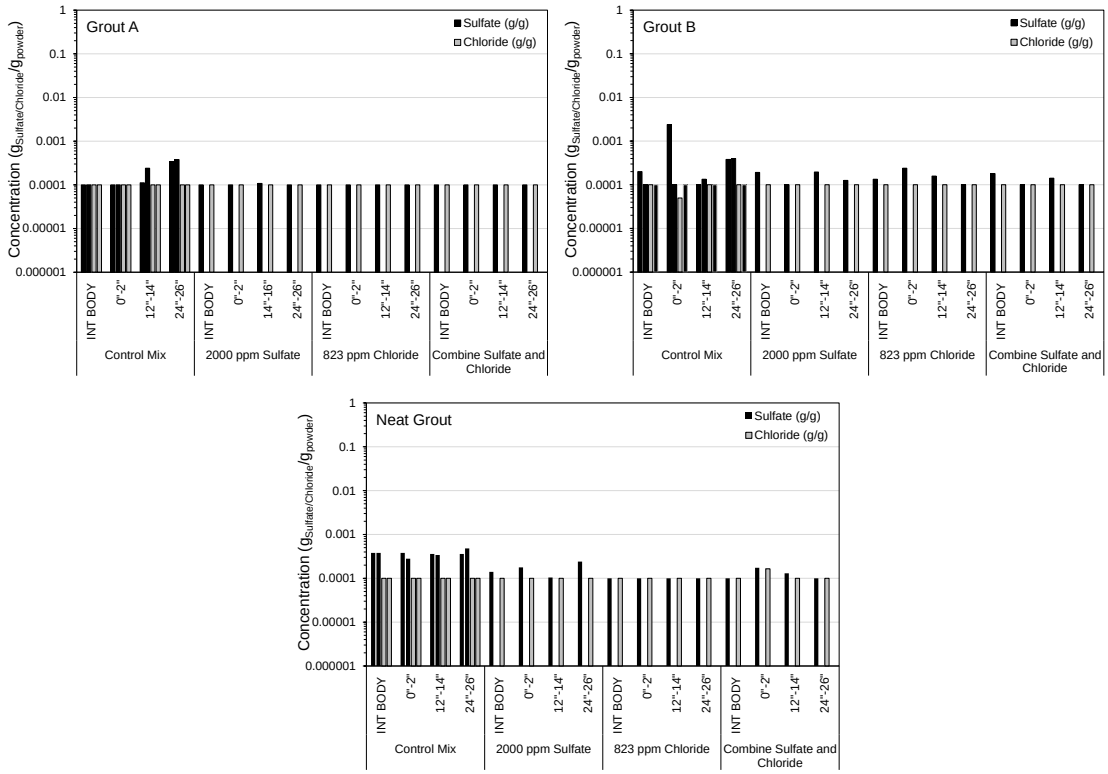

Figure 3.15. Sulfate ion concentration in grout subjected to external contamination

As shown in Figure 3.16, the addition of excess mix water in the INT setup for the grouts allowed for moisture displacement and accumulation of sulfate ions relative to the conditions with no excess mix water. However, the experiments did not show appreciable effects due to the grout flow constriction.

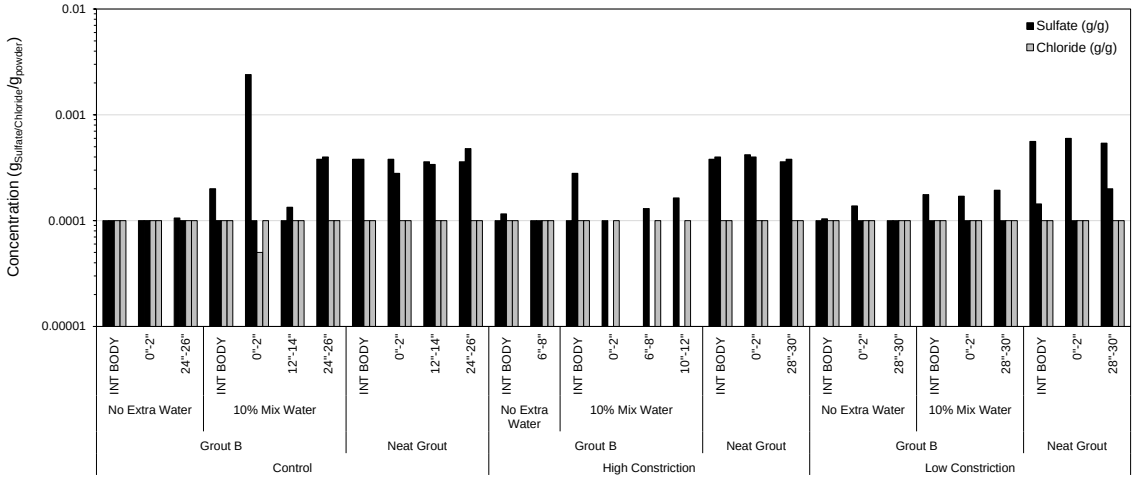

Figure 3.16. Sulfate ion concentration in grout subjected to flow constriction

CHAPTER 4. MODIFIED ACCELERATED CORROSION TEST FOR GROUTS

The preliminary testing using a modified ACT test explored the idea of assessing the robustness of grouts subjected to non-ideal conditioning. These tests incorporated testing of grout subjected to adverse conditioning and mixing to promote grout deficiencies. The results of the testing described next are not representative of performance and durability of strand in the grout if properly handled and are only considered for research purposes to identify test methodologies that can be adopted to address grout robustness.

4.1.ACT for Grouts following PTI M-55

The OCP of each test specimen was obtained prior to the LPR and anodic polarization tests prescribed by the ACT. As shown in Figure 4.1, the steel embedded in the neat grout as well as test specimens cast with grout in the control as-received condition all developed passive potentials in the range of -100 < OCP < -200 mV_{SCE} after 28 and 56 days of curing, regardless of any grout imperfections. Specimens cast with pre-exposed Grout A and Grout B with 10% excess water also developed similar passive potentials. However, specimens cast with pre-exposed Grout C with 10% excess water developed more electronegative potentials at levels that may be interpreted as active corrosion (as negative as -400 mV_{SCE}). This observation was coincident with the physical grout deficiencies described earlier; however, since the specimens were immersed in saturated calcium hydroxide solution prior to testing and were tested in chloride-free saturated calcium hydroxide solution, corrosion activation was not expected.

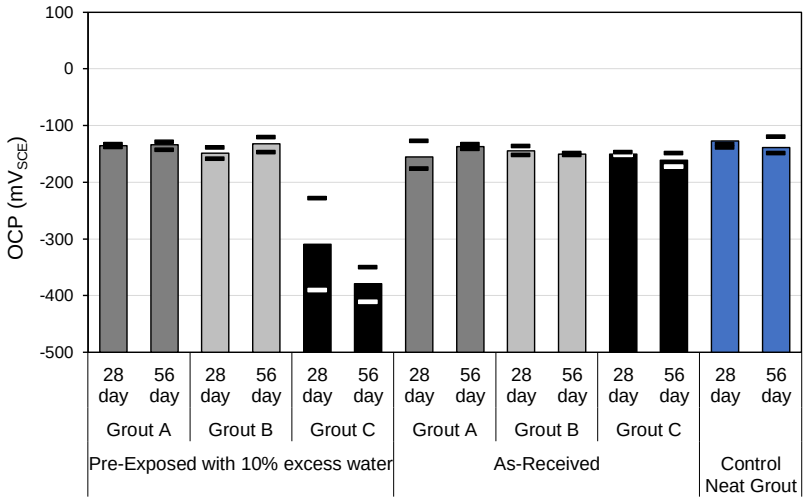

Figure 4.1.Corrosion potentials 28 and 56 days after casting.

The polarization resistance resolved from the LPR test, assuming a nominal steel area of 96.6 cm^2 (surface area of the 7-wire strand within the grout section open to the test electrolyte), is shown in Figure 4.2. Consistent with the OCP measurements, all neat grout specimens and test grout specimens (in both control and adverse pre-exposure/mixing conditions) that developed passive-like potentials all exhibited Rp values that meet or exceed the 700 kΩ-cm^2 criteria established in the ACT. Likewise, the specimens cast with pre-exposed Grout C with excess mixed water had lower Rp values, corresponding to corrosion current densities as high as 0.68 µA/cm^2, further suggesting that low to moderate active corrosion conditions[43] developed in those cases. Of note, specimens cast with Grout C following appropriate procedures (and with generally well hardened and consolidated grout) developed the highest Rp values corresponding corrosion rates as low 0.015 µA/cm^2.

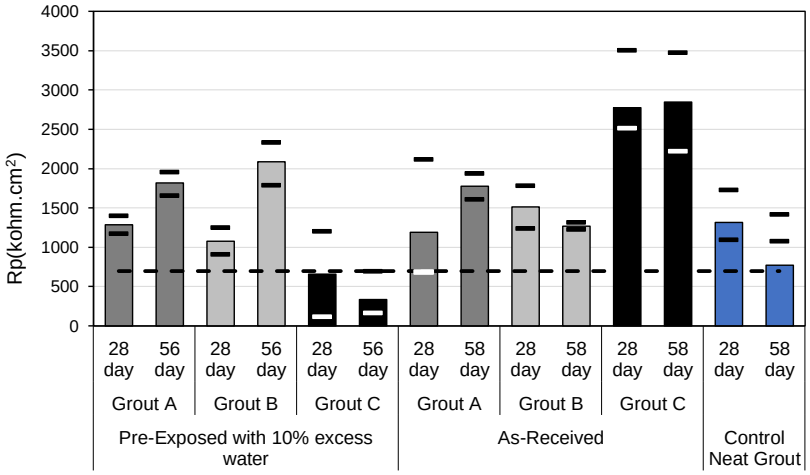

Figure 4.2. Measured polarization resistance 28 and 56 days after casting.
Dashed line represents the limit described in PTI M55 Appendix B[33], 700 kΩ·cm^2.

Further anodic potentiostatic polarization tests for grout after 28-days and 56-days curing at +200mV$_{SCE}$ were made for Grouts A-C and the control neat grout (Figure 4.3). Due to the physical deficiencies described earlier that developed for the aggressive preconditioning and mixing (particularly that for Grout C and the neat grouts), the chloride ions in the test solution for the potentiostatic tests could readily penetrate the grout cover. For the deficient Grout C and the neat grout, it was evident that the embedded strand was depassivated near the onset of testing and large anodic currents developed due to the large anodic polarization. Grouts A and B subjected to adverse mix conditions had a longer time to corrosion as did Grouts A, B, and C when mixed following recommended procedures. The time to corrosion activation (when current exceeded 1μA) for the various test conditions are shown in Tables 4.1-4.4

Table 4.1. Time of corrosion activation when current exceeding 1μA for Neat Grout

Neat Grout (0.45 W/C)		Time of Corrosion (Day)	Current at time of Corrosion (A)
28-day	C2	0.13	0.00147
	C7	0.46	0.00046
	C1	1.4	0.00030
	C8	2.0	0.00242
56-day	C11	0.00052	0.00491
	C12	0.00064	0.00276

Table 4.2. Time of corrosion activation when current exceeding 1µA for Grout A

Grout A			Time of Corrosion (dy)	Current at time of Corrosion (A)
Pre-Exposed Grout with Extra 10% Mix Water	28-day	M51*	1.8	0.0107
		M57*	2.95	0.00015
		M52*	0.00015	0.617[A]
		M56*	12.3	0.00018
	56-day	M58*	0	0.00030
		M53*	5.0	0.00015
		M510*	7.9	0.00469
		M59*	8.5	0.00011
As-Received Grout	28-day	M5A1	5.6	0.00012
		M5A3	13.3	0.00010
		M5A4	26.9	0.00019
		M5A2	45.6	0.00010
	56-day	M5A6	14.5	0.00010
		M5A5	44.3	0.00010

A. Accidental electrode short-circuit.

Table 4.3. Time of corrosion activation when current exceeding 1µA for Grout B

Grout B			Time of Corrosion (dy)	Current at time of Corrosion (A)
Pre-Exposed Grout with Extra 10% Mix Water	28-day	M66*	18.2	0.00068
		M61*	28.3	0.00011
		M62*	34.3	0.00040
		M63*	42.3	0.00082
	56-day	M69*	7.9	0.00083
		M68*	15.9	0.0024
		M67*	21.9	0.00086
		M610*	50.9	0.00099
As-Received Grout	28-day	M6A1	56.6	0.0019
		M6A2	77.6	0.00097
		M6A3	90.7	9.96E-06
		M6A4	93.8	0.00321
	56-day	M6A6	0.27	0.00011
		M6A5	75.82	3.536-05

Table 4.4. Time of corrosion activation when current exceeding 1µA for Grout C

Grout C			Time of Corrosion (dy)	Current at time of Corrosion (A)
Pre-Exposed Grout with Extra 10% Mix Water	28-day	E1'	1.2E-05	0.0208
		E2'	0.00013	0.0351
		E3'	0.00025	0.0412
		E4'	0.00038	0.0437
		E6*	0.00053	0.0255
		E1*	0.00054	0.00074
		E7*	0.00065	0.0303
		E2*	0.00068	0.0126
	56-day	E6'	0.00012	0.647
		E8*	0.00027	0.0302
		E9*	0.00040	0.0225
		E10*	0.00053	0.0353
		E11*	0.00065	0.0339
		E5'	0.0035	0.0123
As-Received Grout	28-day	EA2	0.021	0.00089
		EA1	0.38	0.00010
		EA3	2.89	0.00384
		EA4	2.94	0.00036
	56-day	EA6	1.23	0.00010
		EA5	1.35	0.00010

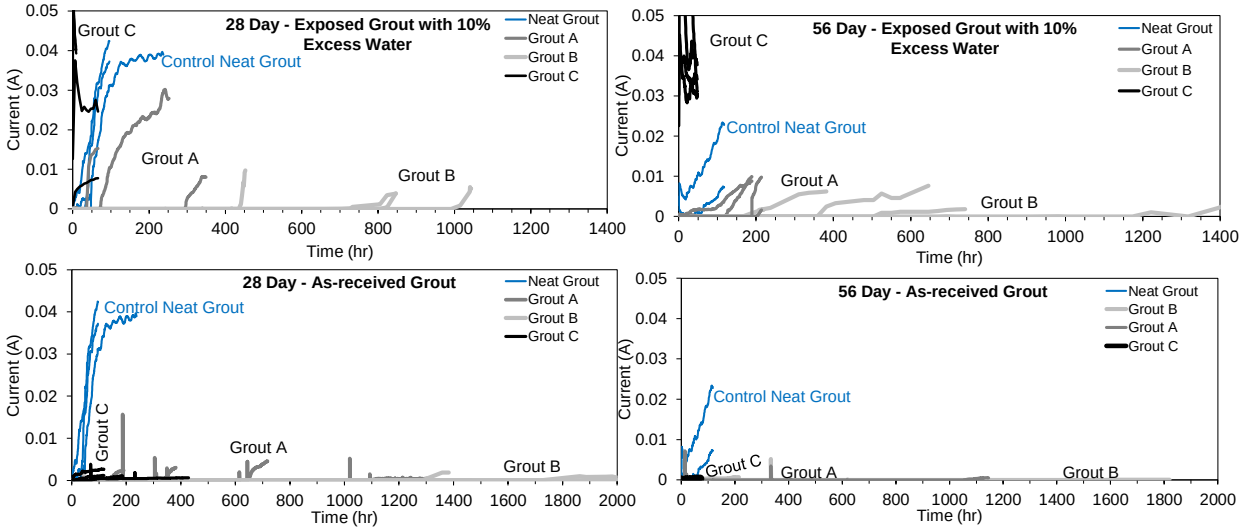

Figure 4.3. Anodic Currents for Steel in Anodic Potentiostatic Polarization Test

4.2. ACT for Grouting following INT test

4.2.1 Corrosion potential and polarization resistance

The OCP of each test specimen was made prior to the LPR and anodic polarization tests prescribed by the ACT. As shown in Figure 4.4, the steel embedded in Grout A and B with or without 10% excess mix water all developed passive potentials in the range of -100 < OCP < -200 mV_{SCE}. Some of the specimens cast with neat grout developed similar passive potentials. However, specimens cast with Grout C, expired Grout C and D developed more electronegative potentials at levels that may be interpreted as active corrosion (as negative as -450 mV_{SCE}) according to ASTM C876. This observation was coincident with the physical grout deficiencies described earlier; however, since the specimens were immersed in saturated calcium hydroxide solution prior to testing and were tested in chloride-free saturate calcium hydroxide solution, corrosion activation was not expected. Testing of the grout pore water for chemical deficiencies (Figure 4.5) showed higher sulfate accumulation in Grout C, expired grout C and D.

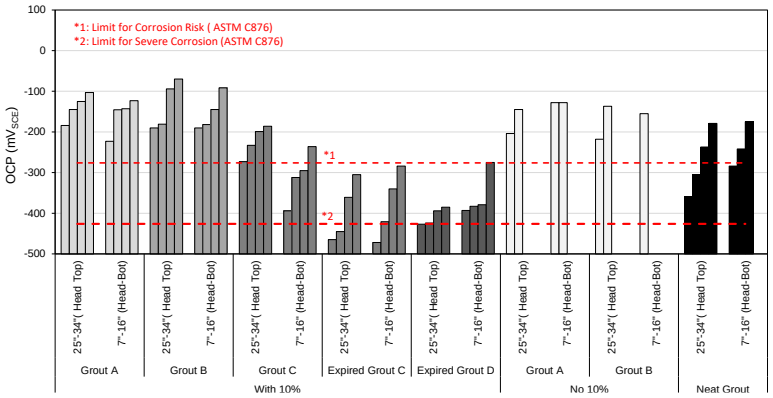

Figure 4.4. Corrosion potentials for INT testing.

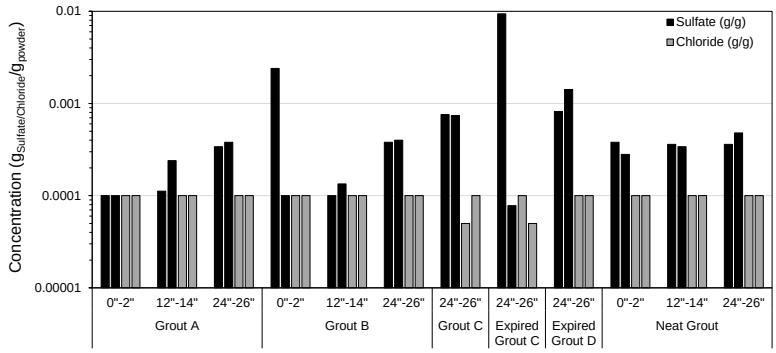

Figure 4.5. Sulfate and chloride concentration for INT specimens.

The polarization resistance resolved from the LPR tests assuming a nominal steel area of 91.20 cm^2 is shown in Figure 4.6. Consistent with the OCP measurements, grout B specimens with or without 10% excess mix water and grout A with no excess mix water developed Rp values that generally meet the 700 $k\Omega$-cm^2 criteria established in the ACT. Grout A with 10% mix water and neat grout which showed lower Rp values. Likewise, the specimens cast with Grout C and expired grout C and D had much lower Rp.

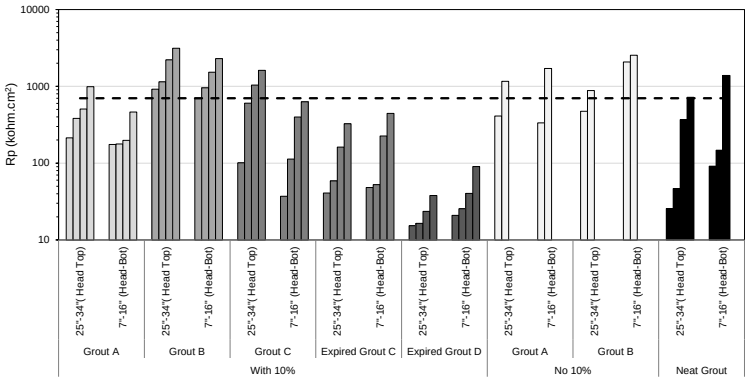

Figure 4.6. Measured polarization resistance.
Dashed line represents limit described in PTI M55 Appendix B, 700 kΩ·cm^2.

4.2.2. Anodic Potentiostatic Polarization

Further anodic potentiostatic polarization tests at +200mV$_{SCE}$ were applied on the specimens (Figure 4.7 and 4.8). Due to the physical deficiencies described earlier (Task 2) that developed from the non-ideal test mixing protocol (particularly that for Grout C, expired Grout C and D), the chloride ions in the test solution for the potentiostatic tests could readily penetrate the grout cover. Grouts A and B, mixed with or without the 10% excess mix water conditions had a longer time to corrosion. The time to corrosion activation (when current exceeded 1µA) for the various test conditions are shown in Table 4.5.

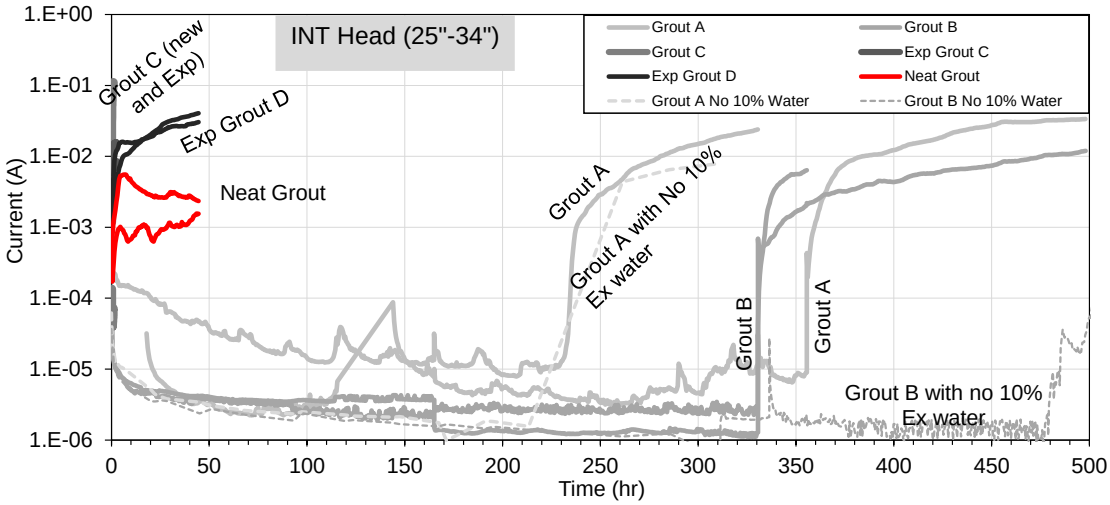

Figure 4.7. Anodic Currents for Steel in Anodic Potentiostatic Polarization Test for INT Header Top Section

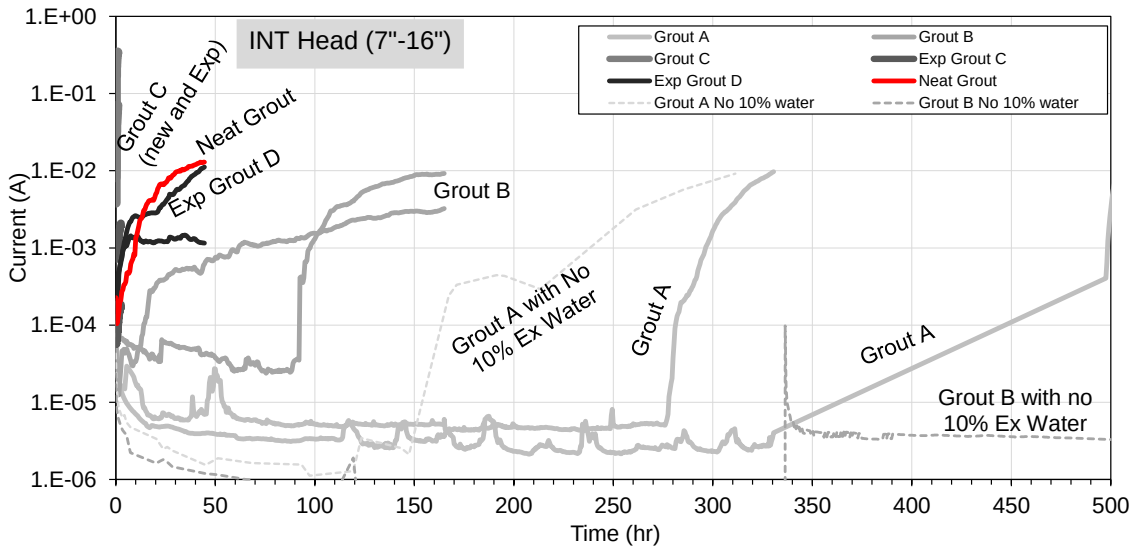

Figure 4.8. Anodic Currents for Steel in Anodic Potentiostatic Polarization Test for INT Header Bottom Section

The results showed that the methodologies prescribed in existing test guidelines can be applicable to assess grout robustness and corrosion propensity in deficient grout. Grout C, expired Grout C and D cast with 10% extra water with the most adverse grout segregation showed results that would be considered not meeting acceptance criteria. Further test developments should consider test configurations that would provide reasonable grout conditioning and handling yet still appropriately assess robustness. The results showed that generally Grout A and B showed a longer time to corrosion. Figures 4.9 and 4.10 show photographs of test specimens after corrosion development by anodic polarization.

Table 4.5. Time of corrosion activation when current exceeding 1μA

Samples Condition				Current at time of Corrosion (A)	Time of Corrosion (hour)
Grout A	Extra 10% Mix Water	INT Head (25″-34″)	IM51*T	0.00020	235
			IM53*T	0.00020	356
		INT Head (7″-16″)	IM51*B	0.00013	282
			IM53*B	0.00064	498
	No Extra water	INT Head (25″-34″)	IM53T	0.0044	261
		INT Head (7″-16″)	IM53B	0.00024	167
Grout B	Extra 10% Mix Water	INT Head (25″-34″)	IM61*T	0.00013	331
			IM63*T	0.00069	330
		INT Head (7″-16″)	IM61*B	0.00042	93
			IM63*B	0.00010	14
	No Extra water	INT Head (25″-34″)	IM61T	0.000062	900
		INT Head (7″-16″)	IM61B	0.000010	1215
Grout C	Extra 10% Mix Water	INT Head (25″-34″)	IE1T	0.0012	0.00028
			IE3T	0.00013	0.0066
		INT Head (7″-16″)	IE1B	0.0082	0.0033
			IE3B	0.0038	0.0097
Expired Grout C	Extra 10% Mix Water	INT Head (25″-34″)	IOE1T	0.0061	0.00028
			IOE3T	0.0066	0.0064
		INT Head (7″-16″)	IOE1B	0.0001	1.069
			IOE3B	0.00078	0.0094
Expired Grout D	Extra 10% Mix Water	INT Head (25″-34″)	IS1T	0.0019	0.00055
			IS3T	0.0010	0.0067
		INT Head (7″-16″)	IS1B	0.00022	0.0036
			IS3B	0.00012	0.0097
Neat Grout		INT Head (25″-34″)	IC3T	0.00036	0.0128
			IC4T	0.00028	0.0158
		INT Head (7″-16″)	IC3B	-	-
			IC4B	0.00023	1215

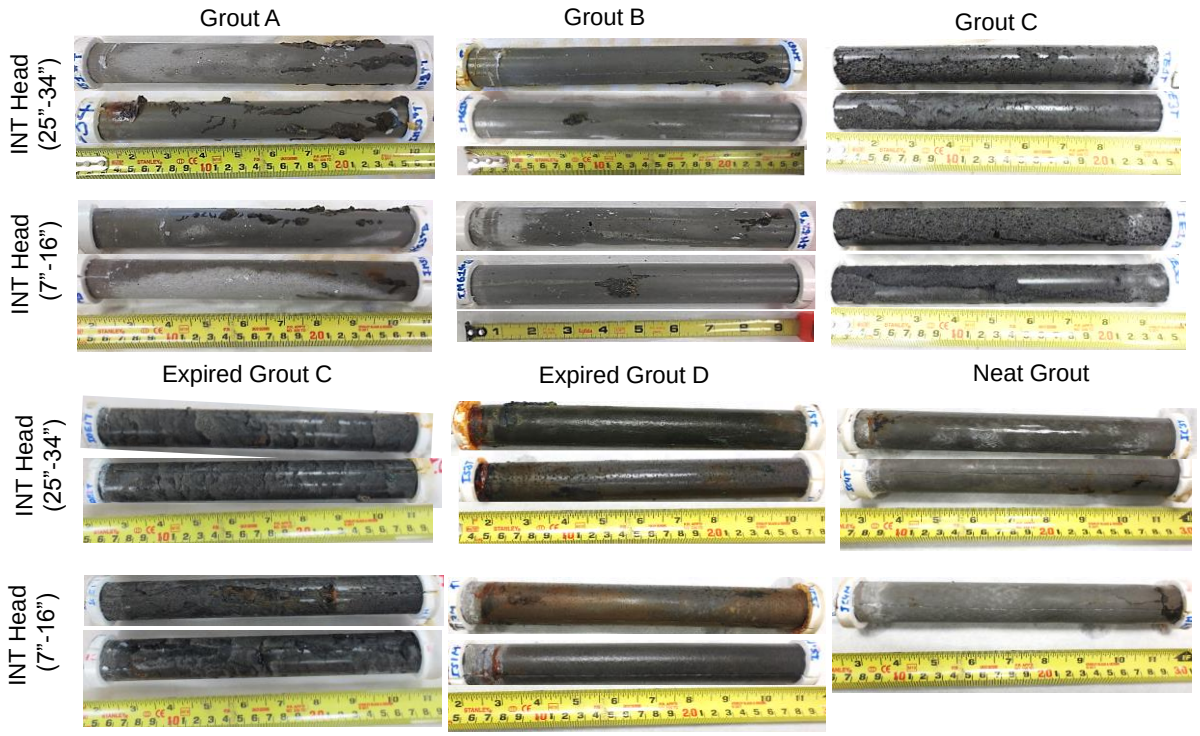

Figure 4.9. PTI test specimens after corrosion development

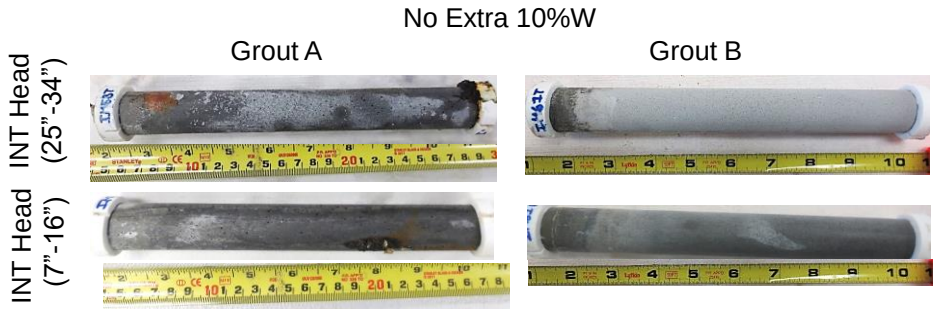

Figure 4.10. PTI test specimens with no extra mix water after corrosion development

4.3. ACT for Grouts with Application of Corrosion Mitigation (Impregnation)

The solution resistance of the grouted specimens with and without the injection of the WD-40 was resolved as the high frequency limit of impedance measured by EIS. As shown in Figure 4.11, the presence of the film increased the solution resistance indicating that there was good coverage of the medium within the grouted specimen. Grout C, which developed physical grout deficiencies, showed the largest increase in solution resistance likely relating to the saturation of the pore spaces with the hydrocarbon film.

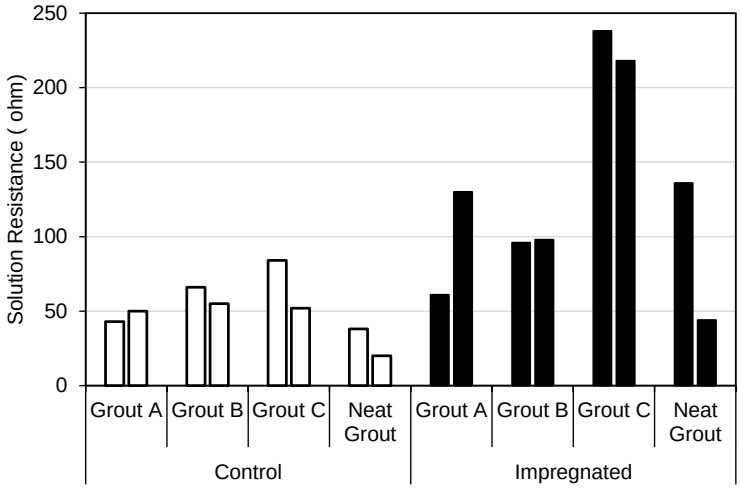

Figure 4.11 Resolved solution resistance

The untreated specimens developed electronegative potentials and high corrosion currents reflective of their corrosion conditions due to testing in salt solution in earlier experiments (Figure 4.12). Grout C specimens, that had physical grout deficiencies, had highly electronegative potentials and high corrosion currents. In contrast, the test specimens injected with the hydrocarbon medium showed increases in the open-circuit potential and significant drop in corrosion current indicating beneficial effect of the injection.

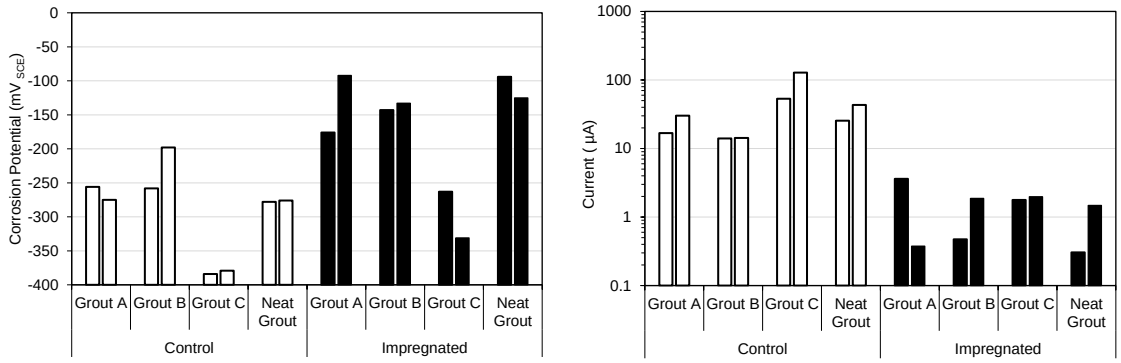

Figure 4.12. Open-circuit potential and corrosion current

Figure 4.13 shows the results of the anodic potentiostatic polarization tests for the test specimens with and without the hydrocarbon film injection, conforming to the PTI Accelerated Corrosion Test. For all tested grout materials and the neat grout, the application of the hydrocarbon film resulted in decreases the anodic currents. Table 4.6 lists the extent of the anodic current reduction for each of the test conditions.

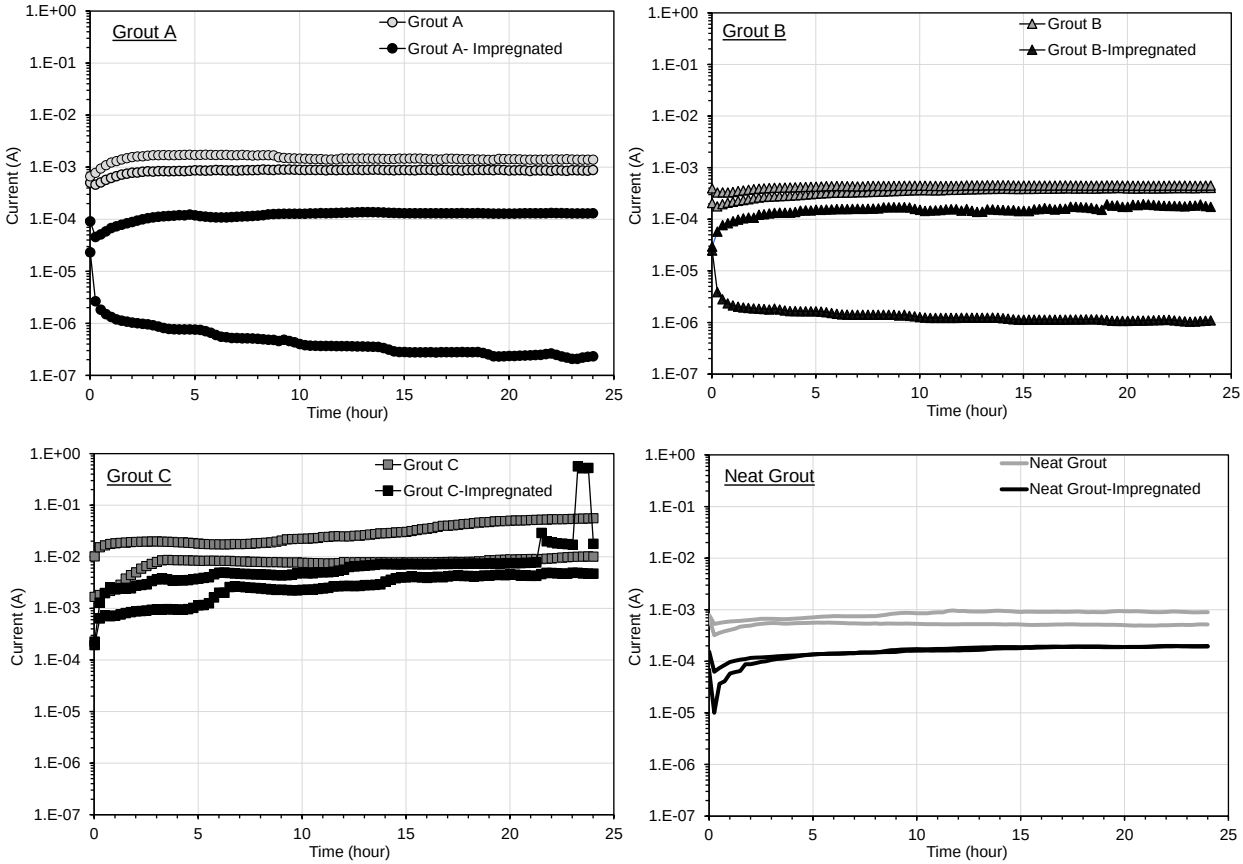

Figure 4.13. Results of anodic potentiostatic polarization tests

Table 4.6. Reduction in current by impregnation

Grout Product	Reduction in Current by Impregnation
Grout A	6.8
(Extra 10% Mix Water)	5987
Grout B	368
(Extra 10% Mix Water)	2.6
Grout C	2.1
(Extra 10% Mix Water)	3.1
Neat Grout	2.6
(0.45W/C)	4.7

Photographs of the test specimens after the anodic potentionstatic polarization tests are shown in Figure 4.14. Corrosion products could be seen emanating from grout C specimens (that had the physical grout deficiencies) with and without the injection of the hydrocarbon film but was visually smaller in the former.

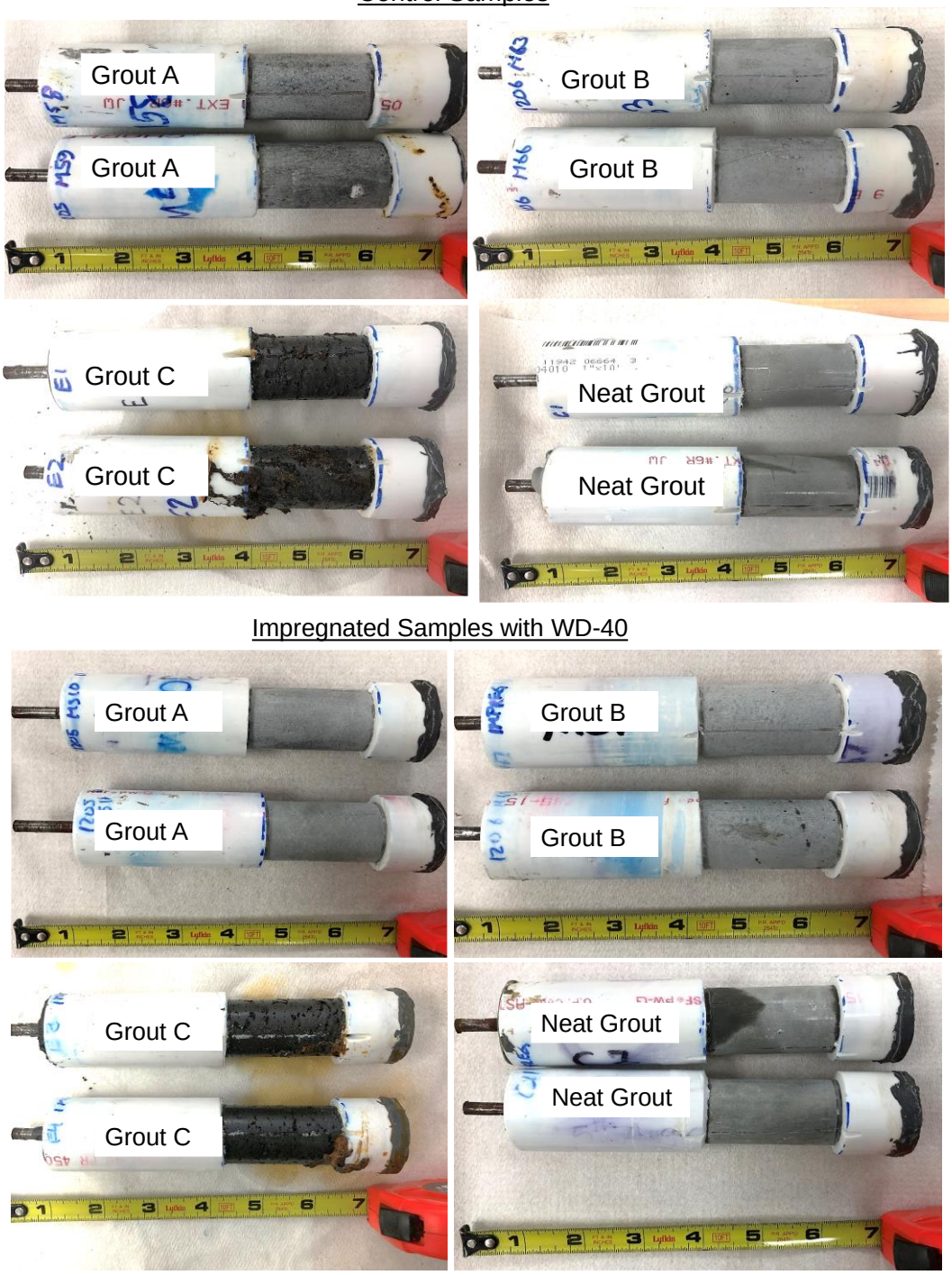

Figure 4.14. Photographs of test specimens after anodic potentionstatic polarization tests.

The results of the testing showed that the accelerated corrosion testing methods to incorporate the consideration of grout material robustness can be applicable to assess passive corrosion mitigation technologies such as impregnation of protective films. The development of the test specimens with grout subjected to adverse mix conditions including excess mix water, grout pre-hydration, and water displacement (such as by the INT setup) produce test conditions where application of the protective films

and inhibitors can be assessed. For illustrative purposes, the testing revealed that in presence of severe grout physical deficiencies, the hydrocarbon film can reduce the corrosion rates, but the continued presence of aggressive chemical species such and chloride ions can still promote corrosion. Development of these corrosion mitigation technologies can consider the effect of the grout deficiencies and the role of the environmental exposure after injection to identify long-term performance.

In summary, it was observed that:

- Accelerated corrosion testing can be used to identify the corrosion performance of passive corrosion mitigation technologies (such as inhibitors and films).
- Application of protective hydrocarbon films into post-tensioned tendons, such as that already commercially developed can reduce, can have beneficial effects to mitigate corrosion.
- The presence of severe grout deficiencies with continued exposure to adverse corrosion environments can reduce the efficacy of the protective film.

Test protocols to assess grout robustness to the effects of adverse construction practices and conditions (such as overwatering, grout pre-hydraton, and water displacement) can be implemented to the accelerated corrosion testing to identify the performance of the corrosion mitigation technology (ie impregnation).

CHAPTER 5. MACROCELL TESTING FOR GROUTS

5.1 Macrocell Testing for following in ASTM A955 Annex 2.28

Figure 5.1 shows the macrocell current in the rapid macrocell testing. In the figure, negative currents represent net oxidation reaction in electrode 1 designated as anode. Test results showed early high macrocell currents that later stabilized to terminal values with time. The steel couple incorporating Grout A showed near terminal values less than 1µA. Consistent with the results from the modified ACT, the steel couple incorporating Grout C that showed separation of a physically deficient material showed larger macrocells in the range of 2-10µA (Figure 5.1A). As shown by comparison of Figures 5.1A and 5.1B, the development of corrosion macrocell currents of steel embedded in the deficient grout can be captured more distinctly using a control neat grout for the cathode cell component than when using the control mix of each grout product. Figure 5.1C-E show the condition when electrodes 1 and 2 were the same material. This test set was used as a control set to verify the differentiation caused by the non-ideal mixing condition.

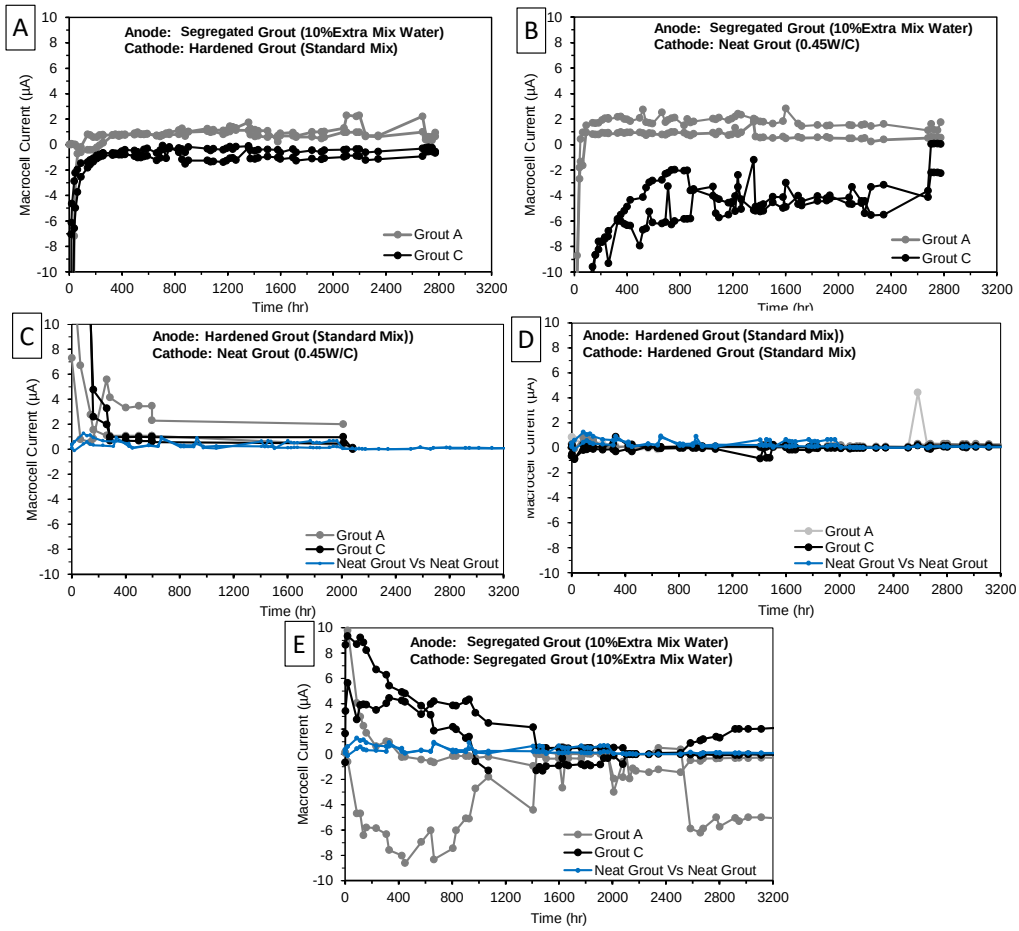

Figure 5.1: Macrocell currents in modified rapid-macrocell test.
Negative values represent electrode 1 is net anodic and electrode 2 is net cathodic.

5.2 Modified Macrocell Testing following INT

5.2.1 First Cycle (No salt addition)

Figures 5.2 and 5.3 shows the macrocell current measured in the rapid macrocell tests. In the figures, negative currents represent net oxidation reaction in the Anode cell. Test results showed early high macrocell currents that stabilized to terminal values with time. For the first 200 hours of testing, all Grout A, B and expired Grout C showed anodic behavior for both INT header sections. Expired Grout D had the largest measured macrocell current (~ -2µA) compared to the other specimens (which ranged from 0 µA to -1µA). After 800 hours of the testing, it was observed that most of the specimens in the Anode cell changed from net anodic to net cathodic behavior as result of possible passivation. In the case for Grout C and expired Grout C (both mixed with 10% excess mix water), cathodic macrocell current was observed throughout the testing, in spite of the different levels of physical grout deficiencies (distinct separation of friable material) that were visually evident for Grout C.

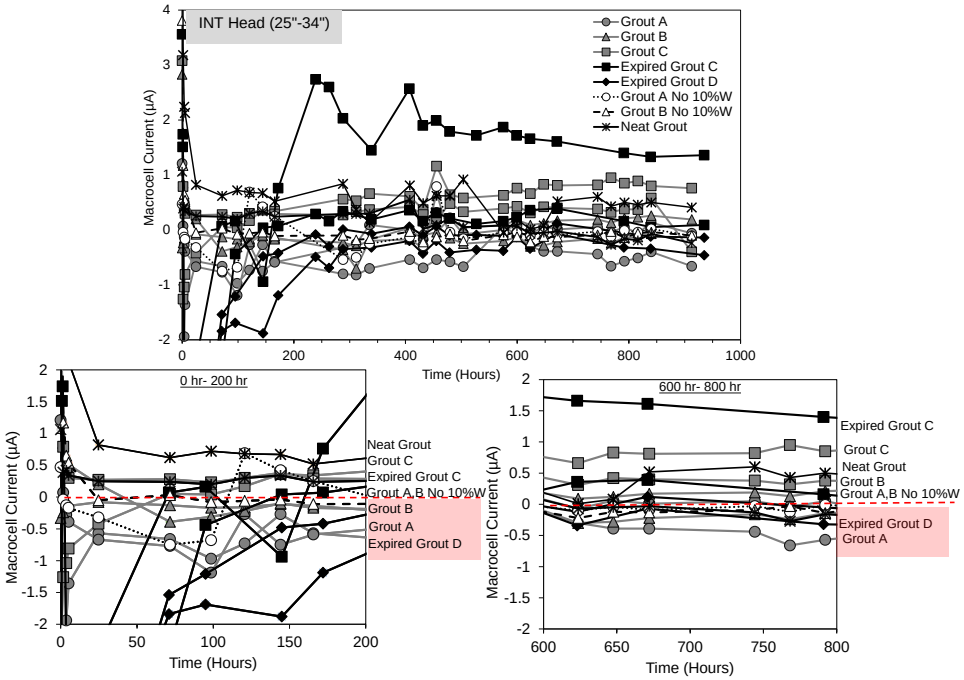

Figure 5.2. Macrocell currents in modified rapid-macrocell test INT Head (25″-34″).

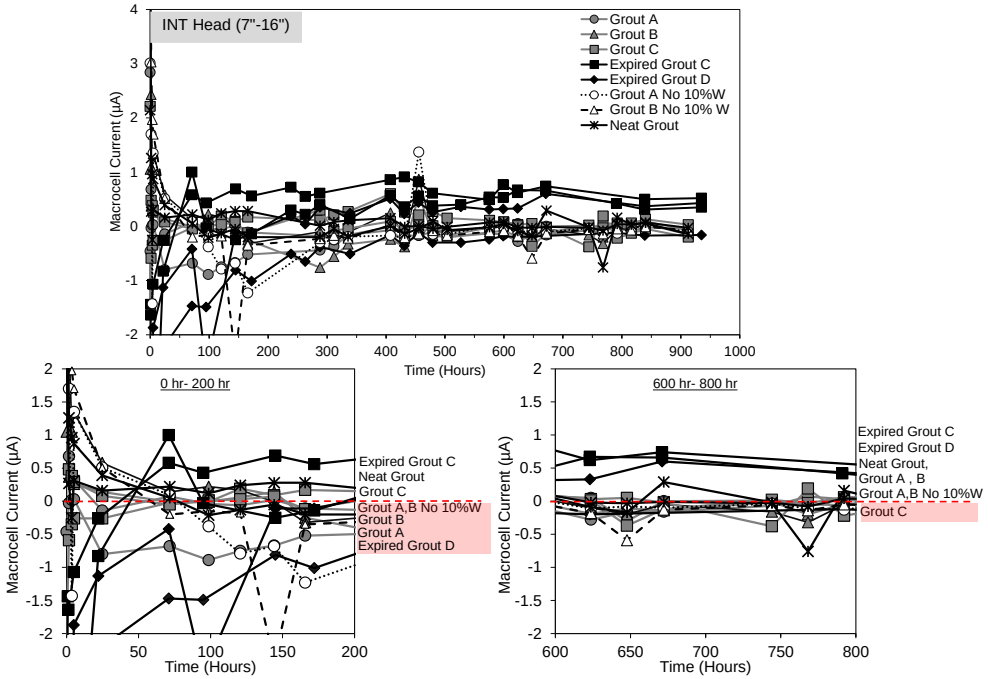

Figure 5.3. Macrocell currents in modified rapid-macrocell test for INT Head (7″-16″).

After 40 days of macrocell measurement, each test cell was disconnected by the electrical switch. The depolarization potential were measured right after disconnection and after 15 min, 1 hr, 2 hr, 24 hr and 48 hr. As shown in Figure 5.4, most of the test specimens showed active potentials. Grout C showed more electropositive potentials. It was observed that the Grout C specimens were cathodically polarized as much as 50 mV during the testing. Overall, there was no significant polarization due to the galvanic coupling of the test cells.

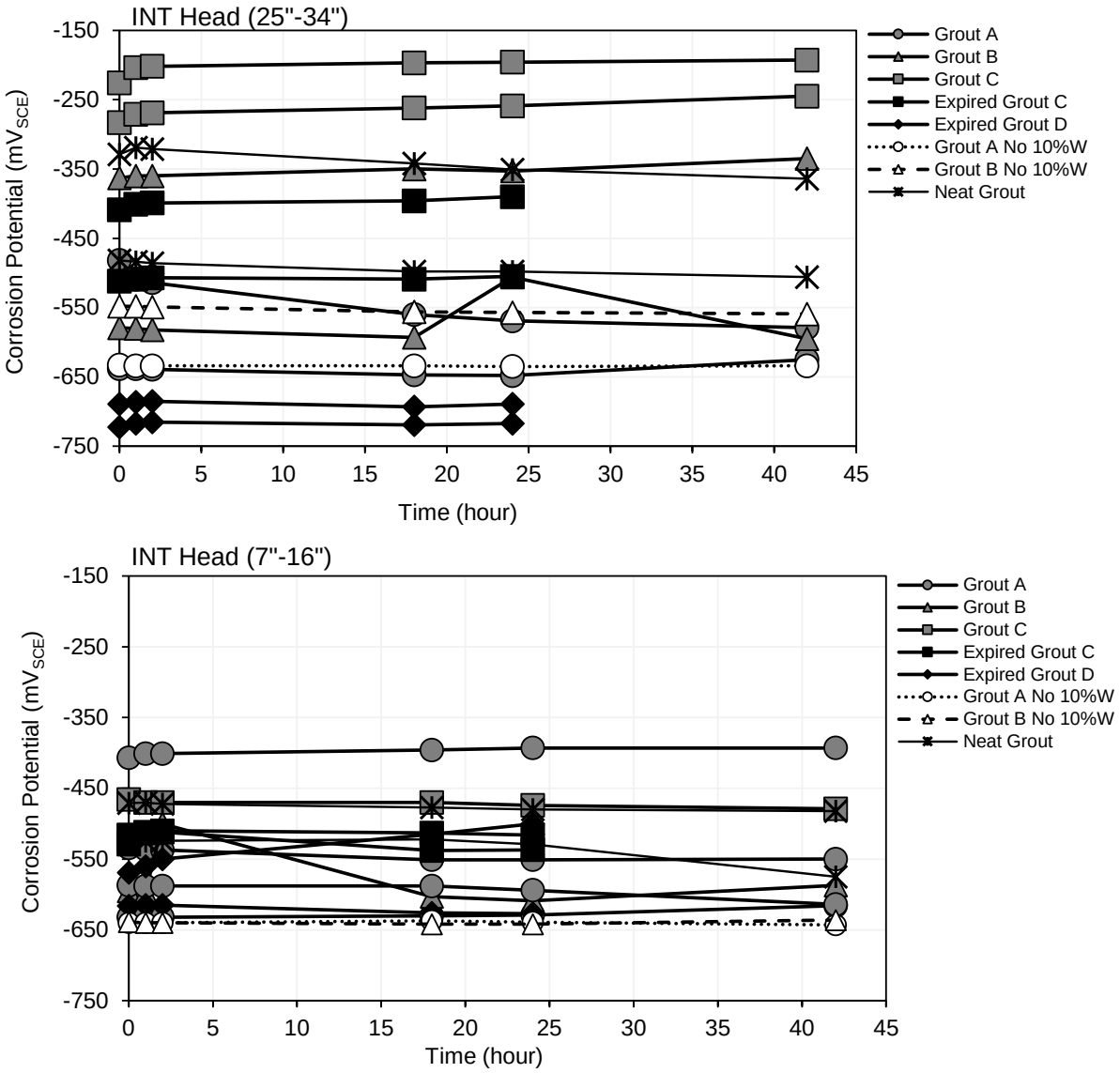

Figure 5.4. Potentials after disconnection (depolarization data)

Figure 5.5 shows a comparison of the corrosion potential and polarization resistance from start and end of the ACT experiment. All specimens showed a shift from noble to active potentials by the end of the testing. The polarization resistance correspondingly showed a decrease in polarization for all specimens except for expired Grout C and D. The spontaneous changes in corrosion activity of the individual cells during the course of the experiment introduce complications in the macrocell testing.

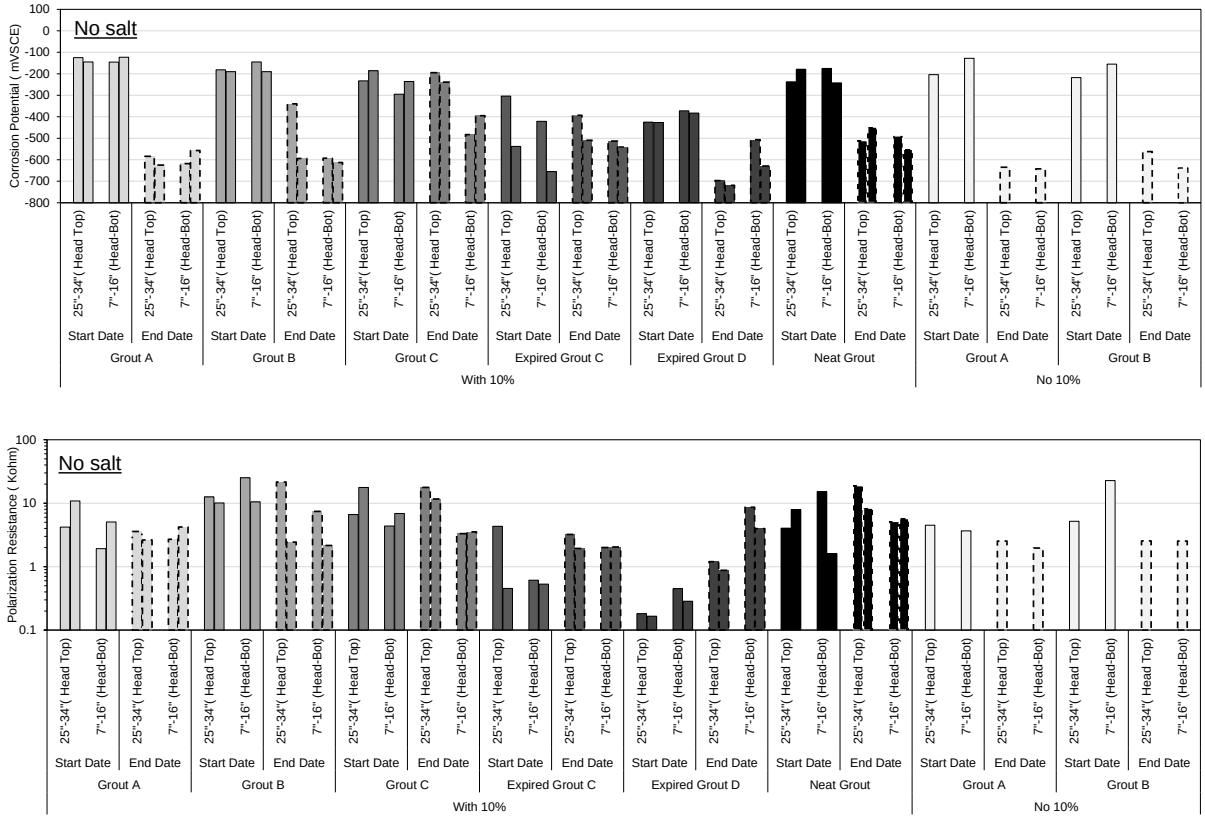

Figure 5.5. Comparison of LPR and OCP data from start to end of experiment

5.2.2 Second Cycle (with salt addition)

The macrocell testing did not reveal strong differentiation in corrosion activity that can be related to the grout deficiencies developed by the INT setup. However, as the INT test setup did provide a means to promote grout deficiencies, the macrocell test could be used to assess grout robustness in accelerated corrosion test conditions in the presence of salt. After the first cycle of measurement, all the solution were renewed and 5% NaCl solution was also added to the Anode test cell. Figure 5.6 and 5.7 show the macrocell current measurements for the second cycle for up to 40 days. Up to 200 hrs of testing, Grout B, Grout C and expired Grout D all showed anodic behavior, however by the end of the testing, most of the test specimens transitioned to net cathodic behavior.

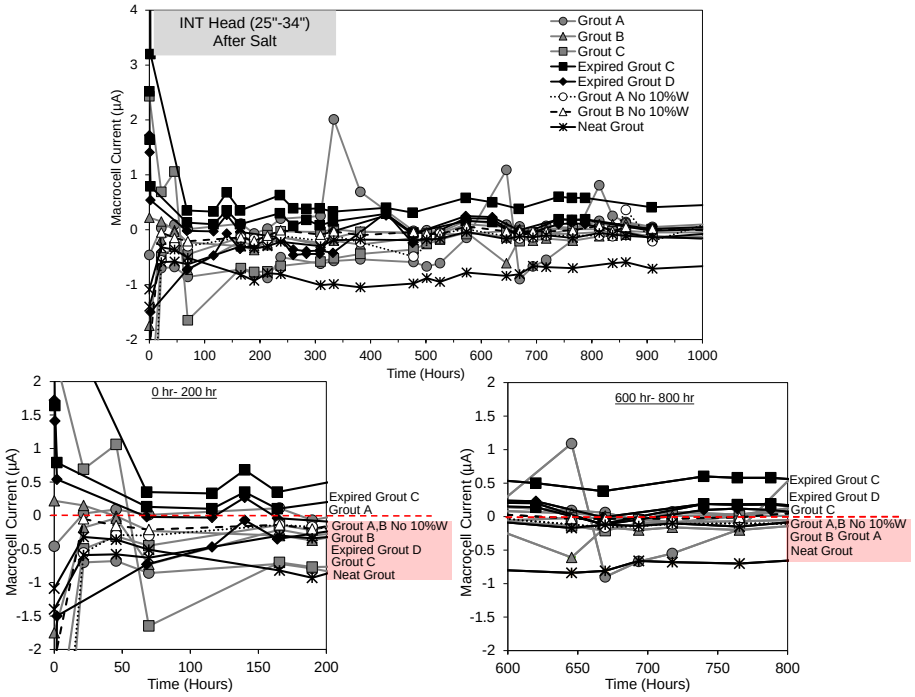

Figure 5.6. Macrocell currents in modified rapid-macrocell test INT Head (25″-34″) after adding salt.

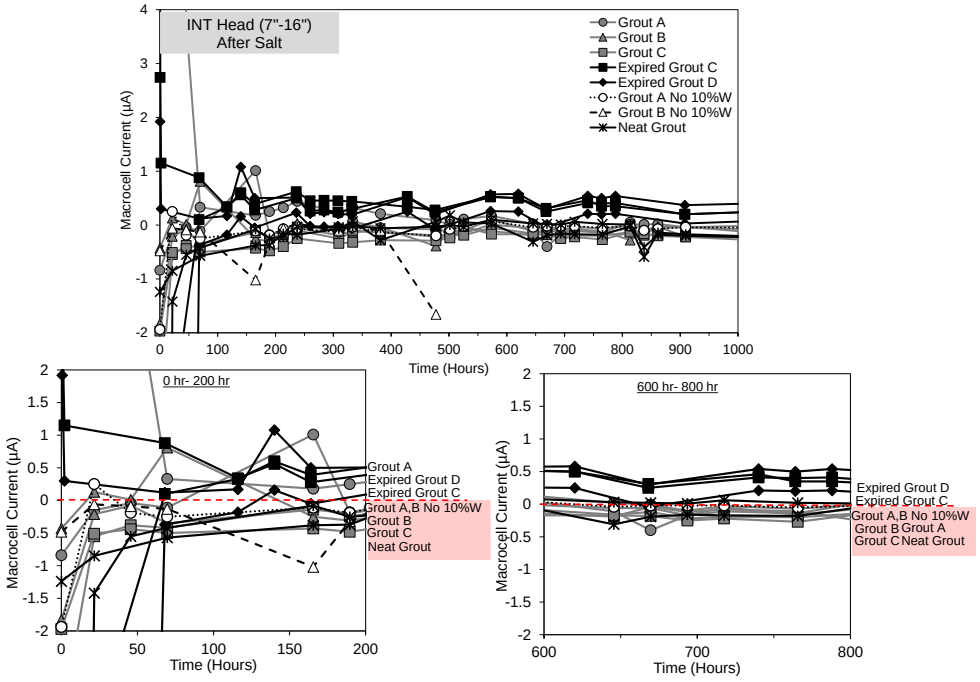

Figure 5.7. Macrocell currents in modified rapid-macrocell test INT Head (7″-16″) after adding salt.

The depolarization data were monitored for (0 hr, 15 min, 1 hr, 2 hr and 24 hr). As with the first test cycle, the galvanic coupling of the anode and cathode cell did not provide significant polarization (Figure 5.8) and any of the effect of the grout deficiencies and the immersion in salt solution were not well captured.

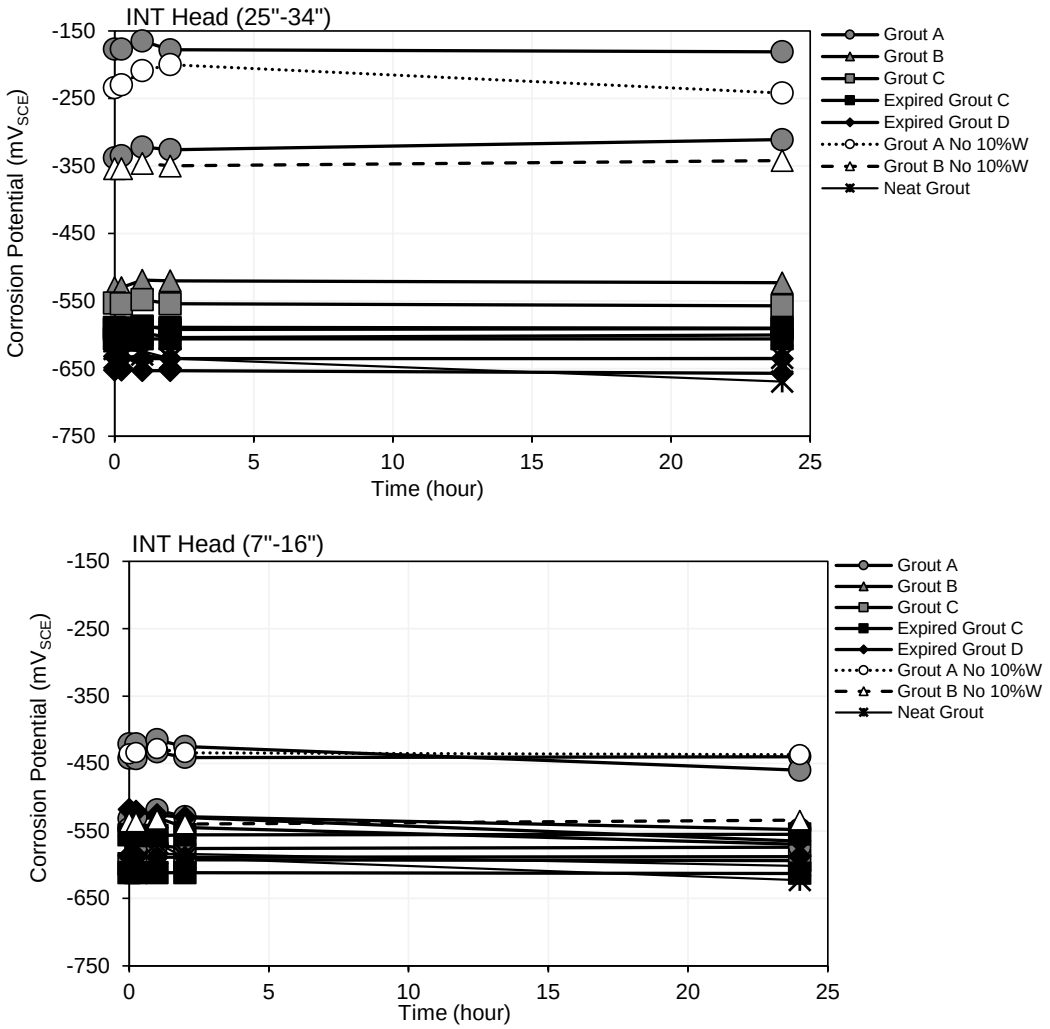

Figure 5.8. Potentials after disconnection (depolarization data) after adding salt.

Figure 5.9 shows the corrosion potential and polarization resistance of the uncoupled test cells at the beginning and end of the testing. After the testing in the salt solution, the grouts that had the most severe physical deficiencies (expired Grout C and D) developed active corrosion potentials by the end of the test and correspondingly all of those specimens developed low polarization resistance.

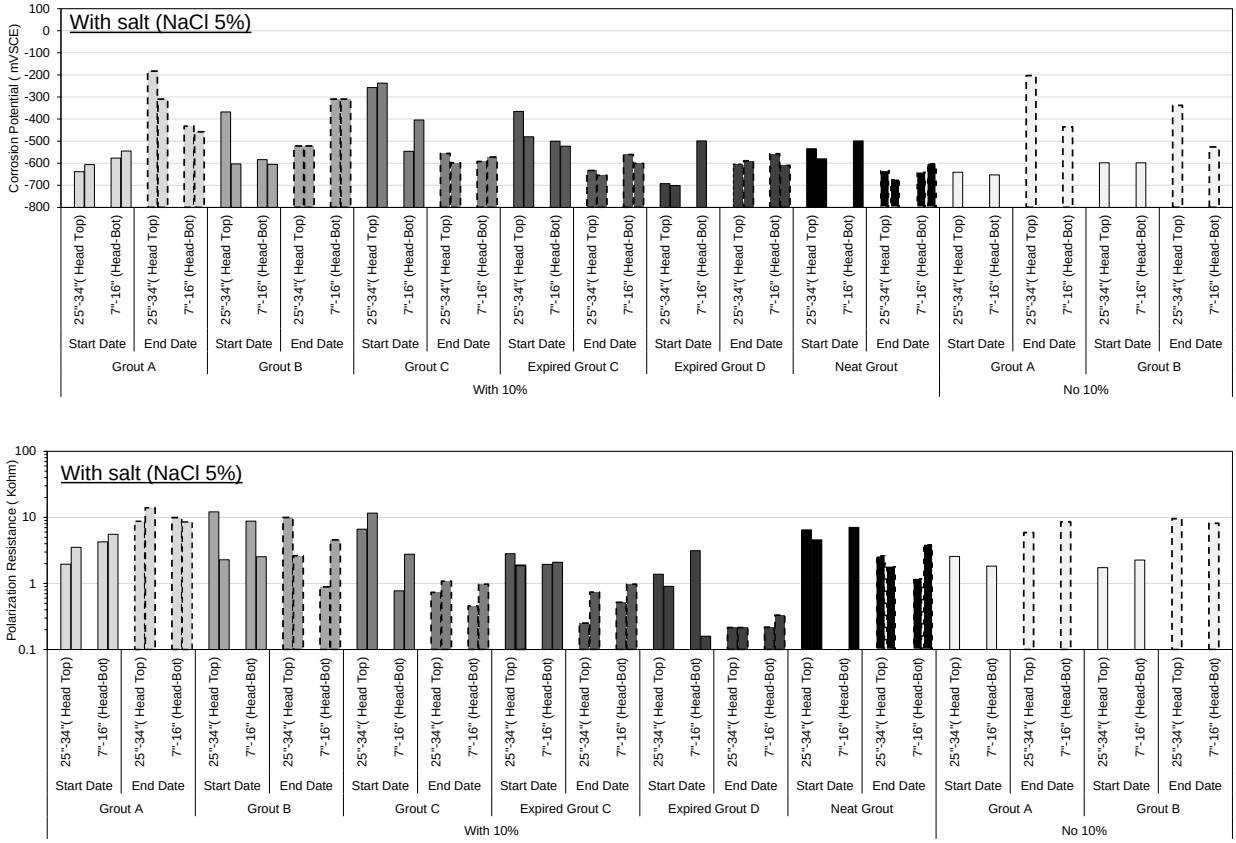

Figure 5.9. LPR and OCP of decoupled macrocell test specimens after 2nd cycle

5.2.3 Summary

The macrocell tests were envisioned to provide an economic alternative to the polarization resistance and potentiostatic tests. However, the outcomes of the research showed that there were complications relating to the electrochemical activity of the individual test cells that would obscure easy interpretation of the galvanic coupling of the cells. Any adverse chemical effects relating to the development of deficient grout by the INT setup was not captured by the macrocell testing. The addition of salt to the anode cell did not provide better outcomes. The INT setup however can be useful to identify the robustness of grout materials to adverse mixing conditions (such as overwatering and prehydration).

Lab testing to identify grout robustness requires aggressive test methods; however, overly aggressive test conditions to promote grout segregation is not representative of the required and necessary appropriate quality expected for field construction. Any development of corrosion test methods to address grout robustness must state the expected use and handling of the materials and provide justification for the level of adverse grout conditioning implemented for construction materials beyond that specified by the manufacturer.

CHAPTER 6. CORROSION TESTING OF MIT SPECIMENS

The corrosion activity of the embedded steel bar was assessed by measurement of the open-circuit potential, polarization resistance (Rp) by the linear polarization resistance method (LPR), and solution resistance by electrochemical impedance spectroscopy (EIS). At the base of each tendon, the embedded steel bar was exposed so that electrical contact can be made for the electrochemical testing. Six portals along the length of the MIT specimen were made to expose the grout within the duct by cutting and removing the PVC cover. A counter electrode made out of activated titanium mesh (4 x 3 inch) was inserted between two wet sponges was affixed to exposed grout surface. A pen copper/copper-sulfate reference electrode was placed at the center of the fixture.

The LPR measurements were made from the open-circuit condition (OCP) and cathodically polarized 25 mV at a 0.1 mV/s scan rate. The Rp was corrected for the solution resistance resolved as the high frequency limit from EIS. EIS was measured at the OCP with a 10 mV a.c. excitation voltage from 100 kHz to 1 kHz.

The OCP for the steel in the MIT specimens are shown in Figure 6.1. The OCP of the steel showed a modest decrease to more electronegative potentials at the upper 5 feet of the tendons. However, the potentials overall were generally indicative of passive conditions. Indeed the resolved Rp shown in Figure 6.2 did not show strong indication for elevated corrosion rates for the steel at the upper elevations.

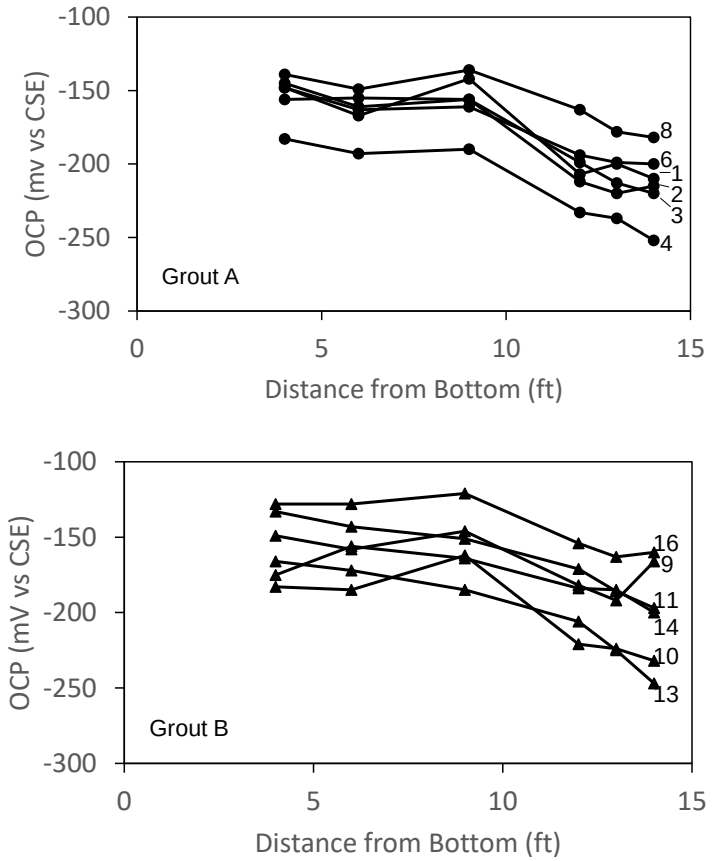

Figure 6.1. Open-circuit potential of steel in MIT specimens

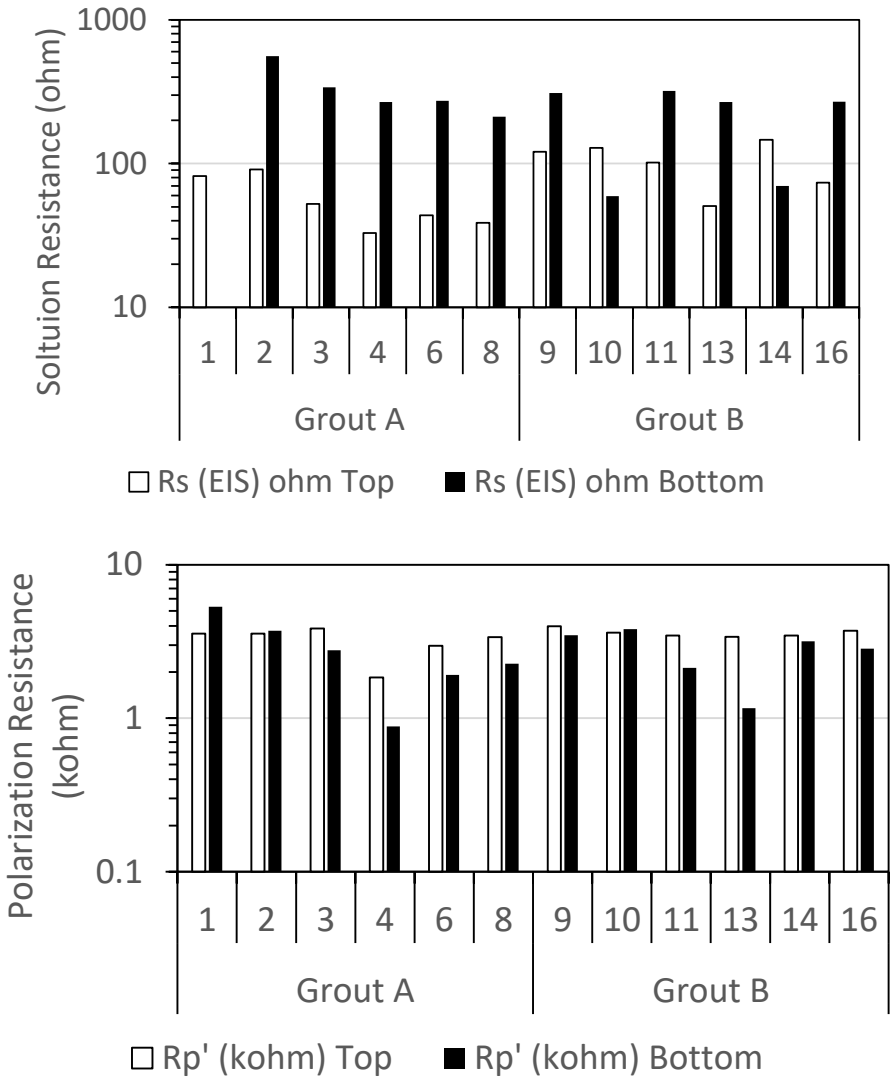

Figure 6.2. Solution resistance and polarization resistance of steel in MIT specimens

The resolved solution resistance of the grout however was strongly differentiated between locations from the top and bottom of the tendon, indicating differentiation in the grout and moisture content (Figure 5.6). Lower solution resistance was resolved for grout at the top of the tendon than at the lower elevations, further supporting the use of the MIT as means to test grout performance. It was noted that greater differentiation in solution resistance between tendon elevations as well as lower values were obtained for Grout A compared to Grout B. Indeed Grout B had better performance as it was designed for vertical PT applications and Grout A has been accepted for only horizontal PT applications. The sulfate content in Grout B was much greater differentiated between the high point elevation (~0.48 mg/g) and the low point elevation (~0.13 mg/g) than for Grout A, but Grout A showed as much as ~0.6 mg/g sulfate at high and low point elevations.

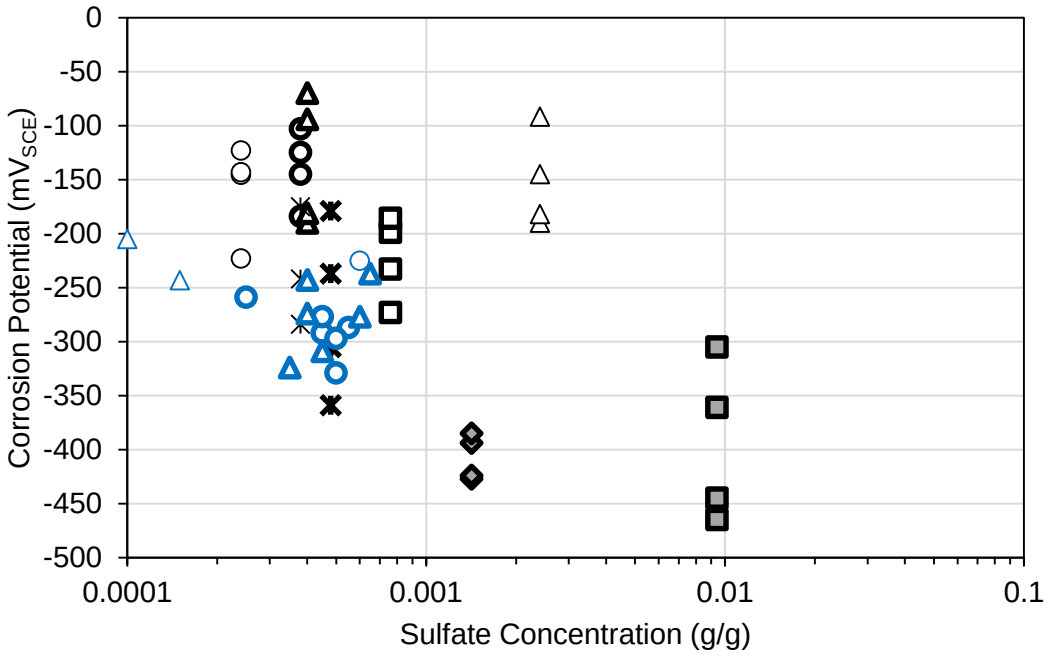

Figure 6.3. Correlation of steel corrosion potential and grout sulfate content.
Circle: Grout A. Triangle: Grout B. Square: Grout C. Diamond: Grout D. Cross: Neat Grout. Filled: Expired Grout. Blue: MIT. Black: INT

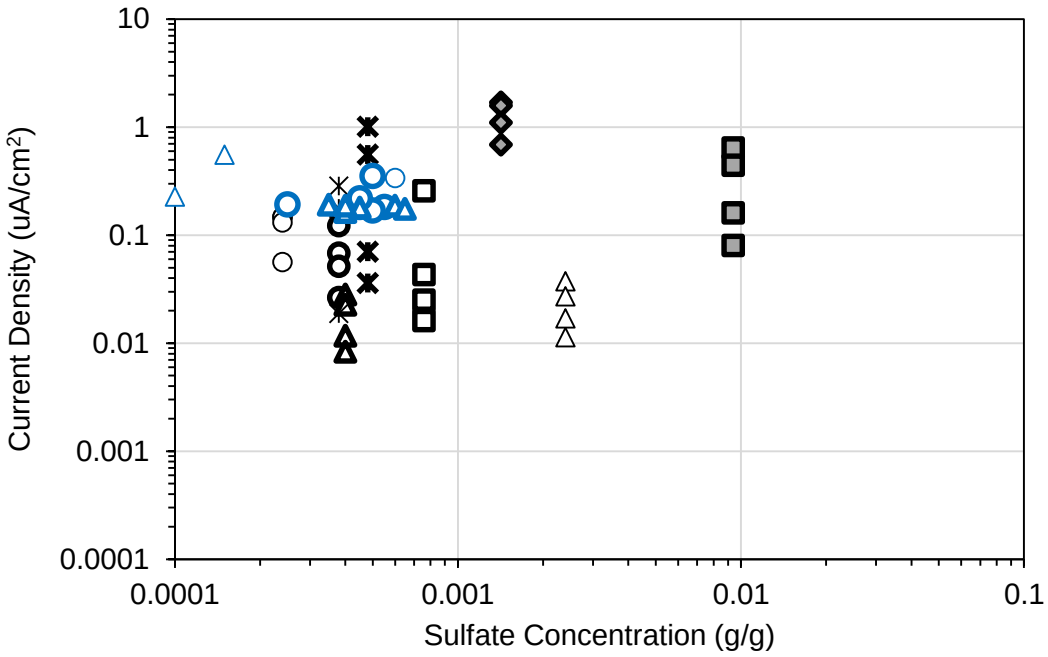

Figure 6.4. Correlation of steel corrosion current density and grout sulfate content.
Circle: Grout A. Triangle: Grout B. Square: Grout C. Diamond: Grout D. Cross: Neat Grout. Filled: Expired Grout. Blue: MIT. Black: INT

The corrosion potentials and corrosion current densities for the steel embedded in the MIT specimens and the INT specimens were correlated to the grout sulfate content. Figure 6.3 and 6.4 show correlation of steel corrosion potential and corrosion current density with grout sulfate content. As shown in Figure 6.3, the corrosion potential decreases to more electronegative values at the higher sulfate concentrations. Likewise, the corrosion current density showed a general increasing trend with the higher sulfate levels (Figure 6.4). The values produced from the test program here were consistent with historical data from earlier research, further verifying the adverse effects of elevated sulfate ion concentrations in the segregate grout. The expired grouts developed the highest sulfate ion concentrations and showed the greatest susceptibility for corrosion development.

CHAPTER 7. ASSESSMENT OF CORROSION BY ELECTROCHEMICAL NOISE

7.1. Electrochemical Noise

In the past 10 years, research on the effects of sulfate ions on steel corrosion has been conducted in response to the observations of premature corrosion of steel strand in cementitious grouts in post-tensioned bridge construction in Europe and in Florida. The steel strand corrosion appeared to be highly localized to regions of deficient grout. The corrosion in these cases were uniquely related to moisture and pore water in the grout that had elevated sulfate ion concentrations. The early presence of sulfate ions in alkaline solutions can impair the formation of the steel passive layer. Carsana and Bertolini, 2011 [10] attributed the corrosion to the development of pore water pH greater than 14. Newton and Sykes, 1987 [43] described how the elevated sulfate ion concentrations in alkaline solutions with excess calcium hydroxide allow for an increase in pH. However, the presence of pozzolans including silica fume would promote reactions to consume hydroxyl ions resulting in lowering the pH [44]. To further complicate the scenario, the localization of the deficient grout in the failed bridge tendons in Florida had low cement content (thus presumably a smaller reservoir of excess calcium hydroxide) and large aggregation of silica fume. Due to the practical nature of the corrosion observations in the grouted PT bridge systems, there remains interest to clarify the electrochemical behavior of steel in alkaline sulfate solutions and to provide rationale for practical material specifications.

The electrochemical noise (EN) technique relating to corrosion of metals in aqueous solution has been developed over the past 50 years [45-54]. The measurement technique was of interest to ideally elucidate the localized corrosion behavior of steel subjected to the early presence of elevated sulfate ion concentrations in alkaline solutions because of the incomplete description of how sulfate ions are related in those systems as well as the observation of localized corrosion in the field. Assessment of additional test parameters in the grout pore water composition by EN can be conducted pursuant to successful implementation of the technique in these systems. The fluctuations of the electrochemical potential and current (typically associated with unique transient events) can be attributed to corrosion processes at the metal-to-solution interface and can ideally identify the development of localized corrosion. Although complications exist [47], —with limitations in electronics for data acquisition, noise data interpretation, and other confounding system noise processes (physical, chemical, and electronic)— EN provides a useful mean to identify corrosion processes for metals in solution without the need for an external polarization that can alter the characteristics of the interface. Results of EN measurements of steel in simulated grout pore solution is described in the following to characterize the development of localized steel corrosion in alkaline sulfate solutions.

7.2 Materials and Methods

EN measurements were made on coupled-pairs of nominally identical steel working electrodes connected across a zero-resistance ammeter (ZRA) where the electrode pair was held at a common system open-circuit (OCP) condition, and the time records for electrochemical potential and current were measured. Each of the working electrodes in the pair was made from a cut section of a 1.27-cm diameter smooth carbon steel bar (0.02% C, 0.16% Mn, 0.003% S, 0.03% Si, 0.006% P, 0.09% Cu and balance Fe) mounted in an epoxy resin to expose one transverse cut face of bar, that was subsequently polished to 0.05 μm following conventional metallographic preparation steps. An insulated copper wire was soldered to the back transverse surface of the steel section via a steel screw prior to encapsulation in epoxy. The working electrode pair was separated 7.5 mm by a plastic spacer and held together with an elastic band. The spacer was also used to secure a micro silver/silver-chloride (Ag/AgCl) reference electrode. Several openings were made in the spacer to accommodate the reference electrode shaft to where the tip of the electrode was centered between the working electrodes as well as to allow mixing with the bulk solution. The test solution consisted of a saturated calcium hydroxide solution (0.2 g $Ca(OH)_2$) and 0, 0.1, 0.6, 1, 2, 3, 5, or 10 g Na_2SO_4 in 100 mL deionized H_2O. The test solution pH was measured with a glass pH/ATC

combination electrode. Table 1 lists the test solution makeup and measured pH. An activated titanium rod was placed for supplemental linear polarization resistance measurements at the end of EN testing. An illustration of the test cell is shown in Figure 7.1.

Table 7.1. Test cell solution

Test Condition (g Na_2SO_4/ L H_2O)	Mix Concentration in 100 mL H_2O	Sulfate Concentration (ppm SO_4^{2-})	pH	$[SO_4^{2-}]$/ $[OH^-]$
0	0.2 g $Ca(OH)_2$	0	12.60	0
1	0.2 g $Ca(OH)_2$ 0.1 g Na_2SO_4	676	12.62	0.17
6	0.2 g $Ca(OH)_2$ 0.6 g Na_2SO_4	4,056	12.61	1.01
10	0.2 g $Ca(OH)_2$ 1.0 g Na_2SO_4	6,760	12.60	1.8
20	0.2 g $Ca(OH)_2$ 2.0 g Na_2SO_4	13,521	12.62	3.4
30	0.2 g $Ca(OH)_2$ 3.0 g Na_2SO_4	20,281	12.70	4.2
50	0.2 g $Ca(OH)_2$ 5.0 g Na_2SO_4	33,803	12.64	8.0
100	0.2 g $Ca(OH)_2$ 10.0 g Na_2SO_4	67,606	12.70	14

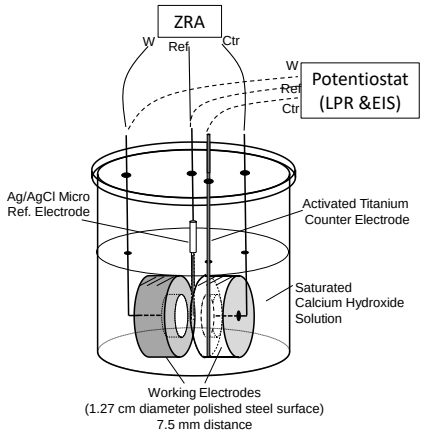

Figure 7.1. Schematic of the test setup.

For EN testing, the test cell was placed in an aluminum enclosure to act as a Faradaic cage with the test instrument grounded to the enclosure. The EN measurements were made in a ZRA-mode using a Gamry Ref600 potentiostat and ESA410 data acquisition program equipped with an anti-aliasing filter, following guidelines described by Huet and Ngo, 2019 [48] and Ritter et al., 2012 [48] with general settings as shown in Table7.2. The I-E stability setting was set to fast. The I-E range was 6-600 nA for testing up to 20 g Na_2SO_4/ L H_2O, 600 nA up to 50 g Na_2SO_4/ L H_2O, and 600 nA to 6 μA at 100 g Na_2SO_4/ L H_2O. The potential channel range and current channel range was typically set to 300 mV for testing up to 20 g Na_2SO_4/ L H_2O and to 3 V at higher concentrations with some deviations to avoid overload conditions. For each test specimen, the electrochemical potential and current time signatures were made at time 6 hr, 24 hr, and 1 week after immersion at 100 Hz (for 170 s), 10 Hz (for 28 min), and

1 Hz (for 70 min) sampling rates to obtain sets of power spectral density (PSD) graphs for noise data interpretation and validation purposes. The indicated test duration for each data sampling rate provided sufficient data points to perform fast Fourier transforms (FFT) and as recommended by Ritter et al., 2012. [48]

Table 7.2**.** EN ZRA test settings

Sulfate Levels	I-E Stability	I-E Range	E Channel Range	V Channel Range
0 to 20 g Na_2SO_4 / L H_2O	Fast	6 – 600 nA	300 mV	300 mV
30 to 50 g Na_2SO_4 / L H_2O	Fast	600 nA	3 V	3 V
100 g Na_2SO_4 / L H_2O	Fast	600 nA -6 μA	3V	3 V

The EN measurements were assessed by statistical evaluation of the electrochemical potential and current time signatures such as the mean, rms, standard deviation, skew, and kurtosis. Spectral analysis also included assessment of the PSD to characterize the characteristic charge (q), characteristic frequency (f_n), and corrosion current, (I_{corr}). Also comparisons of the noise impedance (Z_n), noise resistance (R_n), and polarization resistance (R_p) were made.

For the R_p measurements, supplemental linear polarization resistance (LPR) and electrochemical impedance spectroscopy (EIS) measurements were made after EN testing at 6 hr, 24 hr, and 1 week. Approximately 30 minutes after temporarily disconnecting the electrode pair from the ZRA, LPR and EIS measurements were made for each of the electrode pair. LPR was conducted from the open-circuit potential (OCP) condition to -25 mV_{OCP} at a scan rate of 0.01 mV/s, and EIS was made at the OCP with a 10 mV ac perturbation potential from 100 kHz to 1 Hz. The R_p was calculated as the nominal polarization resistance measured by LPR minus the solution resistance determined as the high frequency limit from EIS.

After the electrochemical measurements for up to 1 week, the steel specimens were removed from the test solution, surface cleaned with cotton, rinsed with ethanol, and dried with warm air. The surface of the steel was photographed with either a metallographic microscope to identify small pitting or a stereo microscope for low magnification of those specimens with more corrosion.

7.3. EN Analysis

The mean, rms, and standard deviation of the measured potential or current (generically described as x below) for data points i=1 to N (where N is the data population for the time signature) is described as in Equation 7-1 to 7-3. Higher order statistics such as skew and kurtosis can be described as in Equation 7-4 and 7-5 [45].

$$\text{Mean} = \overline{x} = \frac{\sum_{i=1}^{N} x(i)}{N} \qquad \text{Eq. 7-1}$$

$$\text{rms} = \sqrt{\frac{\sum_{i=1}^{N} x(i)^2}{N}} \qquad \text{Eq. 7-2}$$

$$\text{Std. Dev. } \sigma = \sqrt{\overline{x(\mathrm{i})^2}} = \sqrt{\frac{\sum_{\mathrm{i}=1}^{\mathrm{N}} \left(x(\mathrm{i}) - \overline{x}\right)^2}{\mathrm{N}}} \qquad \text{Eq. 7-3}$$

$$\text{Skew} = \frac{\sum_{\mathrm{i}=1}^{\mathrm{N}} \left(x(\mathrm{i}) - \overline{x}\right)^3}{\mathrm{N}\left(\overline{x(\mathrm{i})^2}\right)^{3/2}} \qquad \text{Eq. 7-4}$$

$$\text{Normalized Kurtosis} = \frac{\sum_{\mathrm{i}=1}^{\mathrm{N}} \left(x(\mathrm{i}) - \overline{x}\right)^4}{\mathrm{N}\left(\overline{x(\mathrm{i})^2}\right)^{2}} - 3 \qquad \text{Eq. 7-5}$$

The mean of the electrochemical potential and current time signature would likely provide general indication of the corrosion at the open-circuit condition (or rather the mixed potential condition of the electrode pair). Isolated transient corrosion events only have moderate influence on the value for a time signature if the transients have small periods relative to the recording time. Asymmetry in corrosion behavior of the paired electrodes that result in macrocell polarization can cause significant changes in the mean values. The rms and σ would ideally qualify the extent of the occurrence of isolated noise events attributed to corrosion signal transients with magnitudes deviating from the mean, although larger values associated with wide noise bands could mask those phenomena. These values would strongly be affected by heterogeneities between the working electrode pair. Skew (asymmetry) and normalized positive kurtosis (upsurge) of the distribution of the electrochemical potential and current may better reveal localized corrosion if the transient corrosion events exhibit unique short and unidirectional noise signatures as the occurrences of the corrosion events would provide greater statistics not conforming to a normal distribution.

Spectral analysis of EN data include evaluation of the electrochemical potential and current PSD. The PSD can be computed by FFT or the maximum entropy method (MEM). As described by Ritter et al., 2012 [48] and Huet and Ngo, 2019 [47], the EN data require validation of anti-aliasing in the frequency domain by the observation of a drop in PSD near the sampling frequency f_s divided by 2 and good overlap of PSD at different sampling frequencies. The calculated PSD from a time signature with multiple transient events is the culmination of power spectrum of all the individual transient events [45], and therefore systems with more events would be expected to have larger PSD. The random transient events associated with metastable pitting would have short periods, and the associated PSD would ideally show a low frequency limit (Ψ_{E0} for potential and Ψ_{I0} for current). Characteristics of the transient events can be assessed from the PSD by shot noise analysis. The corrosion current was described as

$$I_{corr} = \mathrm{B}\sqrt{\frac{\Psi_{I0}}{\Psi_{E0}}} \qquad \text{Eq. 7-6}$$

where B is the Stern-Geary coefficient and is related to the noise admittance $Z_n^{-1} = (\Psi_{I0}/\Psi_{E0})^{0.5}$. The characteristic charge, q, of the transient events was described as

$$q = \frac{\sqrt{\Psi_{I0} \times \Psi_{E0}}}{\mathrm{B}} \qquad \text{Eq. 7-7}$$

and the characteristic frequency, f_n, of the transient events was described as

$$f_n = \frac{\mathrm{B}^2}{\Psi_{E0}} \qquad \text{Eq. 7-8}$$

In the cases where a low-frequency PSD limit is not observed, calculations for I_{corr}, q, and f_n assuming a nominal Ψ_{E0} and Ψ_{I0} at a low frequency such as at 1 mHz may still provide qualitative comparisons of test parameters. As described by Cottis, 2001 [45] estimates of the PSD at an arbitrary low frequency can be obtained by the MEM using a high order coefficient optimized by comparison with the FFT.

The noise resistance, R_n, has been related to the polarization resistance, R_p, used to calculate the corrosion rate by the equation I_{corr}=B/R_p. R_n was calculated as the quotient of the standard deviation of the EN potential time signature and the complementary EN current time signature for the entire length of each time signature, $R_n = \sigma_E/\sigma_I$. Likewise the noise impedance, $Z_n(f) = (\Psi_E(f)/\Psi_I(f))^{0.5}$ can be computed from the potential and current PSD derived from the MEM with larger order coefficients. Comparisons of R_n and Z_n (at the low frequency limit) to R_p of each of the uncoupled electrode pair measured by the linear polarization resistance method at the end of EN testing were made. The calculated shot noise parameters q and f_n from testing at 1 Hz for 6 hr, 24 hr, and 1 week were used to make simple comparative estimates of cumulative corrosion loss in grams using Faradaic conversion following Equation. 9,

$$\text{Cumulative mass loss} = \frac{\sum_{i=1} (f_n(i)\, q(i)\, t(i))\, M}{nF} \qquad \text{Eq. 7-9}$$

where i is discretized in units corresponding to the length of time t of the sampling rate (i.e. 1 Hz), M=55.85 g/mol, n=2, and F=96,500 C/mol. The f_n and q values for 0-15 hours, 15-96 hours, and 96 hours-1 week were calculated from the 6 hr, 24 hr, and 1 week EN data sets, respectively.

7.4. Results and Discussion

As shown in Table 7.1, the pH of the solution was 12.6-12.7. There was a moderate positive trend of an increase in pH with elevated sulfate concentrations (generally conforming to the findings by Newton and Sykes, 1987 [43]. In the absence of aggressive ions, steel passivation would be expected in this pH range[55]. Indeed as described in the following, the control tests in sulfate-free solution showed low corrosion activity compared to the testing in the sulfate solutions.

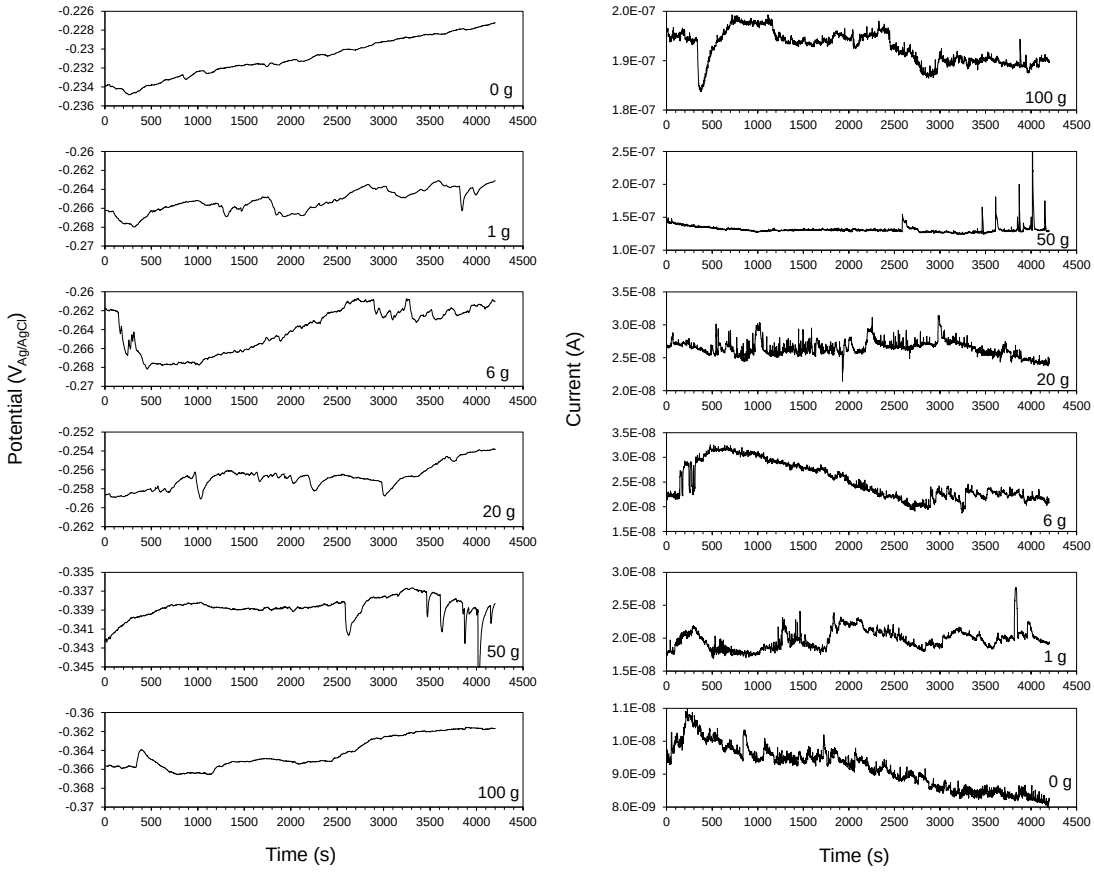

Figure 7.2. Example potential and current noise time signature.
Data collected at 1 Hz after 6 hr immersion. Current plotted as absolute values. Labels indicate g Na_2SO_4 / L H_2O. Sequence of the subplots were ordered by the magnitude of the potential and current.

Typical noise potential and current time signatures for the test specimens exposed in the alkaline sulfate solutions are shown in Figure 7.2. The potentials were more electronegative and currents were greater in the test solutions with greater sulfate concentrations. There was some drift in potential during the noise recordings; however, the differences in potential were typically low (and was less than ~5 mV in 70 minutes as shown in Figure 7.2). As expected, distinct and characteristic noise events exemplified with sharp changes and moderate recovery in potential and current were observed in the sulfate solutions and larger magnitude events were observed at the higher sulfate concentrations.

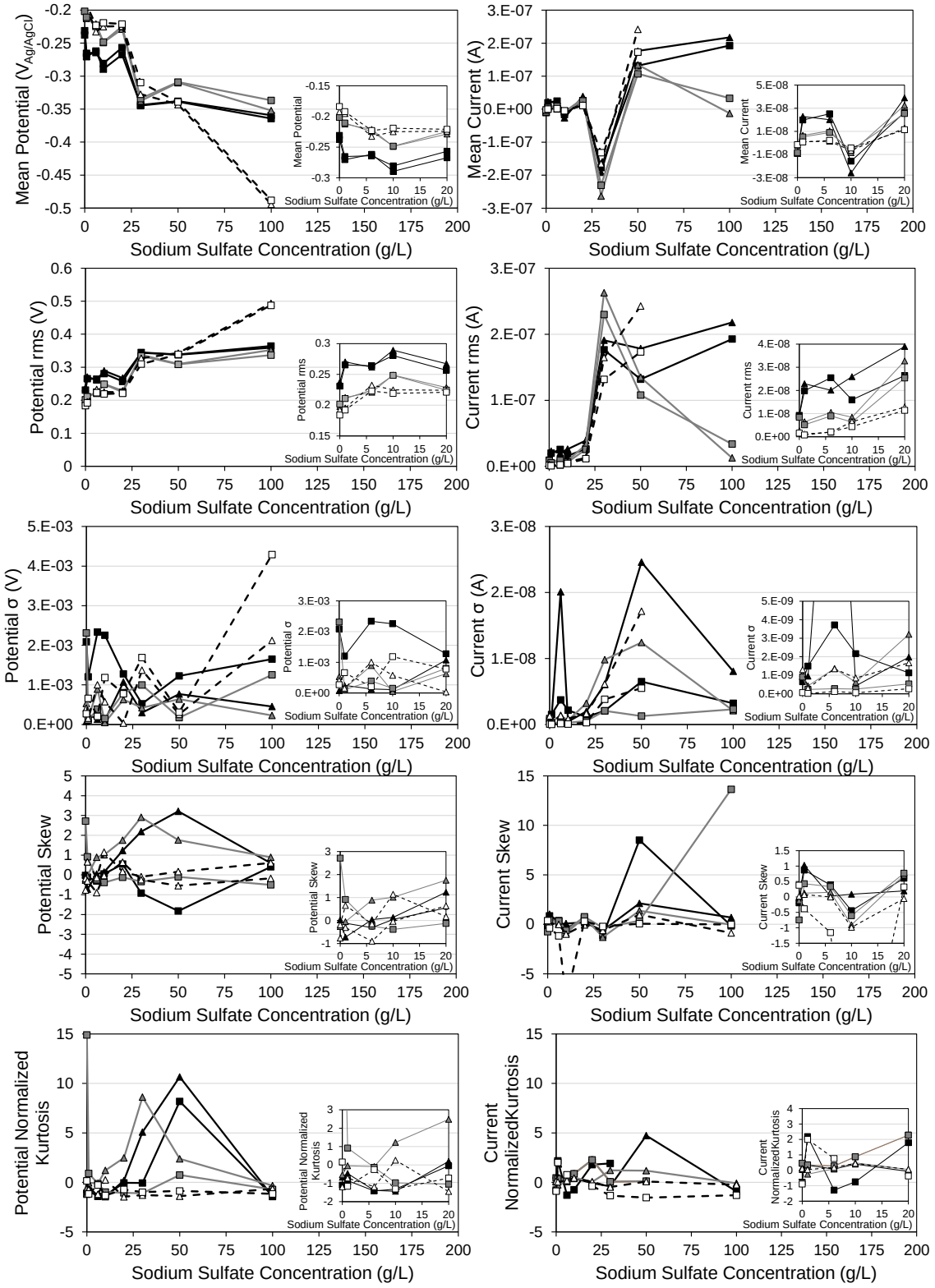

Figure 7.3. Statistics for EN potential and current data.
Square: 1 Hz. Triangle: 100Hz. Black: 6-hr immersion. Grey: 24-hr immersion. White: 1-week immersion.

General statistics of the complete EN potential and current time signatures sampled at 1 and 100 Hz after 6 hours, 24 hours, and 1 week after sample immersion are shown in Figure 7.3. Calculations for time signatures made at 10 Hz did not reveal significant differentiation. Consistent to the potential time signatures in Figure 7.2, the mean potential was more electronegative for steel immersed in the higher concentration sulfate solutions. The mean potential was -0.2 to -0.3 $V_{Ag/AgCl}$ at concentrations less than 20 g Na_2SO_4/L H_2O and more electronegative than -0.3 $V_{Ag/AgCl}$ at higher sulfate concentrations. The development of positive and negative currents indicated that net anodic and net cathodic behavior developed on separate electrodes of the working electrode pair. Nevertheless, , consistent with the developed OCP, the magnitude of the mean current (also exemplified by the I_{rms}) was significantly larger in solutions with more than 20 g Na_2SO_4/L H_2O.

The standard deviation of the EN potential had scatter in the results (attesting to some level of asymmetry of the working electrode pair) but the current σ was overall higher in the test solutions with more than 20 g Na_2SO_4/L H_2O. This was considered to be associated with a wider range of current measured during the isolated noise events due to the more frequent events with larger magnitudes Furthermore, the potential and current skew and kurtosis all showed greater values likewise in solutions with more than 20 g Na_2SO_4/L H_2O reflecting the statistics from the more numerous and greater magnitude noise events at the higher sulfate concentrations.

It was noted that the mean potential showed trend towards more electronegative values and the mean current showed trends to greater current magnitudes also at the low sulfate ion concentrations up to 20 g Na_2SO_4 / L H_2O, albeit to a lesser extent than that observed at the higher sulfate concentrations. Likewise the potential and current rms, σ, skew and kurtosis had larger values at those low sulfate ion concentrations than the control condition, indicating that sulfates also have effect at low concentrations. However, the statistics in the sulfate solutions described above were more appreciable at early times of exposure (ie 6 hrs) than after 1 week indicating that those noise events are reduced with time.

A typical example of the potential and current PSD calculated by FFT as well as MEM from EN measurements made at 1, 10, and 100 Hz sampling frequencies are shown in Figure 7.4. As expected, the PSD computed by MEM with a high order coefficient showed comparable results as the PSD computed by FFT. The PSD showed cutoff frequencies at $f_s/2$ indicating filtering of signal above the Nyquist frequency and good overlap of the three PSD providing validation of the EN measurements. Figure 5 shows the potential and current PSD computed by MEM with an order coefficient of 500 for test specimens (sampled at 1 Hz) immersed in the various sulfate concentration solutions for 6 hours. Figure 6 shows the calculated Z_n for those specimens. Consistent with the general observation of transient noise activity in the EN time signatures and the commensurate noise potential and current statistics for the specimens described earlier, the potential and current PSD were generally larger in magnitude at the higher sulfate concentrations. Likewise, the Z_n was lower for the higher sulfate concentrations. These observations provided consistent indication of greater corrosion activity of steel in alkaline sulfate solutions.

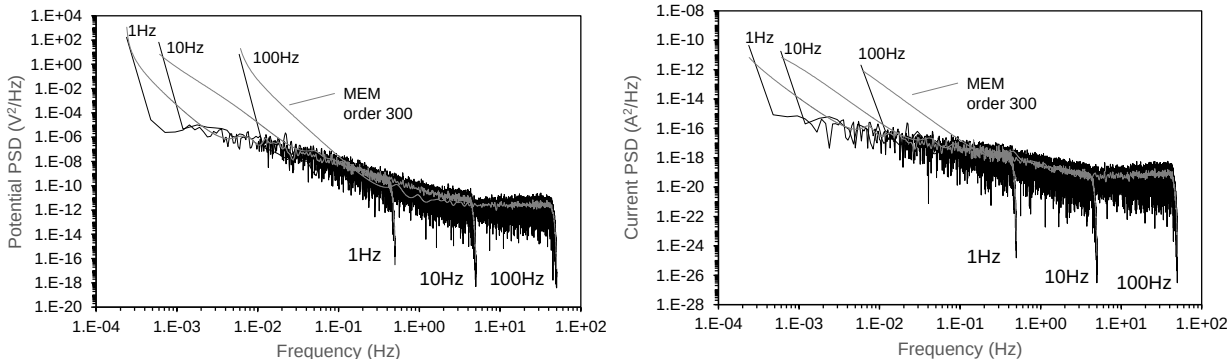

Figure 7.4. Example of potential and current PSD by FFT and MEM (3g Na_2SO_4/ 100 mL H_2O). Data after 6 hr immersion.

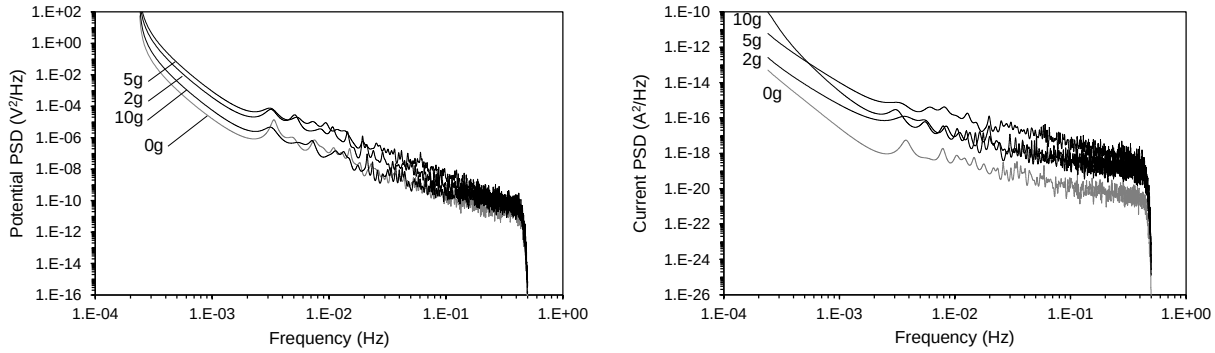

Figure 7.5. Example of potential and current PSD derived from MEM (order coefficient = 500) for sulfate solutions.
Labels indicate g Na_2SO_4 / L H_2O. (Data sampled at 1Hz after 6 hr immersion)

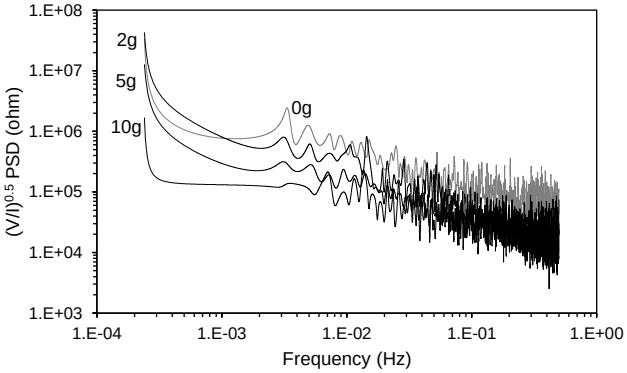

Figure 7.6. Example of $Z_n(f)$ derived from MEM (order coefficient = 500) for sulfate solutions.
Labels indicate g Na_2SO_4 / L H_2O. (Data sampled at 1 Hz after 6 hr immersion)

Table 7.3. Potential and current PSD low frequency limit (1mHz) for EN sampled at 1Hz

Test Condition (g Na_2SO_4/ L H_2O)	Ψ_{E0} (V^2/Hz) (Low frequency limit for potential)			Ψ_{I0} (A^2/Hz) (Low frequency limit for current)		
	6 hr	24 hr	1week	6hr	24hr	1week
0	3.47E-04	7.07E-04	1.25E-05	2.63E-17	5.26E-17	1.06E-18
1	1.93E-03	6.58E-05	1.77E-06	1.49E-15	1.11E-17	1.95E-19
6	1.12E-03	1.27E-03	9.91E-06	6.17E-16	1.05E-16	2.41E-18
10	2.04E-04	7.19E-05	1.46E-04	2.16E-16	1.33E-17	2.05E-17
20	2.69E-03	2.77E-04	1.07E-04	1.09E-15	2.91E-16	7.42E-17
30	4.22E-04	2.35E-04	1.71E-05	1.12E-14	8.00E-15	1.12E-15
50	5.98E-03	3.23E-04	1.19E-05	1.37E-14	4.30E-15	4.54E-16
100	3.49E-04	6.92E-04	1.97E-05	1.61E-14	2.30E-15	4.94E-15

The low frequency limits of the potential and current PSD were masked due to anomalous noise that manifested as an abrupt increase in PSD at the low frequency end of the power spectra. As a general approach, Ψ_{E0} and Ψ_{I0} were estimated as the PSD calculated by MEM with an order coefficient of 500 at a nominal frequency of 1 mHz (Table 7.3). The calculated I_{corr}, q, and f_n for the specimens in the various sulfate concentrations are shown in Figure 7 and Figure 8. The Stern-Geary coefficient was assumed to be 52 mV based on the results of anodic potentiodynamic polarization testing (to be disseminated in a future publication) where passive-like anodic Tafel behavior was observed in test specimens immersed in similar sulfate solutions. The R_n calculated from σ values and Z_n from Ψ values had good correlation [45] as shown in Figure 7.9 and the estimates of Ψ_{E0} and Ψ_{I0} were deemed adequate for comparison purposes. Furthermore, the corrosion current calculated from the measured R_p by LPR for each of the uncoupled electrode pair generally corresponded well with I_{corr} calculated per Equation7-6 even though some level of electrode asymmetry was apparent as described earlier.

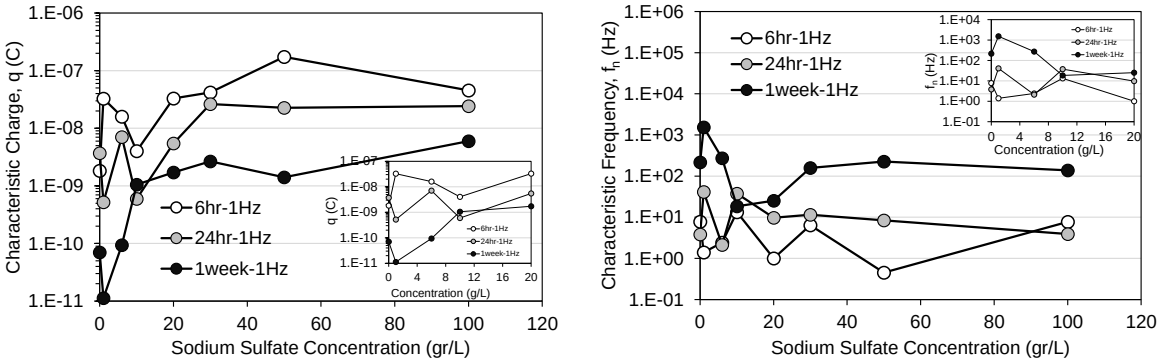

Figure 7.7. EN characteristic charge, q and frequency, f_n in sulfate solutions.

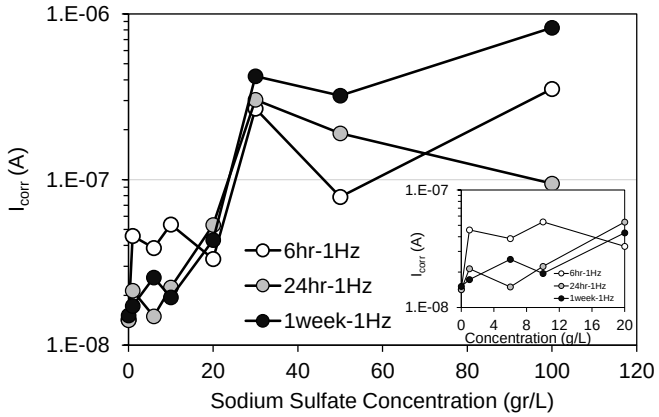

Figure 7.8. Estimated corrosion current in sulfate solutions.

The I_{corr} values (Figure 7.8) showed a distinct increase with the sodium sulfate concentrations but a significant increase was observed at concentrations greater than 20 g Na_2SO_4 / L H_2O. At these higher sulfate concentrations, the corrosion rate showed a trend towards higher overall corrosion rates with time of immersion from 6 hrs to 1 week. These results provide supporting evidence that sulfate concentrations in alkaline solutions allow for elevated general corrosion activity.

In addition, the q and f_n values (Fig. 7.7) provide information on the extent of localized corrosion events. With time, at a given sulfate concentration, the magnitude of charge decreases and the frequency of the events increases. This indicated that larger pitting events (large q and low f_n) that developed at the higher sulfate ion concentrations were more severe at early exposure times. At lower sulfate ion concentrations below 10 g Na_2SO_4 / L H_2O, pitting events seemed significant at early times but appeared to dissipate with time. Above 10 g Na_2SO_4 / L H_2O, pitting events were maintained after longer exposure times (ie 1 week). Overall, the general trend of the collected data indicated that the characteristic charge increases and the characteristic frequency decreases with sulfate ion concentration yet the overall corrosion rate increases. The noise data would indicate that pitting events can be sustained above 10 g Na_2SO_4 / L H_2O and more extensive localized corrosion develops above 20 g Na_2SO_4 / L H_2O.

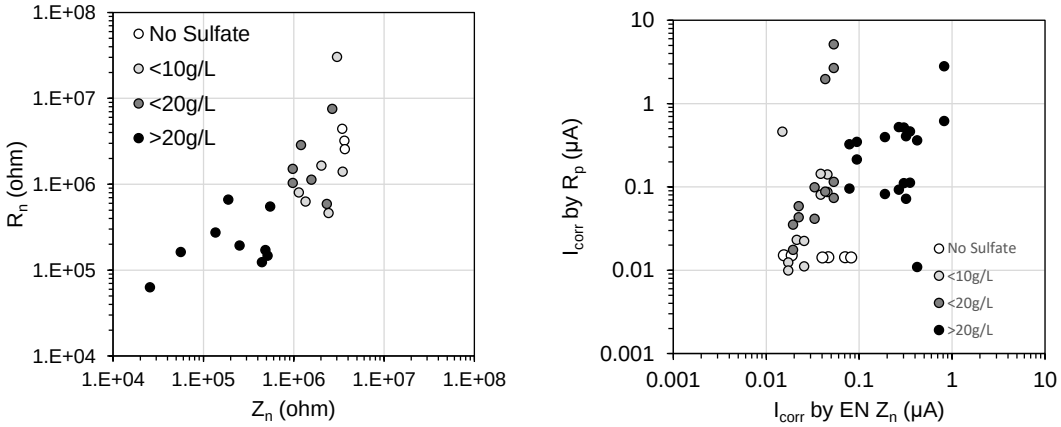

Figure 7.9. Comparison of EN data (R_n, Z_n) and LPR R_p. Labels indicate g Na_2SO_4 / L H_2O.

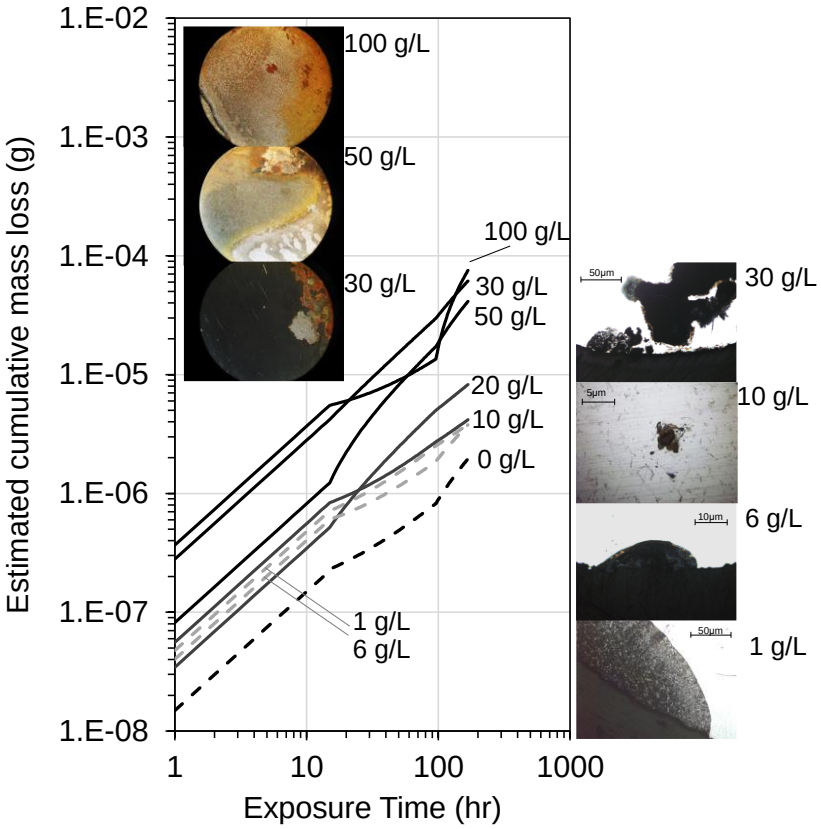

Figure 7.10. Estimated corrosion mass loss and pitting observations. Labels indicate g Na_2SO_4 / L H_2O.

The estimated corrosion mass loss using Faradaic conversion of the calculated EN q and f_n data is shown in Figure 7.10. As expected, the calculated mass loss for steel in the sulfate solutions was greater than in the sulfate-free solutions. The greatest amount of corrosion loss was calculated for steel in the sulfate solutions greater than 20 g Na_2SO_4 / L H_2O and low corrosion loss was calculated for sulfate solutions between 1 and 10 g Na_2SO_4 / L H_2O. The micrographs and low-magnification images of the steel surface showed corresponding levels of pitting and corrosion. As expected, no distinct corrosion artifacts were observed on the steel specimens exposed in the sulfate-free test solutions, consistent with the low calculated corrosion rates and lack of signature noise events. Small pits were observed on specimens immersed in sulfate solutions with less than 30 g Na_2SO_4 / L H_2O. At 30 g Na_2SO_4 / L H_2O and above, significant formation of pits were apparent. The results would indicate that low level sulfates can locally impair the formation of the passive film but the associated corrosion would appear to be modest. However, if localized breakdown or impairment of the passive film occurs at moderate sulfate levels, it may be posited that there are certain environmental conditions that exacerbate corrosion. For example, autocatalytic corrosion with local acidification can develop within the pit similar to that for chlorides as described by Equation 7-10.

$$Fe^{2+} + 2H_2O + SO_4^{2-} \rightarrow Fe(OH)_2 + H_2SO_4 \qquad \text{Eq. 7-10}$$

Furthermore, as observed in the field, sites for iron oxidation reaction were isolated on strand embedded in the deficient grout, and macrocell coupling to the rest of the steel strand otherwise normal hardened grout that can accommodate additional sites for reduction reactions (including oxygen reduction) would allow for accelerated corrosion. High sulfate concentrations greater than 20 g Na_2SO_4/L

H_2O could result in more egregious pitting. Indeed, in the Florida bridge case, the most severe steel strand corrosion developed in the most severe grout segregation with sulfate levels levels (up to 12,000 ppm) commensurate to 20 g Na_2SO_4/L H_2O. That corrosion would also be accelerated due to macrocell corrosion.

State transportation departments have recently developed material testing and specifications to limit free sulfate ion concentrations in deficient grout to mitigate the development of corrosion as observed in 2011[56-62]. Such limits include 30 ppm following a leaching method for 1 g of grout in 100 mL water. Those limits would correspond to ~4,000 ppm SO_4^{2-} and would be conservative value to screen materials with propensity for grout segregation. The results of EN testing indicated similar sulfate levels to where pitting can develop and be sustained and in part provides supporting evidence for development of limits to be implemented in practical application for highway bridge systems.

7.5. Summary

The early presence of sulfate ions in saturated calcium hydroxide solution can allow for local impairment of the passive film. At higher sulfate concentrations (>20 g Na_2SO_4/L H_2O), more egregious pitting and corrosion develops. Electrochemical noise was shown to be an effective measurement technique to assess the development of localized corrosion of steel in alkaline solution when utilizing appropriate anti-aliasing filters and instrument settings. General statistics such as the mean, rms, standard deviation, skew, and kurtosis of the potential and current time signatures have some experimental scatter but generally revealed the negative the effect of elevated sulfate concentrations on electrochemical noise associated with pitting events. Spectral analysis indicated that the characteristic charge increases and the characteristic frequency decreases with sulfate ion concentration yet the overall corrosion rate increases, indicating that pitting corrosion develops. Pitting events could be sustained in solutions above 10 g Na_2SO_4/L H_2O and more extensive localized corrosion developed above 20 g Na_2SO_4/L H_2O.

CHAPTER 8. SUMMARY OF MAJOR FINDINGS

Material Characterization

- The visual observations of the grout from the various test setups provided important findings for the assessment of grout robustness. The thixotropic grouts, when mixed following recommended practices, generally formed visually consistent hardened grout and was more robust to consolidation problems than the neat grout. Different levels of physical grout deficiencies were visually evident for the thixotropic grout when mixed with excess 10% water.

- The results showed that the INT setup with the vertical deviation can produce enhanced transport of moisture towards the top of the tee header. The grout at greater vertical heights had correspondingly greater moisture content and the moisture content of the grout in the tee header was consistently greater than the grout in the tee body.

- The different grout products had different yields of leached sulfate ions in the INT header. Higher sulfate levels were generally observed in the tee header than the tee body likely relating to the displacement of water to the top of the specimen. Consistent with previous research, it was shown that the sulfate ion accumulation in the deficient grout (here in the tee header) can develop without external contamination.

- Similar to the INT results without the flow constriction, the grout in the tee header had higher moisture content than the grout in the tee body. In all test cases, the excess mix water allowed for enhanced water displacement into the tee header. It was apparent that the presence of a high flow constriction amplified this effect. However, the experiments did not show appreciable effect to enhance sulfate accumulation due to the grout flow constriction.

- The casting of grout specimens with adverse handling and excess mix-water can promote grout deficiencies. There is a balance to vet grout materials using aggressive testing methods to identify material robustness to compensate for poor construction practices when engineered materials are designed to be used appropriately. For example, Grout C showed the best relative corrosion performance when appropriately handled but the worst relative corrosion performance when subject to inappropriate handling and mixing.

Modified Accelerated Corrosion Test

- The results showed that the methodologies prescribed in existing test guidelines can be applicable to assess grout robustness and corrosion propensity in deficient grout. Grout C, expired Grout C and D cast with 10% extra water with the most adverse grout segregation showed results that would be considered not meeting acceptance criteria. The results showed that generally Grout A and B showed a longer time to corrosion.

- Accelerated corrosion testing can be used to identify the corrosion performance of passive corrosion mitigation technologies (such as inhibitors and films). Application of protective hydrocarbon films into post-tensioned tendons, such as that already commercially developed can reduce, can have beneficial effects to mitigate corrosion. The presence of severe grout deficiencies with continued exposure to adverse corrosion environments can reduce the efficacy of the protective film. Test protocols to assess grout robustness to the effects of adverse construction practices and conditions (such as overwatering, grout pre-hydraton, and water displacement) can be implemented to the accelerated corrosion testing to identify the performance of the corrosion mitigation technology (ie impregnation).

Macrocell Corrosion Test

- The macrocell tests was envisioned to provide an economic alternative to the polarization resistance and potentiostatic tests. However, the outcomes of the research showed that there were complications relating to the electrochemical activity of the individual test cells that would obscure easy interpretation of the galvanic coupling of the cells. Any adverse chemical effects relating to the development of deficient grout by the INT setup was not captured by the macrocell testing. The addition of salt to the anode cell did not provide better outcomes.

INT Experimental Setup

- The INT setup however can be useful to identify the robustness of grout materials to adverse mixing conditions (such as overwatering and prehydration). However, there is a balance to vet grout materials using aggressive testing methods to identify material robustness to compensate for poor construction practices when engineered materials are designed to be used appropriately. Any development of corrosion test methods to address grout robustness must state the expected use and handling of the materials and provide justification for the level of adverse grout conditioning.

MIT Corrosion Testing

- The resolved solution resistance of the grout however was strongly differentiated between locations from the top and bottom of the tendon, indicating differentiation in the grout and moisture content. Lower solution resistance was resolved for grout at the top of the tendon than at the lower elevations, further supporting the use of the MIT as means to test grout performance.

- The corrosion potentials and corrosion current densities for the steel embedded in the MIT specimens and the INT specimens were correlated to the grout sulfate content. The corrosion potential decreases to more electronegative values at the higher sulfate concentrations. Likewise, the corrosion current density showed a general increasing trend with the higher sulfate levels. The values produced from the test program here were consistent with historical data from earlier research, further verifying the adverse effects of elevated sulfate ion concentrations in the segregate grout. The expired grouts developed the highest sulfate ion concentrations and showed the greatest susceptibility for corrosion development.

Electrochemical Noise Technique

- Electrochemical noise was shown to be an effective measurement technique to assess the development of localized corrosion of steel in alkaline solution when utilizing appropriate anti-aliasing filters and instrument settings. General statistics such as the mean, rms, standard deviation, skew, and kurtosis of the potential and current time signatures have some experimental scatter but generally revealed the negative the effect of elevated sulfate concentrations on electrochemical noise associated with pitting events. Spectral analysis indicated that the characteristic charge increases and the characteristic frequency decreases with sulfate ion concentration yet the overall corrosion rate increases, indicating that pitting corrosion develops.

REFERENCES

1. Naaman, A. E. (1982). Prestressed concrete analysis and design: Fundamentals (pp. 360-364). New York: McGraw-Hill.
2. Hewson, N. R. (2003). Prestressed concrete bridges: design and construction. Thomas Telford.
3. Osborn, B. (2019). Observations from 30 years of inspecting post-tensioned structures. Concrete Bridge Technology, ASPIRE Spring.
4. Corven, J., & Moreton, A. J. (2013). Post-tensioning tendon installation and grouting manual (No. FHWA-NHI-13-026). Federal Highway Administration (US).
5. Powers, R. G. (1999). Corrosion evaluation of post-tensioned tendons on the niles channel bridge. Florida Department of Transportation, Gainesville, FL.
6. Corven, J. (2001). Mid bay bridge post-tensioning evaluation. Final Report, Florida Department of Transportation, Florida.
7. Hartt, W. H., & Venugopalan, S. (2002). Corrosion evaluation of post-tensioned tendons on the Mid Bay Bridge in Destin, Florida (No. Final Report).
8. Hewson, N. R. (2003). Prestressed concrete bridges: design and construction. Thomas Telford.
9. Lau, K., Lasa, I., & Parades, M. (2011). Corrosion Development of PT Tendons with Deficient Grout: Corrosion Failure in Ringling Causeway Bridge. Florida Department of Transportation State Materials Office, Draft Report.
10. Bertolini, L., & Carsana, M. (2011). High pH corrosion of prestressing steel in segregated grout. In Modelling of corroding concrete structures (pp. 147-158). Springer, Dordrecht.
11. Rafols, J. C., Lau, K., Lasa, I., Paredes, M., & ElSafty, A. (2013). Approach to determine corrosion propensity in post-tensioned tendons with deficient grout.
12. Lau, K., Paredes, M., & Rafols, J. C. (2012). Corrosion Evaluation of Post-Tensioned Tendons With Dissimilar Grout. In *CORROSION 2012*. Paper No. C2012-0001738, NACE International: Houston, TX, USA.
13. Lau, K., Powers, R., Paredes, M. (2013) Corrosion Evaluation of Repair-Grouted Post-Tensioned Tendons in Presence of Bleed Water. In CORROSION 2013, Paper No. 2604, NACE International: Houston, TX, USA.
14. Lau, K., Rafols, J., Paredes, M., Lasa, I. Laboratory Corrosion Assessment of Post-Tensioned Tendons Repaired with Dissimilar Grout. In CORROSION 2013, Paper No. 2602, NACE International: Houston, TX, USA.
15. Lau, K., Paredes, M., Lasa, I. (2013) Corrosion Failure of Post-Tensioned Tendons in Presence of Deficient Grout. In CORROSION 2013, Paper No. 2600, NACE International: Houston, TX, USA.
16. Lau, K., Lasa, I. (2016), Corrosion of prestress and post-tension reinforced-concrete bridges. In: Poursaee A, Corrosion of Steel in Concrete Structures, Woodhead Publishing, Cambridge 2016, pp 37-57. https://doi.org/10.1016/B978-1-78242-381-2.00003-1
17. Lau, K., Lasa, I., Paredes, M. Update on Corrosion of Post-Tensioned Tendons with Deficient Grout, In CORROSION 2014. Paper No. 4225, NACE International: Houston, TX, USA.
18. Permeh, S., Krishna Vigneshwaran, K.K, Lau, K. (2016) Corrosion of Post-Tensioned Tendons with Deficient Grout, Florida Department of Transportation, Final Report, Contract No. BDV29-977-04, October 20, 2016.
19. Krishna Vigneshwaran, K.K., Permeh, S., Echeverría, M., Lau, K., Lasa, I. (2018) Corrosion of Post-Tensioned Tendons with Deficient Grout. Part 1. Electrochemical Behavior of Steel in Alkaline Sulfate Solutions, Corrosion 74 :362-371. https://doi.org/10.5006/2541
20. Permeh, S., Krishna Vigneshwaran, K.K., Echeverría, M., Lau, K., Lasa, I. (2018) Corrosion of Post-Tensioned Tendons with Deficient Grout. Part 2. Segregated Grout with Enhanced Sulfate, Corrosion 74 :457-467. https://doi.org/10.5006/2568

21. Permeh, S.,Krishna Vigneshwaran, K.K., Lau, K., Lasa, I. (2019) Corrosion of Post-Tensioned Tendons with Deficient Grout. Part 3: Segregated Grout with Elevated Sulfate and Vestigial Chloride Content, Corrosion 75: 848-864. https://doi.org/10.5006/3097
22. Permeh, S., Krishna Vigneshwaran, K.K., Lau, K., Lasa, I. (2016) Anodic Behavior of Steel in Enhanced Sulfate Solutions. In CORROSION 2016, paper No. 7712, NACE International: Houston, TX, USA.
23. Krishna Vigneshwaran, K.K., Permeh, S., Lasa, I., and Lau, K. Corrosion of Steel in Deficient Grout with Enhanced Sulfate Content. In NACE Concrete Service Life Extension Conference 2015. Paper No. CCC15-6942, NACE International: Houston, TX, USA.
24. Permeh, S., Krishna Vigneshwaran, K.K., Lau, K., and Lasa, I. Corrosion of PT Tendons in Deficient Grout in Presence of Enhanced Sulfate and Chloride Concentration.In NACE Corrosion Risk Management Conference 2016, Paper No. 16-18751, NACE International: Houston, TX, USA.
25. Permeh S, Krishna Vigneshwaran K.K, Lau K, Lasa I, Paredes M. Material and Corrosion Evaluation of Deficient PT Grout with Enhanced Sulfate Concentrations. In CORROSION 2015, Paper No. 5828, NACE International: Houston, TX, USA.
26. ASTM G109-(2013). "Standard Test Method for Determining Effect of Chemical Admixtures on Corrosion of Embedded Steel Reinforcement in Concrete Exposed to Chloride Environments,", West Conshohocken, PA.
27. ASTM A955. -(2019) "Standard Specification for Deformed and Plain Stainless-Steel Bars for Concrete Reinforcement," West Conshohocken, PA.
28. Palumbo, N. (1991). Accelerated corrosion testing of steel reinforcement in concrete (Doctoral dissertation, McGill University Libraries).
29. Trejo, D., Halmen, C., & Reinschmidt, K. (2009). Corrosion performance tests for reinforcing steel in concrete: technical report (No. FHWA/TX-09/0-4825-1). Texas Transportation Institute
30. Deb, S. (2012). Accelerated Short-Term Techniques to Evaluate Corrosion in Reinforced Concrete Structures. The Master Builder, 248-255.
31. Ožbolt, J., Sola, E., & Balabanić, G. (2015). Accelerated Corrosion of Steel Reinforcement in Concrete: Experimental Tests and Numerical 3D FE Analysis. In CONCREEP 10 (pp. 108-117).
32. Thompson, N. G., Lankard, D., & Sprinkel, M. M. (1992). Improved Grouts for Bonded Tendons in Post-Tensioned Bridge Structures. Final Report (No. FHWA-RD-91-092).
33. Schokker, A. J. (1999). Improving Corrosion Resistance of Post-Tensioned Substructures Emphasizing High Performance Grouts. The University of Texas at Austin.
34. Hamilton III, H. R., Wheat, H. G., Breen, J. E., & Frank, K. H. (2000). Corrosion testing of grout for posttensioning ducts and stay cables. Journal of Structural Engineering, 126(2), 163-170.
35. Pacheco, A. R., Schokker, A. J., & Hamilton III, H. R. (2006). Development of a standard accelerated corrosion test for acceptance of post-tensioning grouts in Florida (No. 00026900).
36. PTI M55.1-12, (2013). "Specification for Grouting of Post-Tensioned Structures." Post Tensioning Institute. Farmington Hills, MI.
37. Martinez, S. L., Darwin, D., McCabe, S. L., & Locke Jr, C. E. (1990). Rapid test for corrosion effects of deicing chemicals in reinforced concrete. University of Kansas Center for Research, Inc..
38. Darwin, D., Browning, J., O'Reilly, M., Locke Jr, C. E., & Virmani, Y. P. (2011). Multiple corrosion protection systems for reinforced concrete bridge components. University of Kansas Center for Research, Inc..
39. O'Reilly, M., Darwin, D., & Browning, J. (2013). Corrosion performance of prestressing strands in contact with dissimilar grouts (No. KS-12-4). Kansas. Dept. of Transportation.
40. O'Reilly, M., Darwin, D., & Browning, J. (2015), Corrosion Performance of Prestressing Strands in Contact with Dissimilar Grouts, ACI August 2015.
41. Whitmore, D., & Lasa, I. (2018). Impregnation technique provides corrosion protection to grouted post-tensioning tendons. In MATEC Web of Conferences (Vol. 199, p. 05008). EDP Sciences.

42. Silnutzer, J., Mraied, H., Mullins, G., Sagüés, A., & Alexander, C. L. (2020). Evaluation of Corrosion Inhibiting Materials Applied by Impregnation (Pressure Injection) Methods to Prevent Corrosion of Post-Tensioned Tendons.
43. Newton, C. J., & Sykes, J. M. (1987). The effect of salt additions on the alkalinity of Ca (OH) 2 solutions. Cement and Concrete Research, 17(5), 765-776.
44. Page, C. L., & Vennesland, Ø. (1983). Pore solution composition and chloride binding capacity of silica-fume cement pastes. Matériaux et construction, 16(1), 19-25.
45. Cottis, R. A. (2001). Interpretation of electrochemical noise data. Corrosion, 57(3), 265-285.
46. Bosch, R. W., Cottis, R. A., Csecs, K., Dorsch, T., Dunbar, L., Heyn, A., ... & Zhang, W. (2014). Reliability of electrochemical noise measurements: results of round-robin testing on electrochemical noise. Electrochimica Acta, 120, 379-389.
47. Huet, F., & Ngo, K. (2019). Electrochemical noise—guidance for improving measurements and data analysis. Corrosion, 75(9), 1065-1073.
48. Ritter, S., Huet, F., & Cottis, R. A. (2012). Guideline for an assessment of electrochemical noise measurement devices. Materials and Corrosion, 63(4), 297-302.
49. Xia, D. H., Ma, C., Behnamian, Y., Ao, S., Song, S., & Xu, L. (2019). Reliability of the estimation of uniform corrosion rate of Q235B steel under simulated marine atmospheric conditions by electrochemical noise (EN) analyses. Measurement, 148, 106946.
50. Gabrielli, C., Huet, F., & Keddam, M. (1986). Investigation of electrochemical processes by an electrochemical noise analysis. Theoretical and experimental aspects in potentiostatic regime. Electrochimica Acta, 31(8), 1025-1039.
51. Bertocci, U., Frydman, J., Gabrielli, C., Huet, F., & Keddam, M. (1998). Analysis of electrochemical noise by power spectral density applied to corrosion studies: Maximum entropy method or fast Fourier transform?. Journal of the Electrochemical Society, 145(8), 2780.
52. Sanchez-Amaya, J. M., Cottis, R. A., & Botana, F. J. (2005). Shot noise and statistical parameters for the estimation of corrosion mechanisms. Corrosion Science, 47(12), 3280-3299.
53. Al-Mazeedi, H. A. A., & Cottis, R. A. (2004). A practical evaluation of electrochemical noise parameters as indicators of corrosion type. Electrochimica Acta, 49(17-18), 2787-2793.
54. Monrrabal, G., Huet, F., & Bautista, A. (2019). Electrochemical noise measurements on stainless steel using a gelled electrolyte. Corrosion Science, 148, 48-56.
55. Li, L., & Sagues, A. A. (2001). Metallurgical effects on chloride ion corrosion threshold of steel in concrete.
56. Section 938, Duct Filler for Post-Tensioned Structures, Florida Department of Transportation, Standard specification for road and bridge construction, Florida, July 2020.
57. FM 5-618, Florida Method of Test for Sampling of Post-Tensioned Tendon Grout, Florida Department of Transportation, Tallahassee, FL, 2018.
58. Sonawane, R., Permeh, S., Garber,D., Lau, K., Duncan, M., Simmons, R. Test Methods to Identify Robustness of Grout Materials to Resist Corrosion, In CORROSION 2020, Paper No. 14820, NACE International: Houston, TX, USA.
59. Permeh, S., Sonawane, R., Lau, K., Duncan, M., Simmons, R. (2021) Update on the Evaluation of Grout Robustness and Corrosion by Accelerated Corrosion and Rapid Macrocell Testing, In CORROSION 2021, Paper No. 16339, NACE International: Houston, TX, USA.
60. Sonawane, R., Permeh, S., Lau, K., Duncan, M., Simmons, R. (2021) Review on the Determination of Sulfate Ion Concentrations in Deficient Post-Tensioned Grouts, In CORROSION 2021, Paper No. 16342, NACE International: Houston, TX, USA.
61. Permeh, S., Lau, K., Duncan, M., & Simmons, R. (2021). Identification of steel corrosion in alkaline sulfate solution by electrochemical noise. Materials and Corrosion. https://doi.org/10.1002/maco.202112347
62. Permeh, S., Lau, K., Duncan, M., & Simmons, R. (2021). Initiation of Localized Steel Corrosion in Alkaline Sulfate Solution. Materials and Structures.

APPENDIX A. PHOTOGRAPHS OF GROUTED TEST SPECIMENS

PTI ACT

Figure A1. PTI test specimens after 28-day hydration
(Top: with 10% excess mix water, Bottom: with no 10% excess mix water)

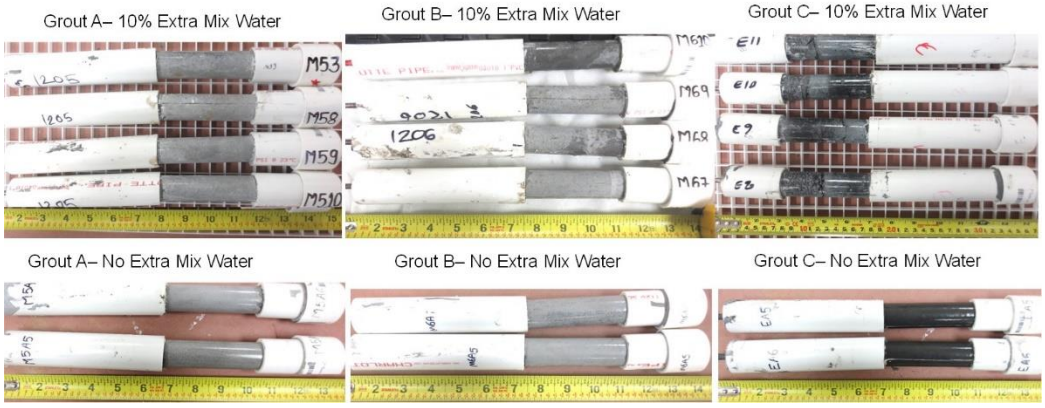

Figure A2. PTI test specimens after 56-day hydration
(Top: with 10% excess mix water, Bottom: with no 10% excess mix water)

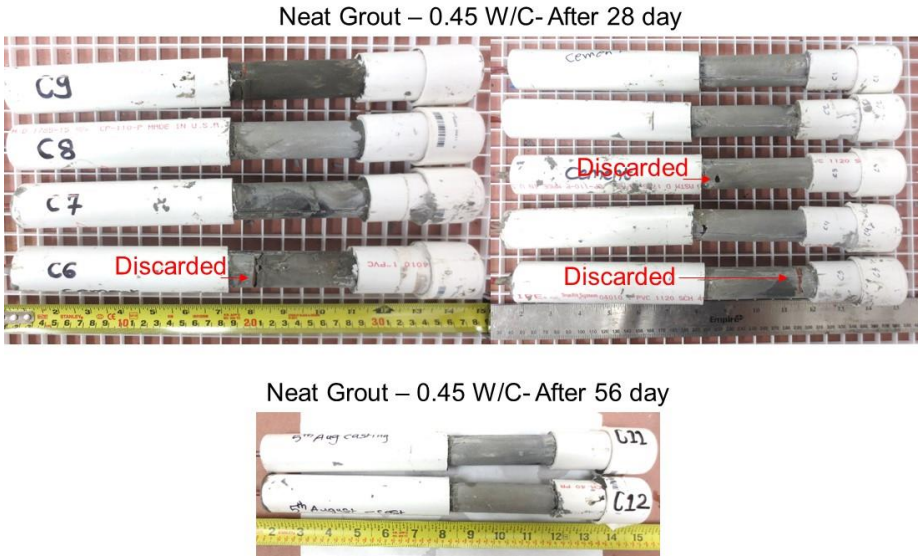

Figure A3. Neat grout test specimens for PTI after 28-day and 56-day hydration

Rapid Macrocell Test

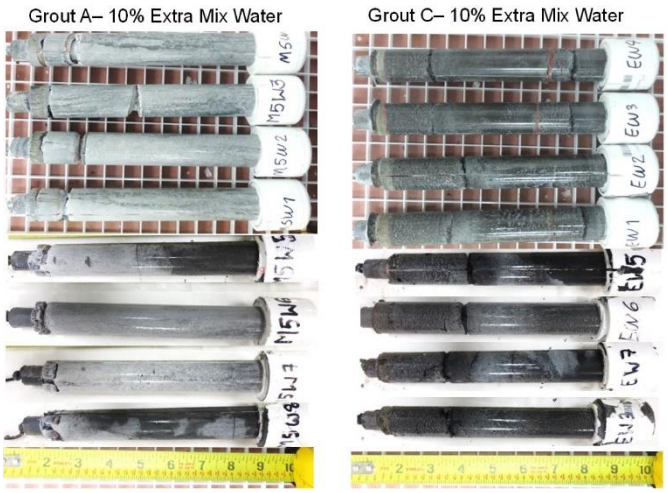

Figure A4. Rapid Macrocell test specimens after 28-day hydration (with 10% excess mix water)

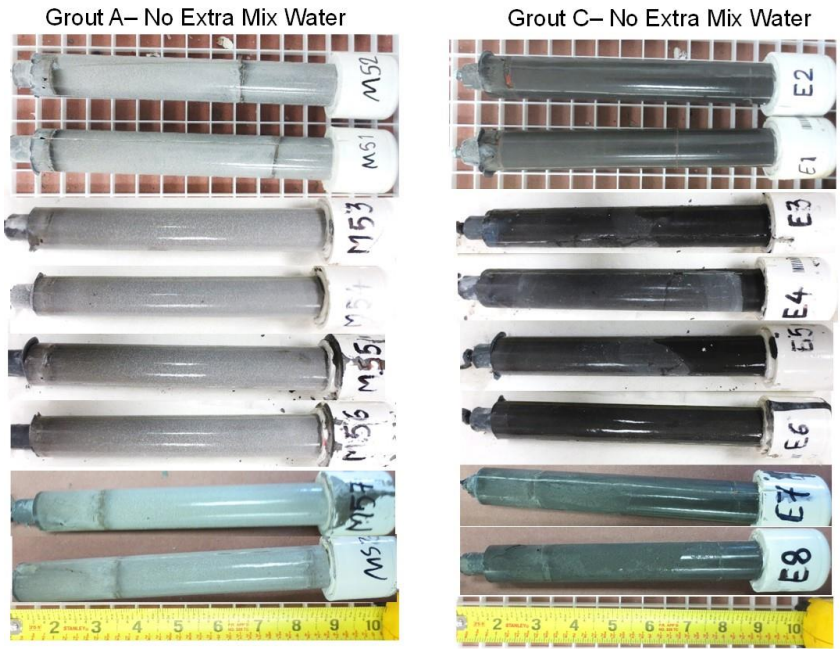

Figure A5. Rapid Macrocell test specimens after 28-day hydration (with no extra mix water)

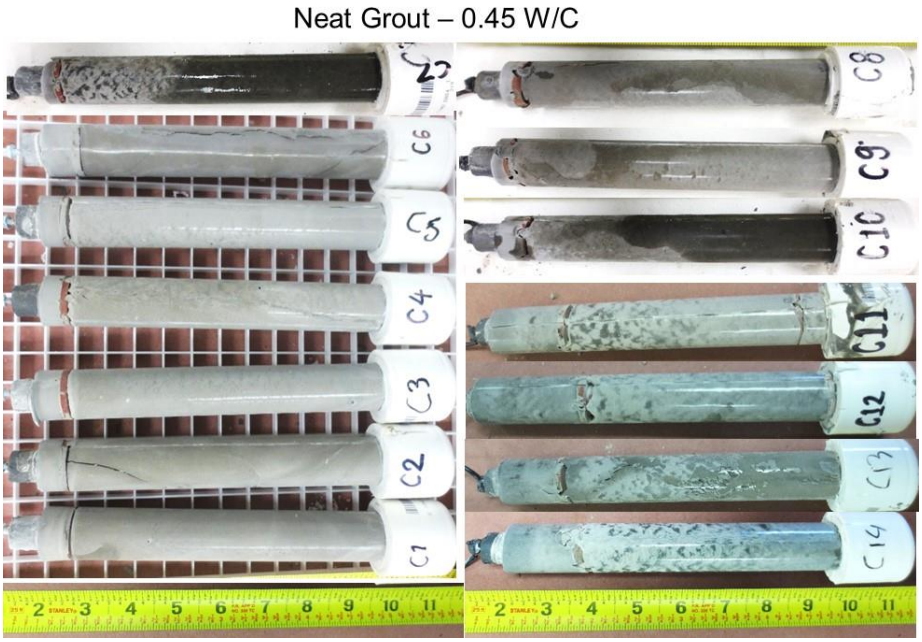

Figure A6. Neat grout test specimens for rapid macrocell testing after 28-day .

INT Grout Test Specimens

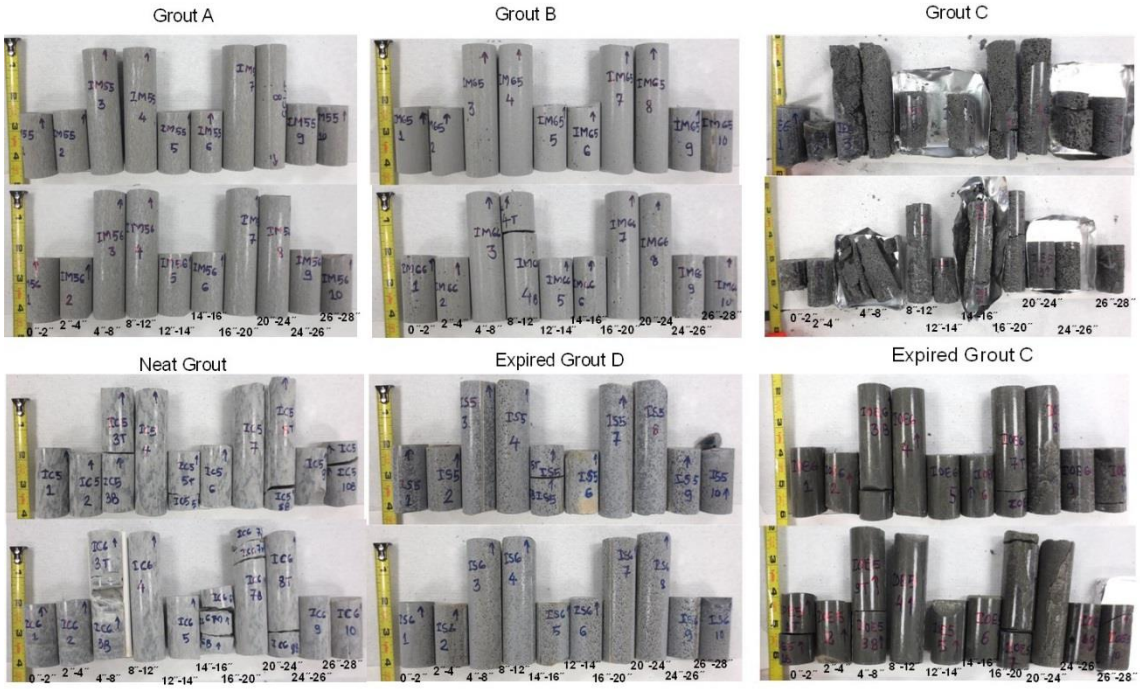

Figure A7. INT Tee-header test specimen after opening, cast with extra 10% mix water

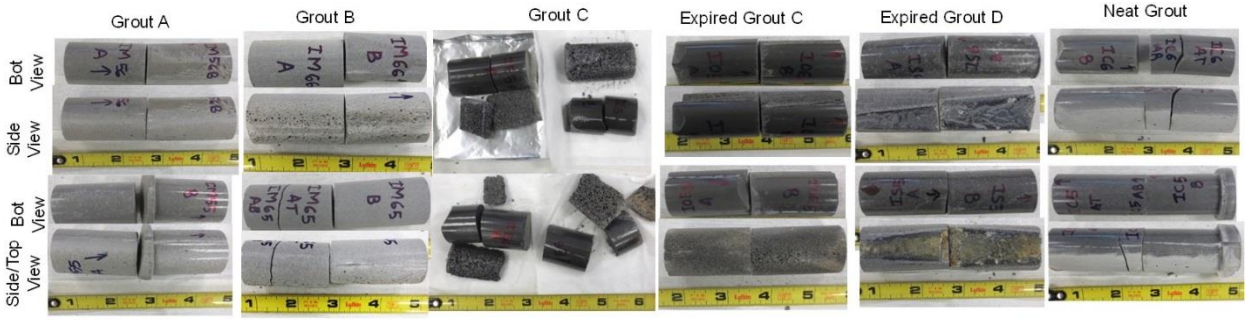

Figure A8. INT Tee-body test specimen after opening, cast with extra 10% mix water

INT Corrosion Test Specimen

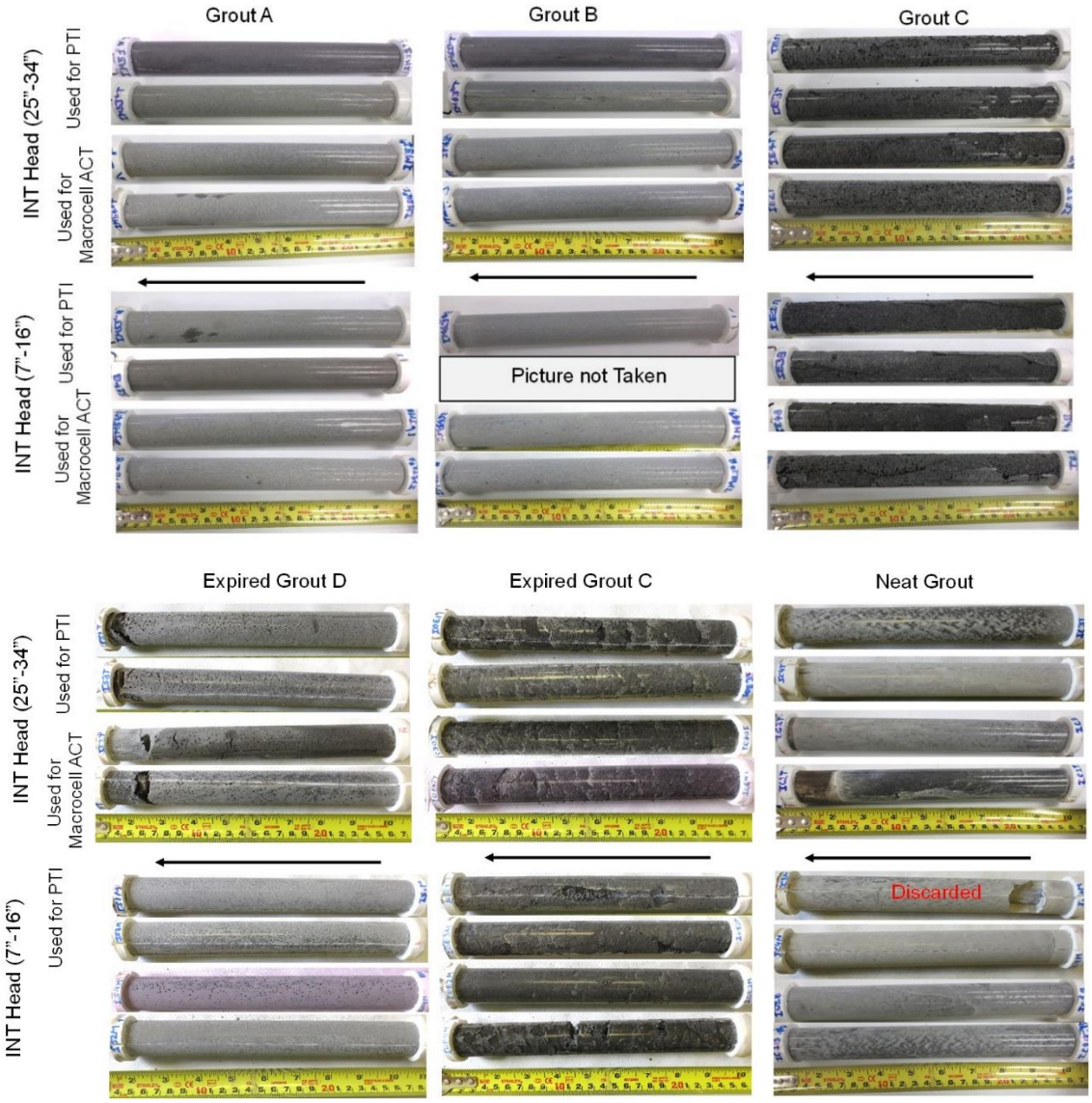

Figure A9. INT corrosion test specimen after opening, cast with extra 10% mix water

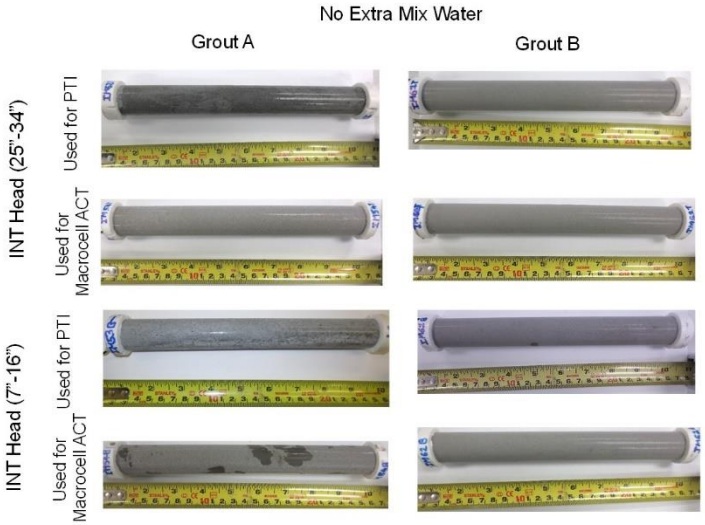

Figure A10. INT corrosion test specimen after opening, cast with no extra mix water.

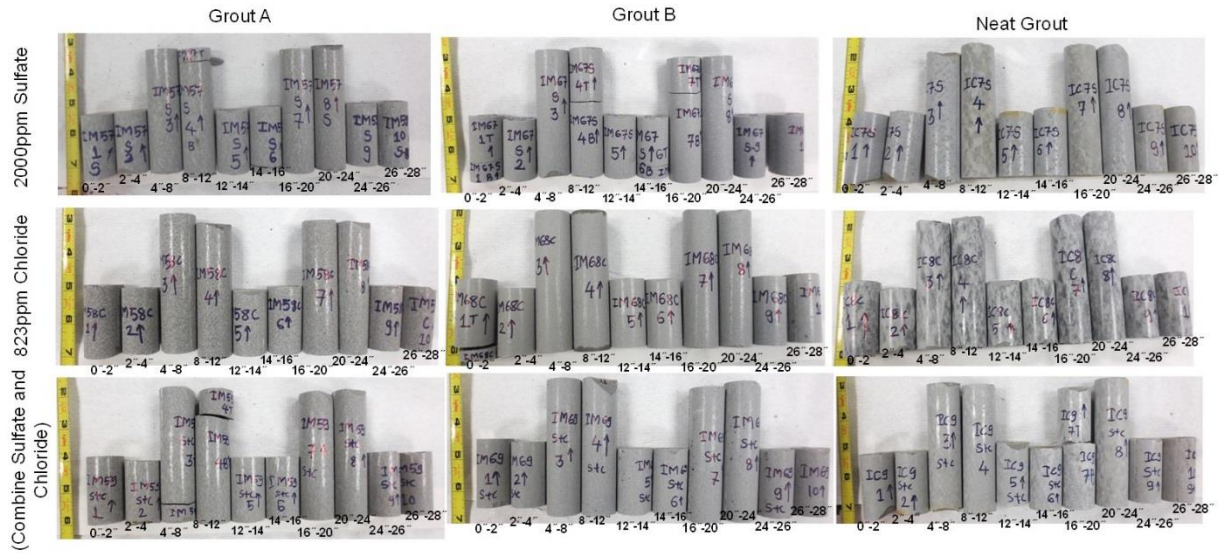

Figure A11. INT Tee-header test specimen after opening, cast with external ion contamination and extra 10% mix water

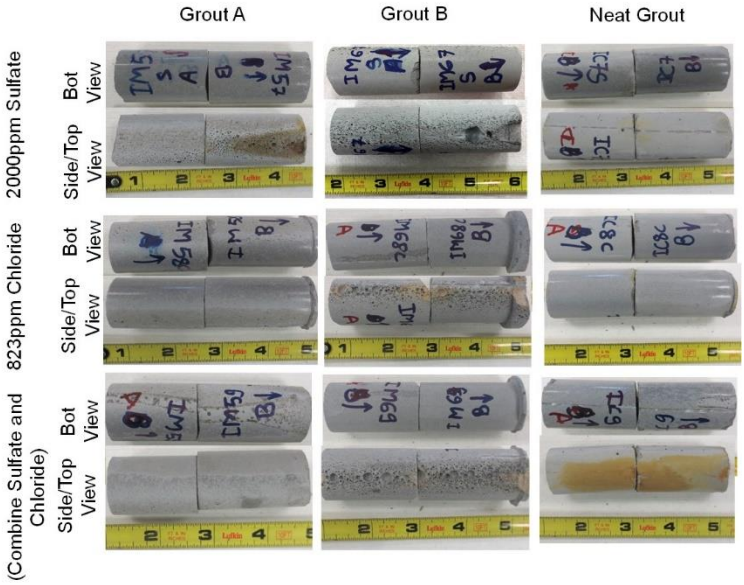

Figure A12. INT Tee-body test specimen after opening, cast with external ion contamination and extra 10% mix water

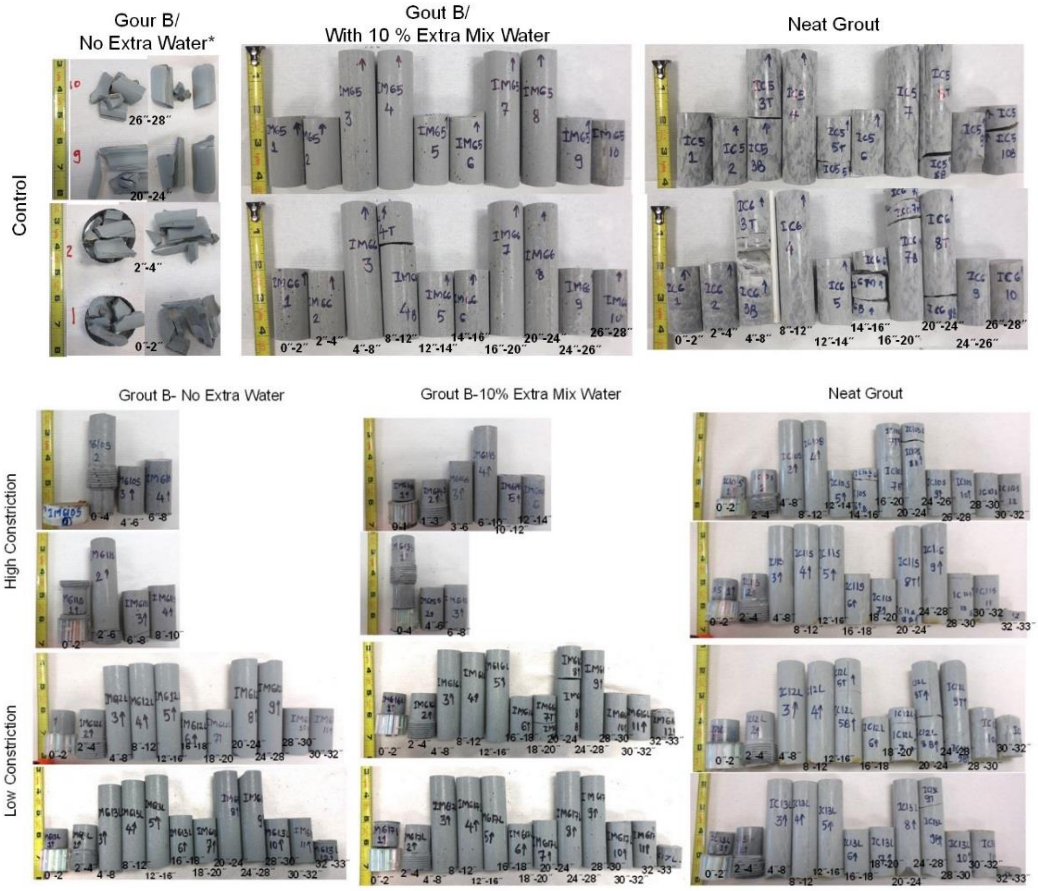

Figure A13. INT Tee-header test specimen after opening, cast with control and physical confinement condition

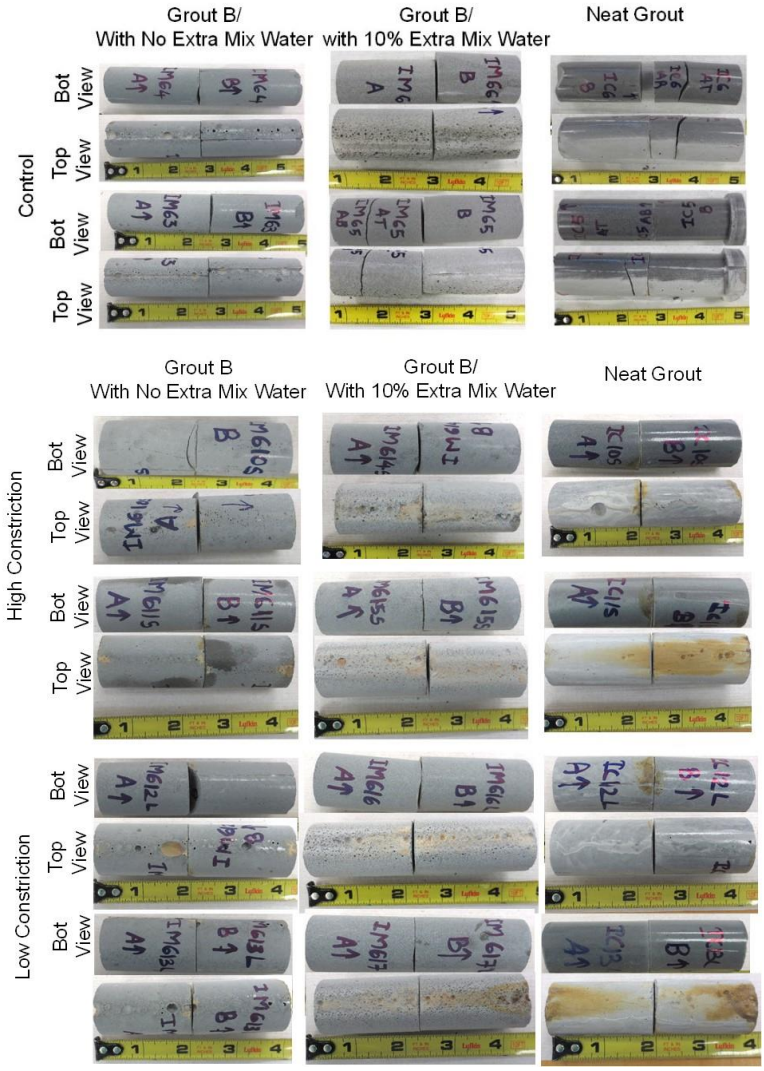

Figure A14. INT Tee-body test specimen after opening, cast with control and physical confinement condition